1990

Spectral hole burning spectroscopy of molecular electronic transitions in amorphous solids

In-Ja Lee
Iowa State University

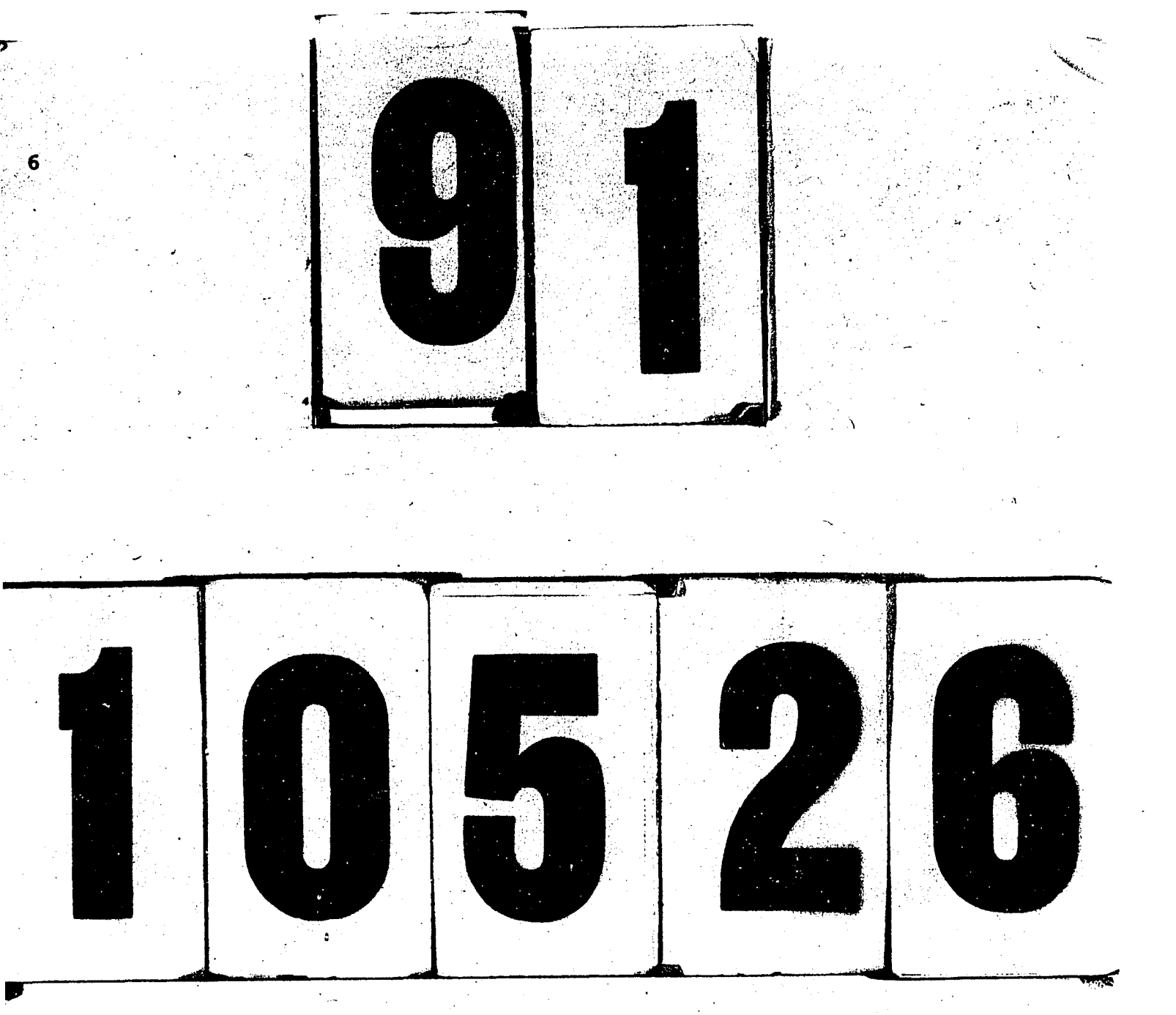

Order Number 9110526

Spectral hole burning spectroscopy of molecular electronic transitions in amorphous solids

Lee, In-Ja, Ph.D.

Iowa State University, 1990

U·M·I
300 N. Zeeb Rd.
Ann Arbor, MI 48106

Spectral hole burning spectroscopy of molecular electronic transitions in amorphous solids

by

In-Ja Lee

A Dissertation Submitted to the
Graduate Faculty in Partial Fulfillment of the
Requirements for the Degree of
DOCTOR OF PHILOSOPHY

Department: Chemistry
Major: Physical Chemistry

Approved:

Signature was redacted for privacy.

In Charge of Major Work

Signature was redacted for privacy.

For the Major Department

Signature was redacted for privacy.

For the Graduate College

Iowa State University
Ames, Iowa

1990

TABLE OF CONTENTS

GENERAL INTRODUCTION

Molecular electronic-vibrational (vibronic) transitions in the solid state are spectrally broadened by a variety of mechanisms which can be classified as homogeneous or inhomogeneous. Homogeneous broadening is the broadening that is common to all chemically identical molecules of the ensemble under spectroscopic investigation. Inhomogeneous broadening in the condensed phase is due to the fact that the environments of chemically identical molecules are not the same. Since the transition frequency is very sensitive to intermolecular interactions, the existence of non-identical environment leads, in a natural way, to a distribution of transition frequencies. This distribution provides a site inhomogeneous contribution, Γ_I, to the transition bandwidth. In what follows the homogeneous contribution to the bandwidth will be denoted by γ. The so-called natural or lifetime broadening of a single vibronic transition is a well known example of homogeneous broadening. For the case when the transition terminates at the vibrationless (zero-point) level of the ground electronic state, γ from the natural broadening is related to the lifetime of the excited state, T_1, by $\gamma=(2\pi T_1)^{-1}$. More generally, γ is given by (1,2)

$$\gamma\pi = 1/T_2 = 1/2T_1 + 1/T_2^*, \qquad (1)$$

where T_2 is the total dephasing time and T_2^* is the pure dephasing time. The spectral lineshape is a Lorentzian (3). To obtain the linewidth in units of cm^{-1}, γ from Eq. 1 should be divided by the speed of light (c) in units of cm/sec.

Pure dephasing is best understood in terms of the density matrix formulation of spectroscopic transitions (4-7). For the purpose of this discussion it suffices it to say that T_2^* is due to the modulation of the single site transition frequency that stems from the interaction of the excited state with the bath phonons and other low frequency excitations. This interaction leads to a decay of the phase coherence of the superposition state initially created by the photons, a decay that occurs without electronic relaxation. The pure dephasing time T_2^* is the time associated with phase memory loss of the superposition state created by the light field. It is strongly temperature dependent: at room temperature $(\pi T_2^* c)^{-1} \approx kT \approx 200\ cm^{-1}$ while at 4 K the linewidth is reduced to $\leq 0.1\ cm^{-1}$ in glasses and crystals (8-10). For a recent theoretical discussion of the relationship between T_2 and T_1 the reader is referred to Refs. 11 and 12.

Figure 1 presents a schematic of an inhomogeneously broadened vibronic origin band, which is a superposition of a very large number of homogeneously broadened single site absorption profiles most often referred to as zero-phonon lines (ZPLs), at low temperatures. In what follows the distribution of ZPLs will be referred to as the site distribution function (SDF). The SDF is determined by the distribution functions for the ground and excited state site energies, and if these functions were identical and perfectly correlated, Γ_I would be zero. This situation never occurs. Furthermore, it has been shown that transition frequencies of different sites can be accidentially degenerate. For amorphous hosts Γ_I~100-500 cm^{-1}. The magnitude of Γ_I for crystals is about 2 orders of magnitude smaller than this.

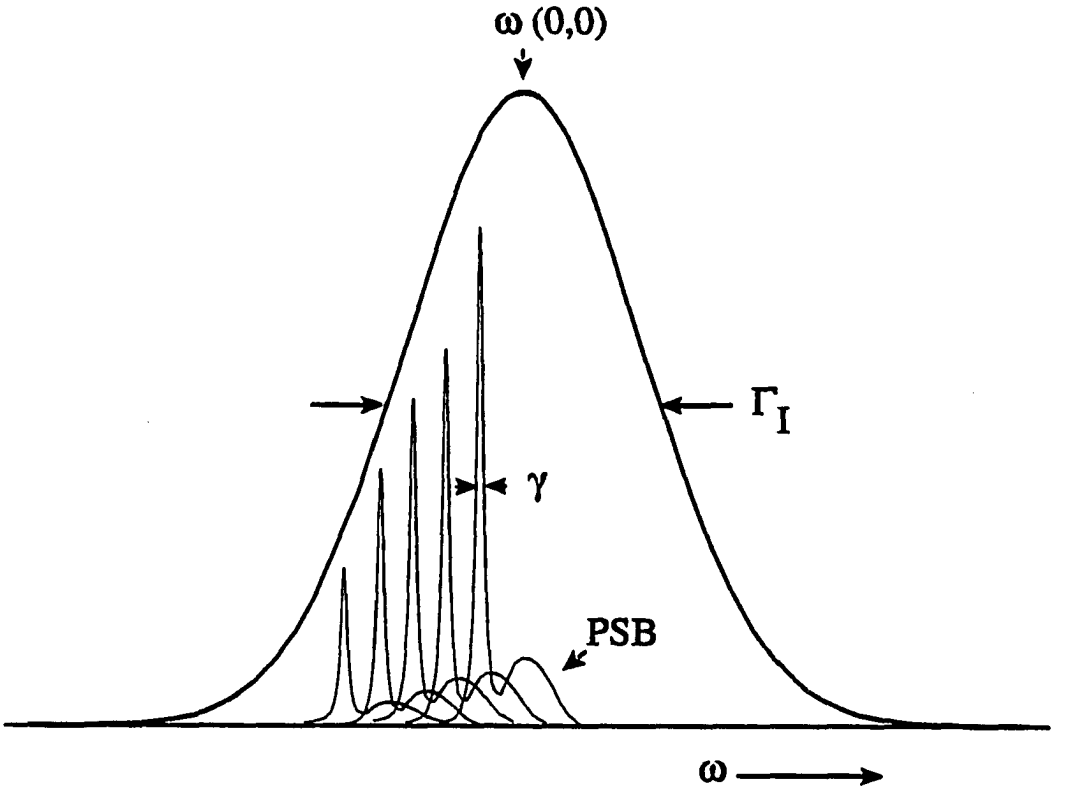

Figure 1. Schematic representation of homogeneous (γ) and inhomogeneous (Γ_I) broadened absorption profoile. ZPL is accompanied by the broad PSB

The broad wings that build to higher energy on the ZPL in Fig. 1 are the phonon sidebands (PSBs), which are a manifestation of the change in the equilibrium lattice geometry that occurs upon electronic excitation. The phonons of organic crystals and glasses provide a continuous distribution of fundamental excitations between 0 and ~150 cm^{-1}. The impurity can introduce localized or pseudolocalized phonons (13) which can lead to relatively sharp features in the PSB. However, such structure is seldom observed for glass or polymer hosts. Rather, the coupling appears to be restricted to the spatially extended phonons. As illustrated in Fig. 1, the PSB resembles a one-phonon profile, i.e., transitions that are accompanied by the creation of 1 phonon. The PSB shape is governed by $g(\omega)D(\omega)$, where ω is measured relative to the ZPL (13,14). Here, $g(\omega)$ is the phonon density of states and $D(\omega)$ is the frequency dependent coupling function. To a very good approximation the probability of the r-phonon process is given by (13,15)

$$P_r = \exp(-S)\, S^r/r! \qquad (2)$$

at liquid helium temperatures. Here S is the Huang-Rhys factor, defined by $S = \Sigma (\mu_i\omega_i/\hbar) (\Delta Q)_i^2/2$ (16,17) where μ_i and ω_i are the appropriate mass and frequency for the ith phonon mode and $(\Delta Q)_i$ is the change in the normal mode coordinate which results from impurity excitation. From Eq. (2), it should be noted that $\Sigma P_r=1$ and the Franck-Condon factor for the ZPL (r=0) is exp(-S). Therefore, the stronger the

electron-phonon coupling the lower the ZPL intensity. For example, the ZPL contribution to the total intensity is ~65% for S=0.45 while ~40% for S=1.0.

Figure 2 represents 0 K single site absorption profiles for S=0.5, 1.0, 2.0, 4.0 and 8.0 which were calculated using the theory of Section I. This theory employs the mean phonon frequency (ω_m) approximation. The one-phonon profile is given a width of Γ. An analytical shape function for the r-phonon profile is obtained by folding the 1-phonon profile r times (15). Typical values of ω_m and Γ for organic amorphous hosts are ~30 cm^{-1}. These results were used for the calculation of the profiles shown in Fig. 2. The distinction between weak and strong linear electron-phonon coupling is usually defined by S=1. For very large S the ZPL becomes highly Franck-Condon forbidden and unobservable. The charge-transfer states of organic donor-acceptor crystals are characterized by such strong coupling (18). A key point is that for sufficiently large coupling (S), the single site absorption profile is exceedingly broad, $\gamma \approx S\omega_m$. This broadening is homogeneous. Line narrowing spectroscopies, vide infra, cannot eliminate such broadening.

In summary, the shape of the vibronic absorption band is determined primarily by the SDF and the linear electron-phonon coupling. It is of fundamental importance to be able to characterize them both as well as γ for the ZPL, particularly the part of γ due to pure dephasing.

That the magnitude and temperature dependence of the pure dephasing of impurity transition at very low temperatures in glasses is fundamentally different from that in crystals was discovered about 10 years ago (19-22). Prior to that it

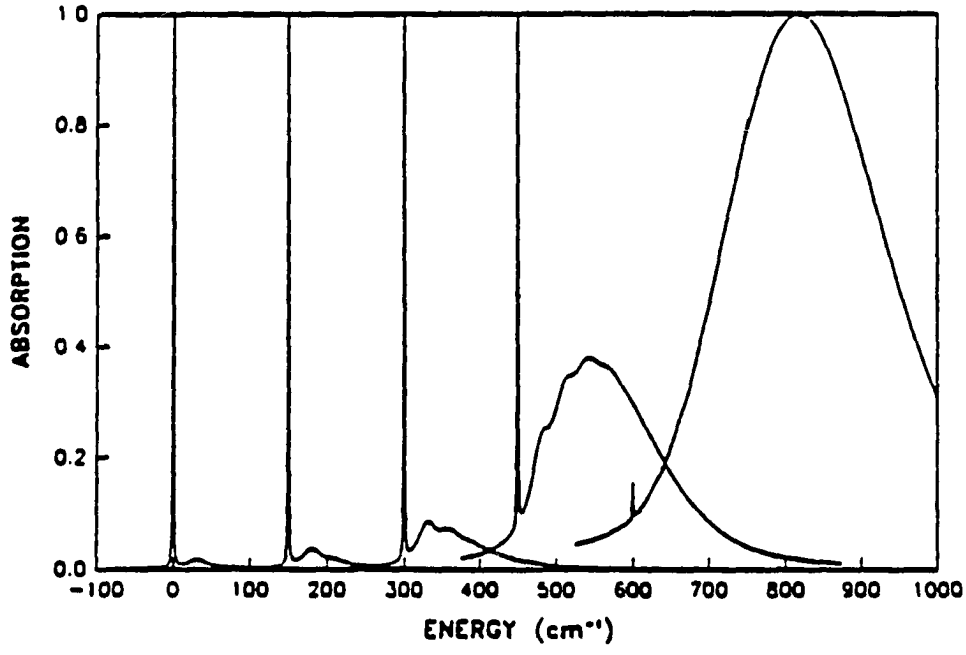

Figure 2. Single site absorption profiles calculated according to the theory of Paper I in Section I. The parameters used were $\Gamma=\omega_m=30\ cm^{-1}$ and $\gamma=1$. From the left to right the values of S are 0.5, 1.0, 2.0, 4.0 and 8.0. For ease of inspection the S=1 to S=8 spectra are artificially shifted in steps of 150 cm^{-1} relative to the S=0.5 spectrum (from Ref. 15)

was known that the thermal properties of glasses at very low temperatures are also anomalous, both in magnitude and temperature dependence. Table I summarizes the anomalous low temperature behavior of pure dephasing and other properties for glasses. In 1971, Zeller and Pohl (23) pointed out that thermal conductivity and heat capacity of several glasses (vitreous SiO_2, selenium, and germanium) behave remarkably different from that of crystalline materials between 70 mK and 1 K. They concluded that a new physical model was required for an understanding of the low temperature thermal properties of amorphous solids. Their results were in accord with the earlier studies (24) and stimulated a number of theoretical and experimental studies (25-30). Besides specific heat and thermal conductivity, the temperature dependence of dielectric and acoustic properties of impurities in amorphous solids were also different from those in crystalline solids. The experimental findings that (30-32) ultrasonic absorption can be saturated in glasses supported the two level system (TLS) tunneling model of Anderson et al. (25) and Phillips (26) because the observed ultrasonic saturation could be explained by considering the scattering of acoustic phonons from the additional low energy degrees of freedom in glasses provided by the TLS.

In 1972, Anderson et al. (25) and, independently, Phillips (26) proposed that in any glass system there should be a certain number of atoms or groups of atoms which can occupy, with nearly equal probability, two equilibrium positions separated by an energy barrier, the so-called TLS. Figure 3 shows a potential energy curve for a TLS along some configurational coordinate. W is the tunneling

Table I. Comparison of glass and crystal properties

PROPERTY	CRYSTAL	GLASS	REL. MAGNITUDE[a]
Specific heat	T^3	$cT + c'T^3$	larger
Thermal conductivity	T^3	$\sim T^2$	smaller
Ultrasonic attenuation		saturates	larger
Sound velocity	T indep.	ln T	10-100
Dielectric constant	T indep.	ln T	10-100
Optical linewidth	T^7	$T\text{-}T^2$	10-100

[a]Glass value relative to crystal value.

frequency, d is the well separation, V is the barrier height and Δ is the asymmetry parameter (energy difference of the two localized states (W=0)). The tunneling parameter $\lambda=(2mV)^{1/2}\, d/\hbar$ where m is the tunneling mass. The tunnel splitting energy, E, is given by $E^2=\Delta^2+W^2$. At very low temperatures, the atoms or groups of atoms cannot be thermally activated over the barrier, but can tunnel through it. Because of the inherent disorder of amorphous solids, consideration of the TLS distribution function $f(\Delta,W)$ is necessary. Initially, a uniform distribution function (25,26) was proposed and later many phenomenological functions were proposed (33-38). Recently, Jankowiak and Small introduced (38-40) analytical forms for the TLS distribution function which were derived under two reasonable assumptions. They are that a Gaussian is the proper distribution function for λ and Δ and that λ and Δ are stochastically independent. The derived distribution functions for TLS were used to calculate the temperature power laws for the thermal conductivity and specific heat. Good agreement with experimental data was obtained (41).

The anomalous dephasing of impurity transitions in glasses has been convincingly attributed to the coupling of TLS to the electronic transition. Several review articles exist (8,42,43). The most detailed treatment of such dephasing in terms of nonphenomenological TLS-distribution functions has been given by Jankowiak and Small (44). As mentioned earlier, the pure dephasing term T_2^* is strongly temperature dependent while T_1 is not. At room temperature, the T_2^* contribution to γ is $\sim kT \sim 200\ cm^{-1}$ which is comparable to Γ_I for glasses. The characteristics of the pure dephasing have been characterized by both two pulse

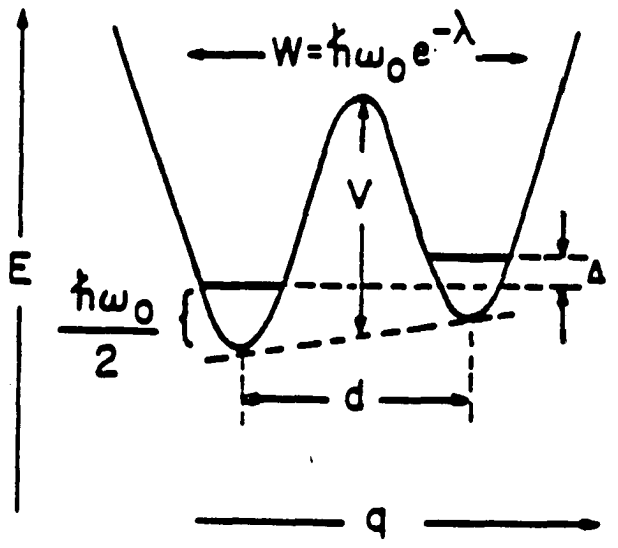

Figure 3. TLS represented in a configuration-coordinate model by a double-well potential. V, barrier height; Δ, asymmetry; and d, distance between two minima. The tunneling frequency between potential wells is given by W

photon echo spectroscopy (45-47) and line narrowing spectroscopy (48-97). For reviews of the former technique and other time domain coherent spectroscopies the reader is referred to Ref. (47). Examples of line narrowing spectroscopies which can eliminate or significantly reduce the contribution of Γ_I to the vibronic bandwidth are: fluorescence line narrowing (FLN) (48-52) and hole burning (53-97). Since γ cannot be eliminated, low temperatures are needed to minimize the contribution by the populated low frequency phonons responsible for γ.

The basic principles of FLN can be understood as follows: if an ordinary broad band light source is used to excite (0,0) transition, all sites whose transition frequencies are different from each other but within the bandwidth of the source will be excited with equal probability and then would result in a broad fluorescence spectrum. On the other hand if a narrow bandwidth ($<<\Gamma_I$) laser excitation is used, only a small subensemble of molecules (an isochromat) whose absorption frequencies overlap the laser profile will be excited and would fluoresce, resulting in a markedly narrowed fluorescence spectrum at low temperature. The fluorescence spectrum consists of an origin ZPL coincide with the laser frequency and many ZPLs corresponding to transitions to the vibrational sublevels of the ground electronic state at the lower energy side of the origin ZPL. Each ZPL is accompanied by a PSB to lower energy. For reviews of FLN, the reader is referred to Refs. 50 and 52.

The basis of hole burning is selective bleaching of the isochromat by laser irradiation. By irradiating a sample with a laser tuned into the inhomogeneously

broadened absorption spectrum, the selected isochromat in the excited state may undergo a phototransformation. The absorption associated with the selected isochromat will be depleted from the absorption spectrum of the sample if the photoproduct absorbs at a different frequency from the frequency absorption of the original sample. This creates a hole in the absorption band coincident with the laser frequency.

Depending on lifetime of hole, hole burning can be classified as [1] transient hole burning due to a temporary depletion of ground state absorbers at ω_B or [2] persistent hole burning due to a permanent depletion which may or may not be reversible. Transient hole burning (53-55) is caused by a population transfer from the ground state to a metastable state (bottleneck state, e.g., a long-lived triplet state) which slows down the decay of molecules to the ground state. In this case the hole decays or fills rapidly, normally μsec to sec, because of a return to the equilibrium populations.

In contrast, persistent holes normally last hours or longer provided the sample is kept at low temperature. Depending on the photoreactivity of the guest molecule, persistent holes can be classified as being formed by photochemical hole burning (PHB) or nonphotochemical hole burning (NPHB). In photochemical hole burning (56-63), the isochromat excited by narrow bandwidth laser undergoes chemical modification of its structure resulting in a hole. Thus what is required for PHB is photoreactivity of the absorbing chromophore. Therefore PHB can be observed for both amorphous and crystalline hosts. For example, dimethyl-s-

tetrazine (DMST) (60) undergoes an irreversible two-photon photodissociation according to DMST $\xrightarrow{h\nu}$ 2 $CH_3CN + N_2$. In this case the fragments absorb in the UV range of the spectrum. Photochemical hole burning was first observed in 1974 by Gorokhovskii et al. (62) for free base phthalocyanine in n-octane where the PHB is caused by an intramolecular hydrogen tautomerization. Other examples of PHB are intramolecular hydrogen tautomerization of porphyrin (56-58), photoionization and trapping of the ejected electron of color centers (59). PHB can be reversible (e.g., phototautomerization, (56-58) or irreversible (e.g., photofragmentation of s-tetrazine (61)). For a review of PHB, the reader is referred to Ref. 63.

Nonphotochemical hole burning, or photophysical hole burning (64-69), is characteristic of molecules in amorphous systems and does not require photoreactivity of the guest molecule. What is needed is a host with a "faulty memory" for its pre-excitation configuration near the absorber. When a photostable isochromat is excited by laser light at ω_B, it may cause a change of the microscopic host configuration around the guest (not of the guest molecule itself). Because the transition frequency of the guest is very sensitive to the environment, the molecule no longer absorbs light at ω_B (resulting in hole production) rather the absorption is at a slightly different frequency (resulting in an antihole) after de-excitation to the ground state. With few exceptions (67,68), NPHB has only been observed with glasses, polymers or proteins because the inherent structural disorder of these matrices provides a faulty memory. In crystalline benzoic acid matrices (67,68), host hydrogen bond rearrangement upon irradiation provides a

faulty memory. Nonphotochemical hole burning was first observed in 1974 by Kharlamov et al. (64) for perylene and for 9-aminoacridine in an ethanol glass. Normally absorption frequencies of the photoproduct of PHB are well separated from that of the original molecules, while the absorption of antihole (increase in absorption due to redistribution of absorber) of NPHB normally lies close to that of the original molecules.

Before introducing the proposed NPHB mechanisms, hole profiles including vibronic and phononic holes will be discussed. As shown in Fig. 4-(a), an absorption spectrum consists of an origin (0-0) band and corresponding vibronic bands (1_α,0) and (1_β,0). When laser light is tuned into the electronic origin band, it excites an isochromat resulting in a zero-phonon hole (ZPH). However, the isochromat also contributes to the (1_α,0) and (1_β,0) vibronic absorption bands. Therefore, a ZPH coincident with the laser burn frequency, ω_B, will be accompanied by vibronic satellite holes to higher energies of ω_B in regions corresponding to vibronic frequencies as shown in the difference hole burned spectrum, Fig. 4-(b). In the same manner, the ZPH is accompanied by the phonon sideband hole (PSBH) at $\omega_B+\omega_m$ since the ZPL in absorption is accompanied by a PSB. Generally SDF's for different electronic states are not correlated (70). Therefore, the narrow isochromat of the transition selected by the laser will correspond to a much broader polychromat in another electronic transition. Full correlation means that the energy difference of two different transitions should be equal for all molecules in the ensemble. Therefore each molecule has ZPLs of both

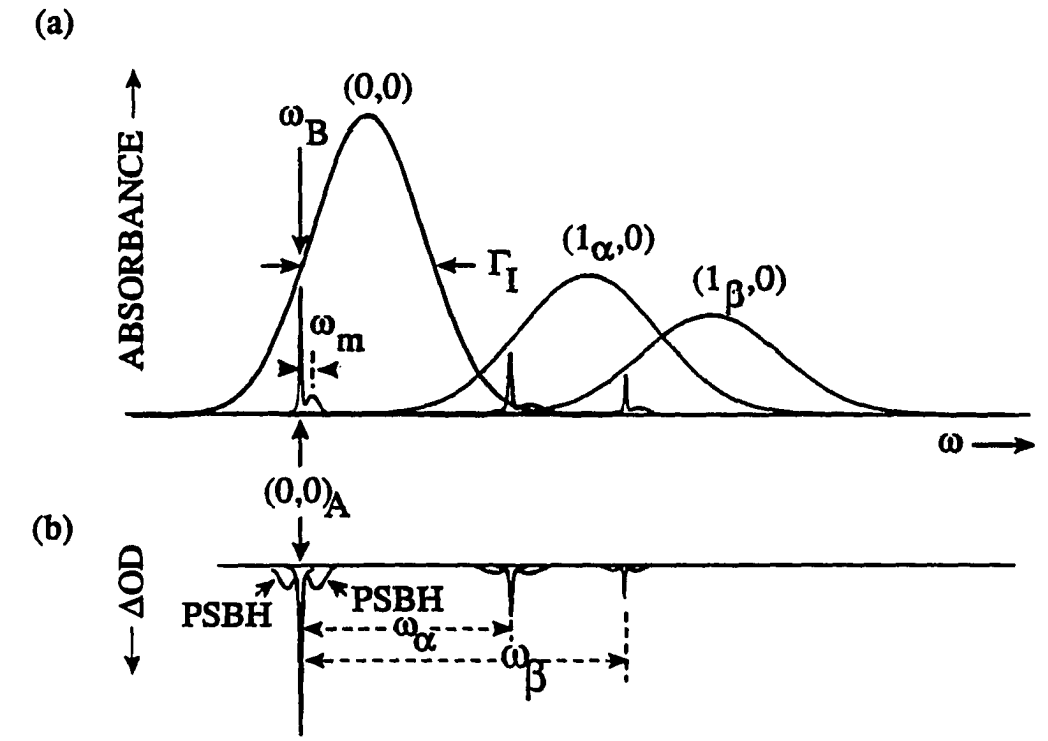

Figure 4. A schematic diagram representing production of the vibronic holes when laser light is tuned into the origin absorption band. (a) an absorption spectrum consists of one origin band (0,0) and two vibronic bands $(1_\alpha,0)$ and $(1_\beta,0)$. ω_B is the laser frequency and Γ_I is the inhomogeneous width. (b) hole spectrum consists of a ZPH, PSBHs and vibronic holes. Here ω_α and ω_β are the vibrational frequencies in the excited states

transitions at the same relative positions within the two inhomogeneously broadened absorption bands. Fortunately, the transition energy distribution of different vibronic levels of the S_1 state are generally highly correlated to the (0,0) transition (71). Therefore the origin ZPH accompanied by reasonably sharp vibronic holes can usually be observed. Because the above mentioned PSBH and the vibronic satellite holes build on the origin ZPH, they are called real-PSBH and real-vibronic holes. The intensity ratio of the ZPH to the real-PSBH or of the ZPH to the real-vibronic satellite holes follow their Franck-Condon factors.

In addition to the real-PSBH, a pseudo-PSBH can also be produced at ω_B-ω_m by sites whose ZPL are located to lower energy of the burn frequency and which absorb laser light via their PSB. In the same manner, pseudo-vibronic holes can be produced. Assume that the molecule under investigation has two vibrations in the excited electronic state with frequencies of ω_α and ω_β as shown in Figure 5-(a). If laser frequency is tuned into the region in which the two vibronic bands (1_α,0) and (1_β,0) overlap, the hole burning at ω_B excites two different isochromats to (1_α,0) and (1_β,0). Since NPHB rate is usually not larger than 10^6 s^{-1}, the vibronically excited isochromats relax to their corresponding zero-point levels in the (0,0) band prior to hole burning. As a result, two origin ZPH (at $(0,0)_A$ and $(0,0)_B$) displaced from ω_B by the two vibrational frequencies will appear in the origin region along with a third at ω_B. The energy difference between the ZPH and ω_B gives the excited state vibrational frequencies.

Vibronic Hole Burning

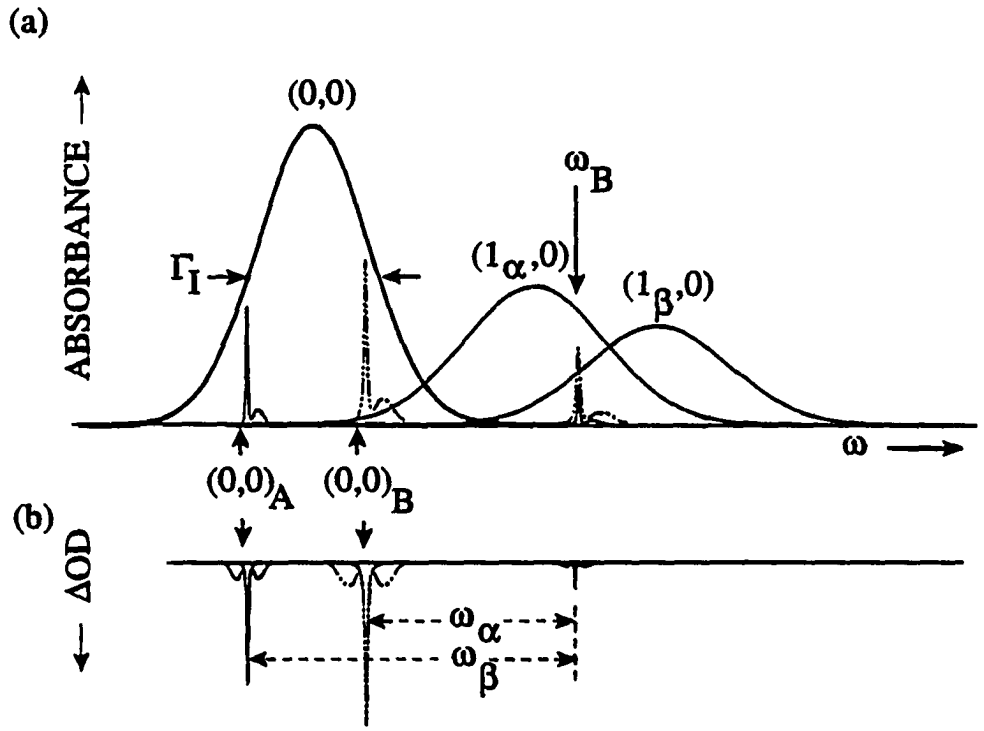

Figure 5. A schematic diagram representing production of the vibronic holes when laser light is tuned into a vibronic absorption band. (a) an absorption spectrum consists of one origin band (0,0) and two vibronic bands $(1_\alpha,0)$ and $(1_\beta,0)$. ω_B is the laser frequency and Γ_I is the inhomogeneous width. (b) hole spectrum consists of a ZPH, PSBHs and vibronic holes. Here ω_α and ω_β are the vibrational frequencies in the excited states

Figure 6 shows nonphotochemical hole burned spectra of Oxazine 720 in glycerol at 1.6 K (72). In this experiment, the burn frequency ω_B=15803 cm^{-1}. The figure shows that the ZPH at ω_B is superimposed on the high energy side of a broad pseudo-PSBH peaked at ω_B-27 cm^{-1}. The increase in absorption to the right of ω_B is the antihole associated with NPHB. The small glitch in the sharply rising edge of the antihole is a consequence of the interference between the positive going antihole and the negative going real-PSBH. The inset of Fig. 6 shows more clearly the existence of the real-PSBH at ω_B+27 cm^{-1}. Pseudo-vibronic holes which occur to lower energy of ω_B are clearly shown while interference with the antihole from the real-vibronic holes at ω_B+302 cm^{-1} and ω_B+592 cm^{-1} is apparent.

In 1978, Hayes and Small proposed (73,74) a mechanism for hole formation by NPHB based on coupling of the electronic transition to the glass TLS_{ext}. Here TLS_{ext} (extrinsic TLS) represents the subset of localized TLS (probe-inner shell) which interact with or are created by the impurity. There is another type of TLS, TLS_{int} (intrinsic TLS) associated with the subset of spatially extended delocalized TLS (outer shell). Bogner and Schwartz have proposed a similar model (75). This model is schematically shown in Fig. 7. TLS_α is the potential energy curve of a TLS coupled to the ground state of the guest molecule while TLS_β is the potential energy curve for the TLS coupled to the excited state. Persistence of the hole by NPHB can be explained if it is assumed that at the burn temperature relaxation between the minima of ground state TLS_α is slow on the time scale of the experiment while it is competitive with the excited state lifetime at TLS_β. The

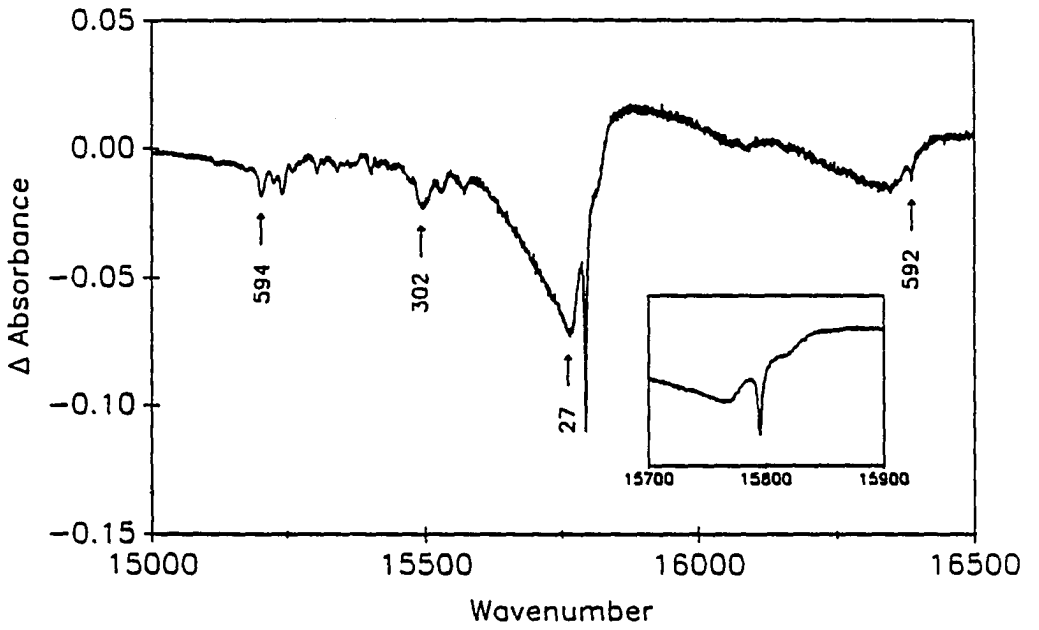

Figure 6. Hole spectrum of Oxazine 720 in glycerol (from Ref. 72). Hole is burnt at ω_B=15803 cm^{-1} at 1.6K. Burn intensity was 1 mW/cm^2 and burn time was 5 sec. A number of pseudo-vibronic holes appear at $\omega<\omega_B$ and real-vibronic holes at $\omega>\omega_B$. Inset shows enlargement of the ZPH region. The pseudo- and real-PSBH are located at ω_B-27 and ω_B+27 cm^{-1}, respectively

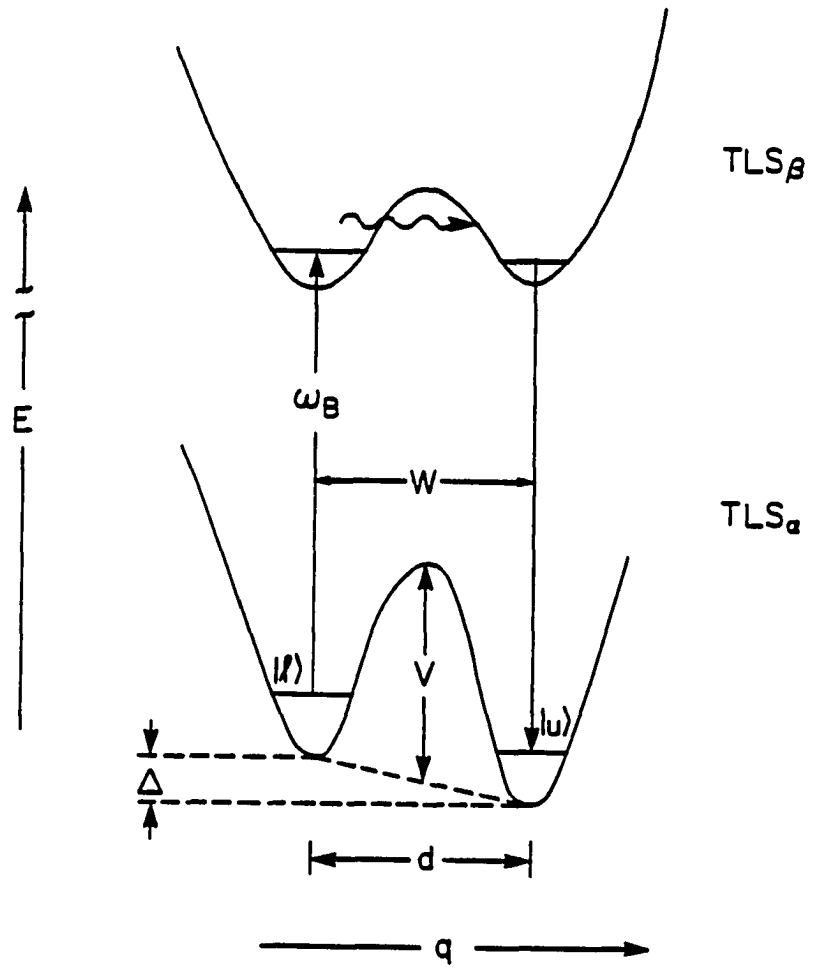

Figure 7. Potential energy curves for a TLS coupled to an impurity in its ground state, α, or excited state, β. The tunneling rate between wells is given by W. ω_B is the laser frequency and $|l\rangle$ and $|u\rangle$ represent the upper and lower well, respectively

degree of competiveness determines the hole burning efficiency. If the burn frequency is resonant with the left well transition, then in the excited state the transition between the minima of TLS_β by phonon assisted tunneling (PAT) or by thermal activation to the right well can compete with the electronic relaxation. In the case of a transition between the minima of TLS_β, after de-excitation to the ground state the absorption frequency will be changed because the microenvironment of the guest molecule has been changed and TLS_α^u and TLS_α^l are nearly kinetically inaccessible to each other (9).

Recent temperature dependent NPHB experiments on cresyl violet perchlorate (CV) in polyvinyl alcohol (76) have shown that there is a strong burn temperature (T_B) dependence of the antihole profile and T_B independence of the hole growth. With this result and an approximation to the static distribution of extrinsic asymmetric double well potentials, one can notice that the above NPHB mechanism predicts a red-shifted antihole. However, based on the published NPHB spectra (75-77) of impurity electronic transitions in amorphous host, it appears that the antihole corresponding to the ZPH plus pseudo-PSBH is often predominately located to higher energy of the ZPH, i.e., blue-shifted, (also see Fig. 6). This indicates that the simple TLS model is inadequate. In Ref. 76, a new NPHB mechanism based on an "outside-in" hierachy of constrained configurational tunneling levels is introduced. The essential idea of this model is that electronic excitation from the pre-burn guest-host configuration triggers rapid tunneling of the delocalized TLS_{int} ("outer-shell") which produces a decrease in the free volume

of the "outer-shell" and an increase in that of the localized TLS_{ext} (probe-inner shell). Subsequently, tunneling occurs causing the hole formation. This new model is shown to be consistent with the experimental data (76,78,79) and can explain why the antihole for $\pi\pi^*$ transitions of organic molecules are produced predominantly to higher energy side of the hole as follows: generally energy stabilization of the ground state and $\pi\pi^*$ state due to the reduction of intermolecular atom-atom repulsion should be nearly identical while the loss of stabilization energy for the $\pi\pi^*$ state associated with attractive interactions would be greater than that for the ground state. With this consideration, the model predicts blue shifted antihole for the $\pi\pi^*$ transitions of organic molecules.

As mentioned earlier, the inherent structural disorder of the amorphous solids leads to a distribution of the TLS parameters. This precludes the observation of a pure exponential decay in time associated with many relaxation processes (80,81) and results in dispersive relaxation processes. This is expected in systems where the hole burning proceeds via the tunneling of TLS. Because the tunneling rate depends exponentially on the tunneling parameter λ by $R = \Omega_0 \exp(-2\lambda)$, the distribution of λ gives rise to a broad distribution of burning rates. Here Ω_0 is defined by the type of the experiment (72,82). The study of hole growth kinetics and spontaneous hole filling (a dark ground state process) are important methods for the investigation of dispersive kinetics in glasses (9,82). For a review of hole growth kinetics, the reader is referred to Ref. 72.

Although a persistent hole can last for long periods of time (~hours to days), slow hole filling (spontaneous hole filling, SPHF) is normally observed in the dark at $T=T_B$. Here, T_B is the burn temperature. This is caused by TLS ground state transitions involving emission or absorption of thermal phonons. Since the electronic transition energy of the impurity molecule also depends on the strain, fluctuation in strain leads to fluctuations of the electronic transition frequencies of the guest. There are two SPHF processes: [1] antihole reversion from the product to reactant state by the TLS_{ext} transition. Under certain circumstances, this process can lead to filling without hole broadening (9); [2] redistribution of the unburned molecules by TLS_{int} transitions. This process, called spectral diffusion, does not change the hole area but changes the hole shape. This causes additional broadening of the optical linewidth. Because the TLS relaxation rate is dispersive in amorphous solids, the broadening of the hole width by spectral diffusion is both time and temperature dependent. If TLS relaxation by spectral diffusion occurs within the lifetime of the excited state of the molecule, it will contribute to the homogeneous linewidth and if not, it will contribute to spectral diffusion (83).

In Refs. 84 and 85, Fayer and his group concluded that the linewidth of resorufin in ethanol glass measured from hole burning was about four times larger than that measured by photon echo as a consequence of spectral diffusion. However this result is somewhat controversial. In Refs. 86 and 87, Völker and her group suggested that hole burning can yield the homogeneous linewidth. This will be further discussed in the introduction to Section II in this dissertation.

Whichever is correct, one can obtain an upper limit of γ from holes burned in the short burn time limit with a monochromatic laser because the holewidth is then greater than or equal to twice γ.

Spectral hole burning is a high resolution line narrowing spectroscopy. Typically holes burned at very low temperatures are very narrow and sensitive to the microscopic environment. Therefore, from detailed linewidth and hole shape studies, one can obtain valuable information about the host as well as the guest. Examples are the degree of inhomogeneous broadening (88), vibrational frequencies (56,78,89) and their Franck-Condon factors (56,78) and symmetry (89), electron-phonon coupling strength (90,91), dephasing (92), spectral diffusion (84-87), bottleneck lifetime (57), etc., as well as TLS parameters (72) by using hole growth kinetics. Also PHB and NPHB have the potential to be used for ultra narrow optical band pass filters (93) and ultra high density optical memory storage devices (94-96).

Application of hole burning to biological systems, e.g., photosynthetic systems (97), is another important recent application. One can obtain the following information on the protein-chlorophyll (Chl) complexes from hole burning spectroscopy: [1] active intramolecular Chl modes (frequencies and Franck-Condon factors) for $S_1 \leftarrow S_0$ transition. When these are compared with those of the same pigment in a non-naturally occuring material, one can obtain information on the extent of the perturbation of the interaction with the protein; [2] linear electron-phonon coupling for the optical transition, where phonon refers to the low energy

intermolecular modes of the protein-Chl complex; [3] the degree of inhomogeneous broadening; [4] the width of the ZPH coincident with the burn frequency which can be used to determine the lifetime of the excited state (zero-point level) due to rapid energy transfer or primary charge separation; [5] the excitonic interaction of strongly coupled Chl aggregates.

In this dissertation, NPHB and PHB techniques are used to study the following: [1] hole and antihole profiles. The theory for hole profiles developed by Hayes et al. (15) was extended to examine the PSBH shapes at arbitrary burn times and at different burn wavelengths. Comparison between the simulated and measured holes provide an approximate method for determination of the antihole profile; [2] the antihole of a porphyrin in an amorphous solid. Using the polarized hole spectra of porphyrin in polymer, it was possible to observe the antihole even though it was broadly distributed throughout the inhomogeneously broadened absorption profile. In addition, vibronic holes and the correlation between the S_1 and S_2 site energy distributions are discussed; [3] spectral diffusion and the power dependence of holes burned with constant fluence. Experimental data are explained in terms of hole burning kinetic models, dispersive kinetics, hole saturation broadening and power broadening; [4] the homogeneous and inhomogeneous contribution to the absorption band of bacteriorhopdopsin. The first report of optical hole burning of bacteriorhodopsin is presented and the results are discussed in terms of the degree of homogeneous broadening and broadening mechanisms.

EXPLANATION OF DISSERTATION FORMAT

This dissertation contains the author's original work on spectral hole burning of 5,10,15,20-tetraphenylporphyrin (TPP), oxazine 720 perchlorate and bacteriorhodopsin in amorphous hosts at low temperatures. The thesis is divided into three Sections. Section I contains an introduction, two published papers on TPP and conclusions. The first paper is concerned with an extension of the linear electron-phonon coupling theory that makes it possible to study the burn time and burn wavelength dependent hole shapes and to extract the antihole profile. The second deals with the observation of an antihole by polarization spectroscopy. Section II contains an introduction, experimental methods, models, results and discussion, and conclusions. It is concerned with the spectral diffusion and the burn power dependence of the depth of holes for oxazine 720 in polyvinyl alcohol burned with the same fluence. Section III contains an introduction, experimental methods, one published paper, and conclusions on the photochemical hole burning of bacteriorhodopsin from *Halobacterium Halobium* S9. It describes the degree of inhomogeneous broadening and mechanism of the large homogeneous broadening of bacteriorhodopsin. The references for the introduction, experimental methods and conclusions are listed at the end of each Section while those for each paper are given at the end of the paper.

REFERENCES

1. Mitchell, A.C.G.; Zemansky, M.W. Resonance Radiations and Excited Atoms, Cambridge University Press: Cambridge, 1934.
2. de Bree, Ph.; Wiersma, D.A. J. Chem. Phys. 1979, 70, 790.
3. Feld, M.S. In Frontiers in Laser Spectroscopy, Balian, R.; Haroche, S.; Liberman, S., Ed.; North Holland: Amsterdam, 1977, vol.1.
4. Louisell, W.H. Quantum Statistical Properties of Radiation, Wiley: New York, 1973, Chap.6.
5. Cohen-Tannoudji, C. In Frontiers in Laser Spectroscopy, Balian, R.; Haroche, S.; Liberman, S., Ed.; North Holland: Amsterdam, 1977, vol.1.
6. Sargent III,M.; Scully, M.O.; Lamb Jr., W.E. Laser Physics, Addison-Wesley; Reading, 1974.
7. Blum, K. In Physics of Atoms and Molecules, Burke, P.G.; Keimpoppen, H., Ed., Plenum Press: New York, 1981.
8. Hayes, J.M.; Jankowiak, R.; Small, G.J. In Persistent Spectral Hole Burning: Science and Applications; Moerner, W.E., Ed.: Springer-Verlag: Berlin, 1988.
9. Jankowiak. R.; Small, G.J. Science, 1987, 237, 618.
10 Berg, M.; Walsh, C.A.; Narasimhan, L.R.; Littau, K.A.; Fayer, M.D. J. Chem. Phys. 1988, 88, 1564.
11. Budimir, J.; Skinner, J.L. J. Status. Phys. 1987, 49, 1029.
12. Sevian, H.M.; Skinner, J.L. J. Chem. Phys. 1989, 91, 1775.

13. Pryce, M.H.L. in Phonons in Perfect Lattices and Lattices with Point Defects, Stevenson, R.W.H., Ed.; Oliver and Boyd: London, 1968, p 403.

14. Sapozhnikov, M.N. Phys. Status. Solidi (b) 1976, 75, 11.

15. Hayes, J.M., Gillie, J.K.; Tang, D.M. Biochim. Biophys. Acta 1988, 932, 4928.

16. Imbusch, G.F.; Kopelman, R.C., In Laser Spectroscopy of Solids, Springer-Verlag: Berlin, 1982.

17. Small, G.J. In Spectroscopy and Excitation Dynamics of Condensed Molecular Systems, Agranovich, V.M., Hochstrasser, R.M., Eds.; North-Holland Publishing Company: Amsterdam, 1983.

18. Haarer, D.; Philpott, M.R. In Spectroscopy and Excitation Dynamics of Condensed Molecular Systems, Agranovich, V.M., Hochstrasser, R.M., Eds.; North-Holland Publishing Company: Amsterdam, 1983.

19. Selzer, P.M.; Huber, D.L.; Hamilton, D.S.; Yen, W.M.; Weber, M.J. Phys. Rev. Lett. 1976, 36, 813.

20. Morgan, J.R.; El-Sayed, M.A. Chem. Phys. Lett. 1981, 84, 213.

21. Hayes, J.M.; Stout, R.P.; Small, G.J. J. Chem. Phys. 1980, 73, 4129.

22. Hayes, J.M.; Stout, R.P.; Small, G.J. J. Chem. Phys. 1980, 74, 4266.

23. Zeller, R.L.; Pohl, R.O. Phys. Rev. B 1971, 4, 2029.

24. Berman, R. Phys. Rev. 1949, 76, 315.

25. Anderson, P.W.; Halperin, B.I.; Varma, C.M. Phil. Mag. 1972, 25,1.

26. Phillips, W.A. J. Low Temp. Phys. 1972, 7, 351.

27. Redfield, D. Phys. Rev. Lett. 1971, 27, 730.

28. Fulde, P.; Wagner, H. Phys. Rev. Lett. 1971, 27, 1280.

29. Phillips, W.A.; Ed., Amorphous Solids-Low Temperature Properties, Springer-Verlag: Berlin, 1981.

30. Hunklinger, S. Festkörperprobleme 1977, XVII, 1.

31. Golding, B.; Graebner, J.E.; Halperin, B.I.; Schutz, R.J. Phys. Rev. Lett. 1973, 30, 223.

32. Hunklinger, S.; Arnold, W.; Stein, S.; Nava, R.; Dransfeld, K. Phys. Lett. A 1972, 42, 253.

33. Doussineau, P.; Frenois, C.; Leisure, R.G.; Levelut, A.; Prieur, J.-Y. J. Physique 1980, 41, 1193.

34. Golding, B.; Graebner, J.E.; Kane, A.B.; Black, J.L. Phys. Rev. Lett. 1978, 41, 1487.

35. Jackle, J Z. Phys. 1972, 257, 212.

36. Black, J.L.; Halperin, B.I. Phys. Rev. B 1977, 16, 2879.

37. Anthony, P.J.; Anderson, A.C. Phys. Rev. B 1979, 20, 763.

38. Jankowiak, R.; Small G.J.; Athreya, K.B. J. Phys. Chem. 1986, 90, 3896 and references in therein.

39. Jankowiak, R.; Small, G.J. Chem. Phys. Lett. 1986, 128, 377.

40. Jankowiak, R.; Small, G.J. J. Phys. Chem. 1986, 90, 5612.

41. Jankowiak, R.; Small, G.J. Phys. Rev. B 1988, 37, 8407.

42. Lyo, S.K. In Optical Spectroscopy of Glasses, Zschokke, I. Ed.; D. Reidel Publishing Company: Dordrecht, 1986.

43. Huber, D.L.; Broer, M.M.; Golding, B. Phys. Rev. B 1986, 33, 7297.

44. Jankowiak, R.; Small, G.J. J.Phys. Chem. 1986, 90, 5612.

45. Walsh, C.A.; Berg, M.; Narasimhan, R.; Fayer, M.D. Acc. Chem. Res. 1987, 20, 120.

46. Skinner, J.L.; Anderson, H.C.; Fayer, M.D. J. Chem. Phys. 1981, 75, 3195.

47. Hesselink, W.H.; Wiersma, D.A. In Modern Problems in Condensed Matter, Agranovich, V.M., Maradium, A.A., Eds.; North-Holland; Amsterdam, 1983, Vol. 4, p 249.

48. Personov, R.I.; Al'shits, E.I.; Bykovskaya, L.A. Opt. Common. 1972, 6, 169.

49. Szabo, A. Phys. Rev. Lett. 1970, 25, 924.

50. Jankowiak, R.; Small, G.J. Anal. Chem. 1989, 61, 1023A.

51. Bykovskaya, L.A.; Personov, R.I.; Romanovskii, Yu.V. Anal. Chem. Acta 1981, 125, 1.

52. Personov, R.I. In Spectroscopy and Excitation Dynamics of Condensed Molecular Systems, Agranovich, V.M., Hochstrasser, R.M., Eds,; North-Holland: Amsterdam, 1983, vol.4.

53. Moerner, W.E., Ed., Persistent Spectral Hole Burning: Science and Applications; Springer-Verlag: Berlin, 1988.

54. Szabo, A. Phys. Rev. B 1975, 11, 4512.

55. Völker, S.; Macfarlane, R.M. Chem. Phys. Lett. 1979, 61, 421.

56. Lee, I,-J.; Small, G.J.; Hayes, J.M. J. Phys. Chem. 1990, 94, 3376.

57. Romagnoli, M.; Moerner, W.E.; Schellenberg, F.M.; Levenson, M.D.; Bjorklund, G.C. J. Opt. Soc. Am. B 1984, 1, 341.

58. Thijssen, H.P.H.; Dicker, A.I.M.; Völker, S. Chem. Phys. Lett. 1982, 92, 7.

59. Macfarlane, R.M.; Shelby, R.M. Phys. Rev. Lett. 1979, 42, 788.

60. de Vries, H.; Wiersma, D.A. Phys. Rev. Lett. 1976, 36, 91.

61. de Vries, H.; Wiersma, D.A. Chem. Phys. Lett. 1977, 51, 565.

62. Gorokhovskii, A.A.; Kaarli, R.K.; Rebane, L.A. JETP Lett. 1974, 20, 216.

63. Völker, S. In Relaxation Processes in Molecular Excited States, Fünfschilling, J., Ed., Kluwer Academic Publisher: Dordrecht, 1989.

64. Kharlamov, B.M.; Personov, R.I.; Bykovskaya, L.A. Opt. Commun. 1974, 12, 191.

65. Carter, T.P.; Fearey, B.L.; Hayes, H.M.; Small,G.J. Chem. Phys. Lett. 1983, 102, 272.

66. Macfarlane, R.M.; Shelby, R.M. Opt. Commun. 1983, 45, 46.

67. Olson, R.W.; Lee, H.W.H.; Patterson, F.G.; Fayer, M.D.; Shelby, R.M.; Burum, D.P.; Macfarlane, R.M. J. Chem. Phys. 1982, 77, 2283.

68. Clemens, J.M.; Hochstrasser, R.M.; Trommsdorf, H.P. J. Chem. Phys. 1984, 80, 1744.

69. Spitzer, R.C.; Ambrose, W.P.; Sievers, A.J.; A.J. Opt. Lett. 1986, 11, 428.

70. Lee, H.W.H.; Walsh, C.A.; Fayer, M.D. J. Chem. Phys. 1985, 83, 3948.

71. Dick, B. Chem. Phys. 1983, 136, 413.

72. Kenney, M.J.; Jankowiak, R.; Small, G.J. Chem. Phys. in press.

73. Hayes, J.M.; Small, G.J. Chem. Phys. 1978, 27, 151.

74. Hayes, J.M.; Small, G.J. Chem. Phys. Lett. 1978, 54, 435.

75. Bogner, V.; Schwartz, Phys. Rev. B. 1981, 24, 2846.

76. Shu. L.; Small, G.J. Chem. Phys. 1990, 141, 447.

77. Child, A.F.; Francis, A.H. J. Phys. Chem. 1985, 89, 466.

78. Gillie, J.K.; Small, G.J.; Golbeck, J.H. J. Phys. Chem. 1989, 93, 1620.

79. Köhler, W.; Friedrich, J.; Fischer, R.; Scheer, H. J. Chem. Phys. 1988, 89, 871.

80. Wong, J.; Angell, C.A. Glass Structure by Spectroscopy, Marcel Dekker: New York, 1970.

81. McGrum, N.G., Read, B.E.; Williams, G. Anelastic and Dielectric Effects in Polymeric Solids, Wiley: London, 1978.

82. Jankowiak,R.; Shu, L.; Kenney, M.J.; Small, G.J. J. Lumnin. 1987, 36, 293.

83. Rebane, K.K.; Gorokhovskii, A.A. J. Lumin. 1987, 36, 237.

84. Littau, K.A.; Bai, Y.S.; Fayer, M.D. Chem. Phys. Lett. 1989, 159, 1.

85. Littau, K.A.; Fayer, M.D. submitted to Chem. Phys. Lett.

86. van den Berg, R.E.; Völker, S. J. Lumin 1987, 38, 25.

87. van der Zaag, P.J.; Galaup, J.P.; Völker, S. Chem. Phys. Lett. 1990, 166, 263.

88. Lee, I.-J.; Gillie, J.K.; Johnson, C.K. Chem. Phys. Lett. 1989, 156, 227.

89. Dick, B. Chem. Phys. 1989, 136, 429.

90. Friedrich, J.; Haarer, D. Angew. Chem. Int. Ed. Engl. 1984, 23, 113.

91. Friedrich, J.; Swalen, J.D.; Haarer, D. J. Chem. Phys. 1980, 73, 705.

92. van den Berg, R.; Voelker, S. Chem. Phys. Lett, 1986, 127, 525.

93. Kikas, J. In Zero-Phonon Lines and Spectral Hole Burning in Spectroscopy and Photochemistry, Sild, O., Haller, K., Eds.; Springer-Verlag: Berlin, 1986.

94. Sild, O.; Haller, K.; Eds, Zero-Phonon Lines and Spectral Hole Burning in Spectroscopy and Photochemostry; Springer-Verlag: Berlin, 1986.

95. Kikas, J.V.; Kaarli, R.K.; Rebane, A.K. Opt. Specktrosk. 1984, 56, 387.

96. Moerner, W.E. J. Mol. Electronics 1985, 1, 55.

97. Johnson, S.G.; Lee, I.-J.; Small, G.J. In Chlorophylls, Scheer, H., Ed; CRC Press: Boca Raton, in press.

SECTION I.

HOLES AND ANTIHOLES

INTRODUCTION

During the past decade, hole burning spectroscopy has been widely used in high resolution laser spectroscopy of impurity centers in crystalline (1,2) and amorphous solids (3-5). The high resolution results from the frequency selective photochemical or photophysical reaction of a isochromat of impurity centers induced by a narrow linewidth laser.

As discussed earlier in the general introduction (see Fig. 6), hole spectrum exhibits a complex shape consisting of ZPH, real- and pseudo- PSBH and satellite vibronic holes and the antihole. Therefore, several theoretical models (6-11) were developed to explain the hole shapes. Most of these models (7-11) share common features.

Friedrich et al. (7,9,11) compared the hole spectra of quinizarin in ethanol-methanol (3:1) burned near the center of the SDF with calculated burn time dependent hole profiles. For qualitative agreement with experimental data, they required a variation in the Debye-Waller factor by a factor of 5 to 10.

Model calculations by Sapozhnikov (10) showed a strong dependence of the hole profile on the burn frequency and burn time. Specifically, when the burn frequency was near the center of the SDF, the real- and pseudo-PSBHs were observed to grow in concert as the burn time increases.

Hayes et al. (6) derived an expression for the hole burned profile which is valid for arbitrary strong electron-phonon coupling. In their model, single site absorption profile consists of the ZPL and multi-phonon transitions (instead of only one-phonon transitions) were used. This model was tested for the short burn time limit and also showed a strong dependence of the hole shape on the burn

frequency. This model was used to explain the hole burned spectra of the primary electron donor state of isolated reaction centers of *Rhodopseudomonas viridis, Rhodobacter Sphaeroides* and Photosystem I. Each of these systems was characterized by strong linear-electron phonon coupling.

In Paper I of this section, the theory for the hole burned profile (6) is extended to examine the PSBH shapes at arbitrary burn time and at different burn wavelengths. The results are compared with the experimental hole spectra of 5,10,15,20-tetraphenyl porphyrin (TPP). This paper introduces an approximate method for extracting the antihole profile in amorphous solids by comparing the experimental and simulated hole profiles.

Porphyrins have been the subject of extensive research (1,12-17) because of their biological importance, e.g., photosynthesis (chlorophyll), oxygen transport (hemoglobin) and biological oxidation (cytochrome). The skeleton of porphyrins consists of four pyrrole rings connected by four methine bridges as shown in Fig. 1. The hydrogens at any outer position may be substituted, the central region may be occupied by two hydrogen atoms (free base porphyrins, D_{2h} symmetry) or by any of metals (metalloporphyrins, D_{4h} symmetry). In some porphyrins, the outer position of one (chlorins) or more pyrrole rings may be reduced by hydrogenation. This section is concerned with only free base porphyrins.

The sample used in this section was TPP. The steric repulsion between ortho-phenyl and β-pyrrole hydrogens results in the phenyl rings being almost perpendicular to the molecular plane (33,34). The vibrational frequencies of TPP in the first excited singlet state have been studied by various methods, e.g.,

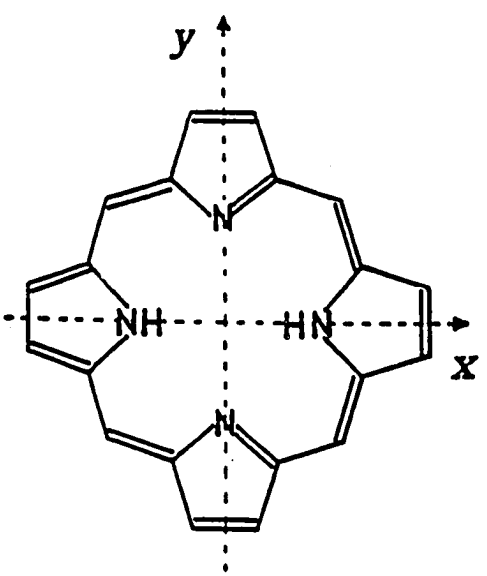

Figure 1. Basic porphyrin skeleton

supersonic jet spectroscopy (35), fluorescence excitation spectroscopy in polystyrene (36) and in nitrobenzene crystal (37) and by hole burning in polymethacrylate (4).

X-ray crystallographic studies on free base porphyrin (H_2P) and tetraphenyl porphyrin (TPP) were reported by Tulinsky and co-workers in Refs. 18 and 19. They determined that the central two hydrogen atoms in porphyrins are located on opposite pyrrole rings. From ^1H and ^{13}C NMR studies in liquid solution, it was reported that these central hydrogen atoms undergo tautomerization (20,21). The inner hydgrogen tautomerization can occur as a dark ground state process (20,21) or as a photoinduced process (1,4,22-24). The photoinduced tautomerization still occurs even at liquid helium temperatures while the dark process ceases at 77 K (1). The photoinduced tautomerization was discovered by Zallesskii et al. (24) from the time dependent fluorescence polarization studies of porphyrins. They found that at 77 K the fluorescence of porphyrins in glass showed considerable depolarization with time and concluded that the depolarization is due to reorientation of the absorption oscillator involving displacement of the imino hydrogens in the center of the porphyrin rings. Up to now, two tautomerization mechanisms have been proposed: two-step transfer in which the hydrogen atoms move asynchronously (25,26) and one-step transfer in which the hydrogen atoms move synchronously (27). The two-step mechanism is supported by a theoretical study (28) and NMR studies (20,29,30) which considered rate of transfer of the two inner hydrogens as a function of temperature and isotopic hydrogen mass.

The free porphyrin molecule will oscillate back and forth between two equivalent isomers. If molecule is embedded in a medium, site symmetry will normally be lower so that one of the isomer is expected to be at a lower energy than the other. The absorption spectrum of H_2P in n-alkane (31) as well as the ESR spectrum (32) show two absorption lines at each site for the $Q_{x,0\text{-}0}$ ($S_1 \leftarrow S_0$, 0-0) transition that corresponds to the two tautomers. Many hole burning experiment of porphyrins (1,31) in crystalline media showed that after a period of monochromatic irradiation in one of the two lines, the other component in the fluorescence had obtained intensity (antihole) from the original line. This is clear evidence that the mechanism of the hole burning of porphyrin is photochemical tautomerization.

However, up to now the antihole of porphyrins in amorphous solids has not been observed. The antihole in amorphous matrices can be detected in polarized absorption spectra because the absorption bands of the reactants and products are oppositely polarized. Paper II of this section of this dissertation is concerned with this subject. In addition, a correlation between the S_1 and S_2 site energy distributions is demonstrated.

PAPER I. HOLE AND ANTIHOLE PROFILES IN NONPHOTOCHEMICAL HOLE-BURNED SPECTRA

41

Hole and Antihole Profiles in Nonphotochemical Hole-Burned Spectra

In-Ja Lee, John M. Hayes and Gerald J. Small

Jounal of Chemical Physics 1989, 91, 3463

ABSTRACT

The shapes of the real-phonon and pseudo-phonon sideband holes (PSBH) which occur in hole-burned spectra in amorphous solids are both wavelength and burn time dependent. The theory previously proposed to simulate hole shapes in the short burn time limit is extended to examine the PSBH shapes at arbitrary times and at different burn wavelengths. The simulated spectra are compared with experimental data for tetraphenyl porphyrin in polystyrene. It is also shown the stimulated spectra may be used to deconvolve the antihole spectrum from the hole spectrum.

INTRODUCTION

During the past decade, research on spectral hole burning of impurity electronic transitions in amorphous solids has undergone substantive growth (1). To a large measure the increase in activity was stimulated by the fact that spectral hole burning provides a new window on the dynamics of configurational tunneling processes which occur in glasses and polymers at very low temperatures (2). In this regard the study of different properties of nonphotochemical hole burning (NPHB) can provide information on relaxation processes whose time scales vary over about 15 decades (picoseconds to hours).

Nonphotochemical hole burning is the manifestation of the production of a final impurity-glass ground state that is thermally inaccessible (3), at T_B (burn temperature), to the preburn state. This production accompanies completion of the cycle which takes the impurity from its ground electronic state to the excited state and back to the ground state. The difference between the excitation energies for the final and preburn ground state is less than or roughly equal to the inhomogeneous linewidth of the impurity transition Γ_I. For electronic transitions Γ_I is typically a few hundred cm^{-1}. The mechanism for NPHB put forth by Hayes and Small (4) is based on the existence of a distribution of impurity-glass asymmetric intermolecular double-well potentials (extrinsic two-level systems, TLS_{ext}) for both ground and excited states of the impurity. The TLS_{ext} appear to be distinct from the intrinsic TLS of the glass which are responsible for optical dephasing and spectral diffusion (2,5-7).

In this paper we are concerned with the nature of the antihole (increase in absorption) which accompanies NPHB. This problem has received limited attention for amorphous solids (8-11) despite its obvious importance for understanding the hole-burning mechanism. For pentacene in benzoic acid, a mixed-crystal system which exibits NPHB, the antiholes have been extensively studied (12,13). An approximate method for extracting the antihole profile in amorphous solids is described in the present paper which depends, in part, on theoretical analysis of the linear electron-phonon coupling.

PHONON SIDEBAND HOLE (PSBH) ANAYSIS

Figure 1 reveals the features of NPHB spectra which are of interest. The spectrum is for the native antenna complex of photosystem I (PSI-200) at 1.6 K. The preburn absorption spectrum is also shown. The hole-burned spectrum was obtained with λ_B = 670.0 nm located at the center of the inhomogeneously broadened origin band for chlorlphyll *a*. For the high fluence used the ZPH (zero-phonon hole) coincident with λ_B is saturated (has attained maximum depth). The difference spectrum, inset of Fig. 1, reveals more clearly the broad asymmetric hole displaced by 22 cm^{-1} to lower energy of ZPH (λ_B). As proven in Ref. 14, this hole is the pseudo-PSBH due to chlorophyll *a* sites that absorb λ_B via phonon-sideband transitions which build on their zero-phonon transitions. The combined intensity of ZPH plus pseudo-PSBH can be seen to be reasonably well compensated for by the antihole just to the left of the ZPH. Therefore, the mechanism for hole buring is nonphotochemical.

There are, however, two types of PSBH, the pseudo-PSBH and real-PSBH (15-17). The latter *builds* on the ZPH and is located to higher energy of the ZPH. In the Condon approximation the relative intensities of the ZPH and real-PSBH are solely governed by Franck-Condon factors and are burn time independent. The situation is more complex for the pseudo-PSBH. In Fig. 1 the real-PSBH is largely masked by the antihole. On the other hand, to obtain the true antihole shape the real-PSBH must be deconvolved from the apparent antihole.

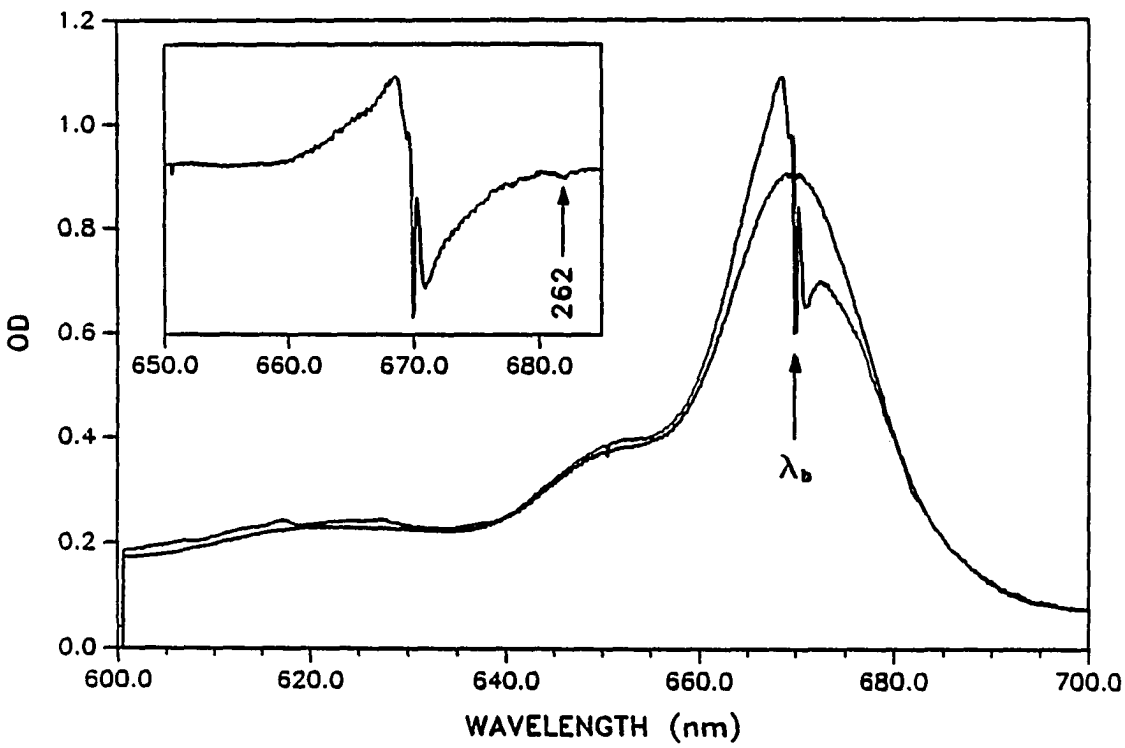

Figure 1. The absorption spectrum of PSI-200 at 1.6 K, before and after hole burning at λ_B=670.0 nm, for 20 min with 4 W/cm^2. The antihole is evident to the left of λ_B. The difference between the two spectra is shown in the inset

Recently, Hayes et al. (18) relaxed the assumption of weak linear electron-phonon coupling and derived an analytic expression for the hole-burned profile (short burn time limit) which is valid for arbitrarily strong coupling. The theory was used to interpret the hole-burned spectra of the primary electron donor state of photosynthetic reaction centers (18,19). The theory predicts a significant λ_B dependence of the ZPH plus PSBH profile. It is clear also that (15) for each λ_B the profile should be burn time dependent. However, the theory of Hayes et al. has not been adequately tested with data from simpler hole-burning systems. One objective of this paper is to do so.

Hayes et al. (18) utilized the mean phonon frequency (ω_m) approximation (11) to write

$$L(\Omega-\nu)=\sum_{r=0}^{\infty}\frac{S^r e^{-S}}{r!}l_r(\Omega-\nu-r\omega_m) \qquad (1)$$

for the single-site absorption profile in the low-temperature limit ($kT < \hbar\omega_m$). Here ν is the zero-phonon transition frequency and r=0, 1, 2,... labels the zero-, one-, two-, etc., phonon processes. The parameter S is the Huang-Rhys factor and the coefficient of l_r is the phonon Franck-Condon factor. The shape of the r-phonon profile is l_r. For the zero-phonon transition, l_0 can be a Lorentzian with FWHM γ (homogeneous linewidth). The one-phonon profile is centered at $\nu + \omega_m$ and is given a width Γ. Impurity electronic transitions in amorphous solids typically exhibit a Γ of ~ 50 cm^{-1}. When a Gaussian with FWHM equal to Γ is utilized for

l_1, the width of the r-phonon profile is $r^{1/2}\Gamma$ for the case where the one-phonon profile is due to coupling to host phonons. Utilization of a Lorentzian yields a width of $r\Gamma$ and an r-phonon profile which is also Lorentzian. However, a width of $r\Gamma$ ($r \geq 2$) is most likely an overestimate of the true width. For this reason Hayes et al. (18) employed Lorentzians for l_r ($r \geq 1$) with a width of $r^{1/2}\Gamma$. An advantage over utilization of Gaussian is that an analytical expression for the hole profile can be obtained in the short burn time limit (18). Our calculations have shown that for S < 1 there is no significant difference between the hole profiles calculated with the two types of function. For larger S values more accurate profiles are obtained using Gaussian or asymmetric phonon profiles. For the calculations presented, Lorenztian profiles were used for the multiphonon profiles. The preburn absorption spectrum is given by the convolution of Eq. (1) with the zero-phonon site excitation distribution function (SDF):

$$A_0(\Omega) = \sum_{r=0}^{\infty} \frac{S^r e^{-S}}{r!} \int d\nu \frac{N_0(\nu - \nu_m)}{N} l_r(\Omega - \nu - r\omega_m) \qquad (2)$$

where $N_0(\nu-\nu_m) / N$ is the probability of a site with zero-phonon transition frequency equal to ν. A Gaussian is the physically reasonable choice for N_0 (centered at ν_m), but a Lorentzian was found to yield hole profiles which do not differ significantly from those obtained with a Gaussian for the relatively small values of S employed ($S \leq 1$).

Following a burn at ω_B with intensity I for a burn time τ, the number of sites with zero-phonon frequency equal to ν is defined by

$$N_\tau(\nu-\nu_m) = N_0(\nu-\nu_m)\exp[-\sigma I\phi\tau L(\omega_B-\nu)],$$

where σ is the absorption cross section and ϕ is the hole-burning quantum yield. The hole-burned absorption spectrum is, therefore,

$$A_\tau(\Omega) = \sum_{r=0}^{\infty} \frac{S^r e^{-S}}{r!} \int d\nu \frac{N_0(\nu-\nu_m)}{N} e^{-\sigma I\phi\tau L(\omega_B-\nu)} l_r(\Omega-\nu-r\omega_m) \qquad (3)$$

Equation (3) does not allow for dispersive kinetics due to a distribution of quantum yields, which is known to be very important for NPHB, specifically for the growth of the ZPH (5). In the absence of interference from the antihole the determination of S from the ZPH and real-PSBH can always be made on the basis of their relative intensities even when dispersion is important. This is not necessarily true when the pseudo-PSBH is employed as will be discussed later.

The calculated hole-burned spectra reported below were obtained by numerical integration (Bode's approximation) of Eqs. (2) and (3); the hole profile is $A_\tau(\Omega) - A_0(\tau)$. For the Huang-Rhys factor employed, sufficient accuracy was obtained by truncating the series at r = 6. The product $\sigma I\phi$ is taken as a constant and only the burn time is considered as a variable. In utilizing Eq. (3) it is

assumed that the linewidth of the burn laser is narrow relative to the homogeneous linewidth γ.

Figure 2 shows a series of ΔOD (change in optical density) hole-burned spectra calculated as a function of burn time for the case where the burn frequency ω_B is equal to ν_m, the center of the SDF. The values of the parameters used are given in the caption. It was found that the hole spectra calculated using a Lorentzian and Gaussian for the SDF were essentially identical. The spectra in Fig. 2 were calculated using a Gaussian SDF with a width of 200 cm^{-1}. Because the experimental systems we consider are characterized by weak coupling with S close to 1, an S=1.0 was used to obtain Fig. 2. Furthermore, a rather small value of Γ = 20 cm^{-1} was employed for the width of the one-phonon profile so that the PSBH would be clearly resolved. The ΔOD scales for all spectra in Fig. 2 are the same and ΔOD value for the ZPH of spctrum (c) corresponds to a 20% OD change. For the shorter burn times [spectra (a) and (b)], corresponding to a percentage of OD changes for the ZPH of $\leq$ 10%, the intensities of the pseudo- and real-PSBH are comparable as expected in the short burn time limit (18). For longer burn times the intensity of the pseudo-PSBH relative to the ZPH increases while, at the same time, the width of the ZPH increases beyond the value of 2γ expected from homogeneous broadening. The latter effect is due to the contribution to the ZPH from off-resonant sites which absorb ω_B via the wings of their zero-phonon absorption profiles. Our calculations indicate that to avoid this type of broadening short burn time spectra, whose ZPH depths are less than 30% of the saturated ZPH

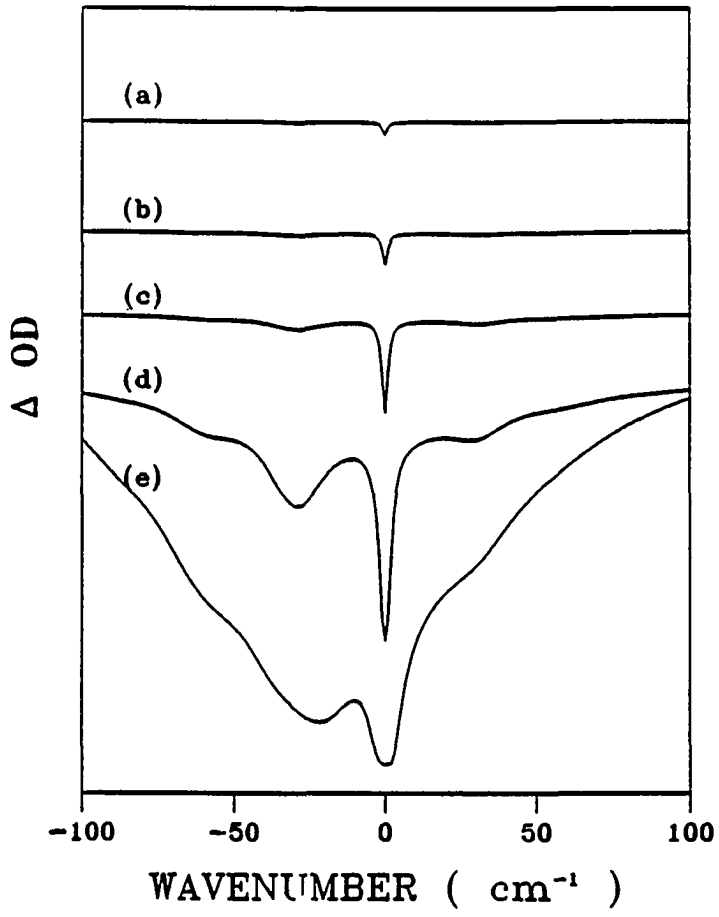

Figure 2. Hole-burned spectra for $\omega_B=\nu_m$ as a function of burn time, calculated as the difference between Eqs. (2) and (3) with burn times of (a) 10 μsec, (b) 25 μsec, (c) 100 μsec, (d) 1 msec, and (e) 10 msec. The parameter used are S=1.0, $\omega_B = \nu_m = 0.0$ cm^{-1}, $\omega_m = 30$ cm^{-1}, $\gamma = 1.0$ cm^{-1}, $\Gamma = 20$ cm^{-1}, $\Gamma_{inh} = 200$ cm^{-1}, and $\sigma I\phi=4.4\times10^4$ cm^{-1} s^{-1}

depth, should be used. The ZPH of spectrum (d) in Fig. 2 is saturated. For NPHB, where the burning kinetics are dispersive, it is apparent from earlier work (5) that this percentage could be significantly smaller. For S values significantly larger than 1 (strong coupling), the burn time development of the hole spectra would be qualitatively different than shown in Fig. 2 in that pseudo-PSBH would saturate before the ZPH (15). However, in general, the time development of the hole profile should also depend on the location of ω_B within the absorption profile.

From the analytic expression for the hole profile in the short burn time limit, Hayes et al. (18) demonstrated that the hole profile does depend on the location of ω_B. The dependence becomes stronger as S increases. This can be qualitatively understood by noting that as ω_B is tuned sufficiently into the low- and high-energy sides of the absorption profile, the ratio of zero-phonon to multiphonon ($r \geq 1$) excitation will increase and decrease, respectively, for a fixed S. The effects of this on the hole-burned spectra could be incorrectly interpreted in terms of a site excitation energy dependence of S.

Figures 3 and 4 show the results of the calculations obtained with the same values for S, Γ, ω_m, and Γ_I as used for Fig. 2 except that $\omega_B = \nu_m - 100$, respectively. Comparison of Figs. 3 and 4 clearly illustrates that there is a pronounced dependence of the hole profile on ω_B which becomes more apparent as the burn time inceases. Whereas the centroid of the hole profile in Fig. 4 is always located near ω_B, the centroids for the two longest burn times in Fig. 3 are shifted about 50 cm^{-1} to the red of ω_B. Spectra (c) of Figs. 3 and 4 can be directly

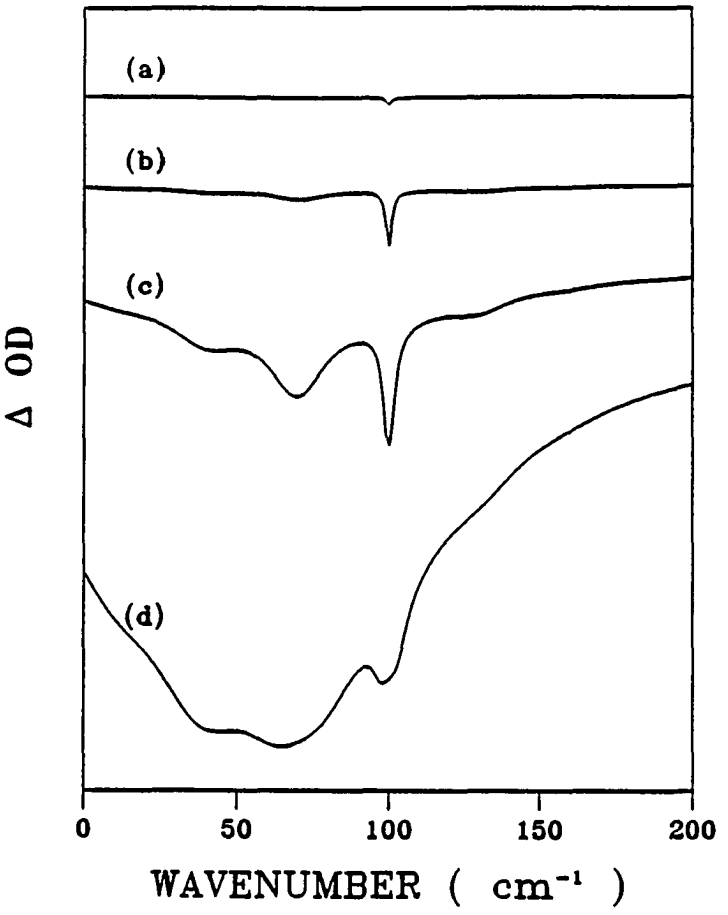

Figure 3. Hole-burned spectra for $\omega_B=\nu_m+100$ cm^{-1} as a function of burn time, calculated as for Fig. 2. The burn times are (a) 10 μsec, (b) 100 μsec, (c) 1 msec, and (d) 10 msec. The other parameters are as in Fig. 2

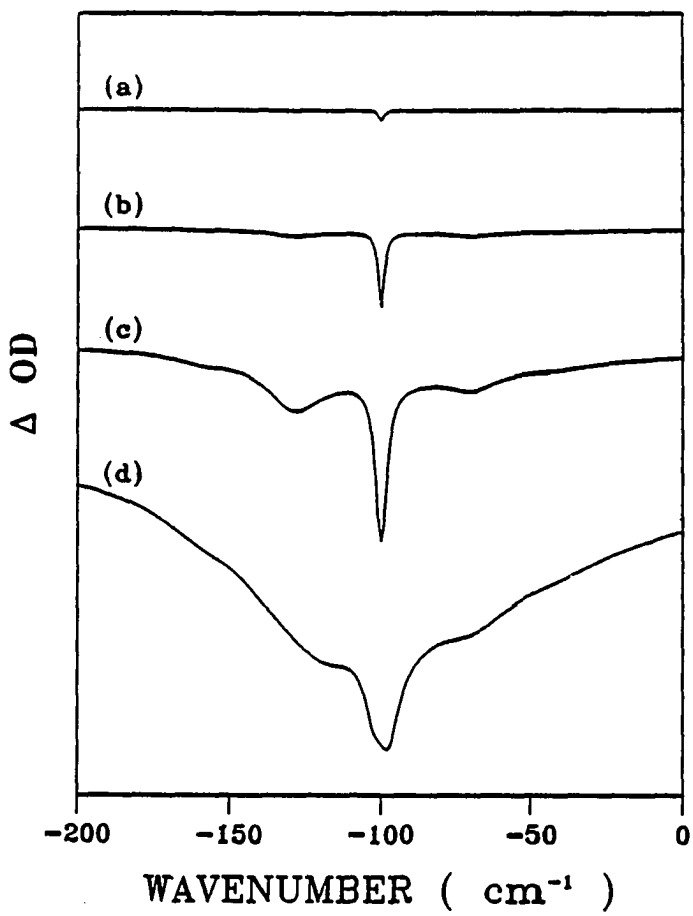

Figure 4. Hole burned spectra for $\omega_B=\nu_m$-100 cm^{-1} as a function of burn time, calculated as for Fig. 2. The burn times are (a) 10 μsec, (b) 100 μsec, (c) 1 msec, and (d) 10 msec. The other parameters are as in Fig. 2

compared with spectrum (d) of Fig. 2. Of particular interest is the behavior shown in Fig. 4 which is that the real- and pseudo-PSBH have comparable intensities for a wide range of burning times.

To test the predictions of the calculations we have begun experiments on a number of hole-burning systems. The preliminary survey studies yielded encouraging results and indicate that the predictions are qualitatively correct. Here we present some illustrative spectra for 5-, 10-, 15-, 20-tetraphenyl-porphin (TPP) in polystyrene films. For this system, the hole-burning mechanism is photochemical (proton tautomerism) and the antihole is distributed over the original inhomogeneous absorptions (21). Because of its broad distribution to wavelengths on both sides of λ_B, interference of the antihole with the real- and peudo-PSBH is minimized. The origin absorption maximum of TPP in polystyrene at 4.6 K is located at 645 nm (FWHM = 350 cm^{-1}). Holes were burned with a cw dye laser possessing a linewidth of $\leq$ 1 MHz and read with a Bruker IFS-120 FT spectrometer operated at a resolution of 2 cm^{-1}. Hole-burned spectra for λ_B = 652, 645 and 638 nm [(A)-(C)] are shown in Fig. 5. The burn fluences for (A) and (C) are identical (see Fig. 5). The fluence used to obtain spectrum (B) was a factor of 2 lower. All spectra correspond to "hard" burns designed to mimic the behaviors of the lowest calculated spectra in Figs. 2-4. Comparison of spectra (e) and (d) of Figs. 2 and 3 with spectra (B) and (C) of Fig. 5 (respectively) and spectrum (d) of Fig. 4 with spectrum (A) of Fig. 5 indicates that TPP in polystyrene behaves in accord with the basic predictions of the theory. The approximate symmetric

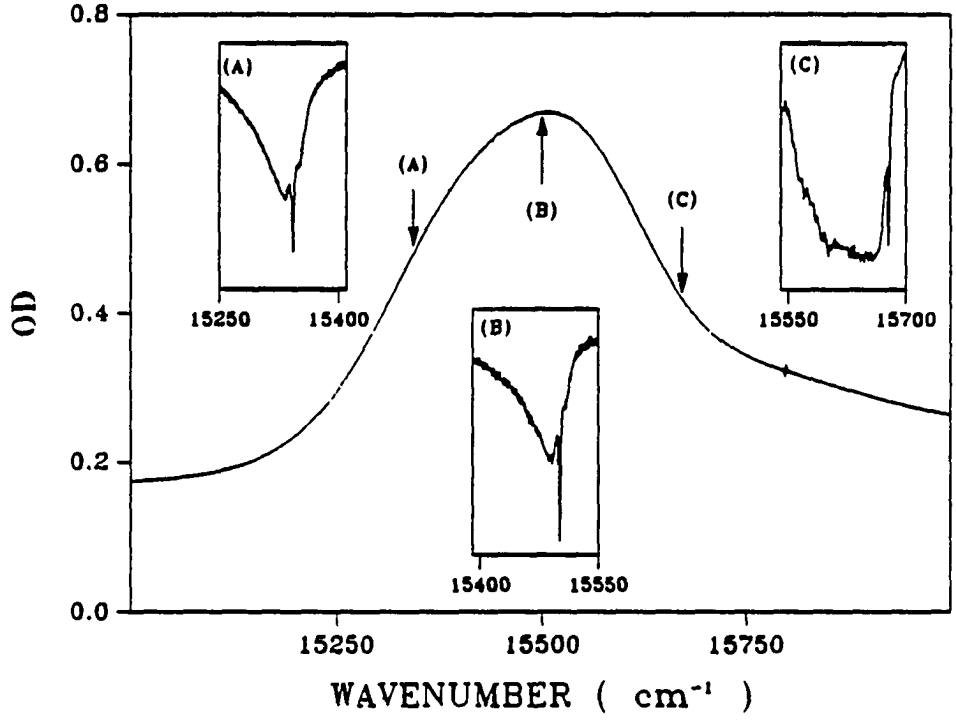

Figure 5. The abroption spectrum for the Q_x transition of 5,10,15,20-tetraphenylporphyrin in polystyrene film. The insets shows hole spectra burned at the labeled positions. Burn conditions are (A) λ_B=652 nm, 10 min at 10 mW/cm^2; (B) λ_B=645 nm, 10 min at 5 mW/cm^2; and (C) λ_B=638 nm, 10 min at 10 mW/cm^2

disposition of the real- and pseudo-PSBH about the ZPH in spectrum (A) of Fig. 5 is particularly interesting. Shorter burn time spectra of TPP in polystyrene indicate that the coupling is weak (S ~ 1). Experiments are planned which will provide us with the burn time dependent spectra for several ω_B values necessary to test the quantitative accuracy of the theory. It shoud be emphasized that the ω_B dependence of the hole spectra is a sensitive function of S, ω_B, and Γ_I. The value of Γ, the width of the one-phonon profile, primarily determines the degree of resolution of the multiphonon sideband holes.

DETERMINATION OF THE ANTIHOLE IN NPHB SPECTRA

Based on published NPHB spectra of impurity electronic transitions in amorphous hosts (9, 10), e.g., oxazine 720 in polyacrylic acid films (11), it appears that the antihole corresponding to the ZPH plus pseudo-PSBH is often predominantly located to higher E of the ZPH. The spectra of chlorophyll *a* of PSI-200 are no exception (Fig. 1). In this section we are interested in determining a reasonable approximation to the true antihole profile for chlorophyll *a* of PSI-200. The approach used is as follows: because the antihole contribution in the region of the pseudo-PSBH is relatively small, the values of ω_m and Γ as well as a good estimate for S can be determined from burn time dependent spectra of the ZPH plus pseudo-PSBH. These values together with a value of Γ_I are then used with the above theory to fit the experimental ZPH plus pseudo-PSBH spectrum of interest. In so doing the value of $\sigma I \phi \tau$ in Eq. (3) is the only adjustable parameter. The fitting procedure provides a calculated hole-burned spectrum for the ZPH, pseudo- and real-PSBH, which is then subtracted from the observed spectrum to yield the antihole profile.

From burn time dependent spectra (λ_B = 669.5 nm) for chlorophyll *a* of PSI-200, Gillie, Small, and Golbeck (14) determined approximate values of 0.8, 20, and 40 cm^{-1} for S, ω_m, and Γ, respectively, and a value of 200 cm^{-1} for Γ_I. The value of S was obtained from the integrated intensities of the ZPH and pseudo-PSBH in the short burn time limit. A comparable value for S was obtained from the deconvolution of the pseudo-PSBH for a longer burn time into one- and two-phonon

contributions. The experimental profile selected by us for fitting is shown in Fig. 6. The parameter values used for the calculation are given in the caption. We note that the value of ν_m used is based on the estimate that the center of the SDF is located to the red of the absorption maximum by ~$S\omega_m$ (18). A Gaussian was utilized for the SDF. The calculated hole-burned spectrum in Fig. 6 exhibits reasonable agreement with the experimental ZPH plus pseudo-PSBH spectrum, except in the region between the maximum of the pseudo-PSBH and the ZPH. We have determined that improved agreement in this region can be obtained by using an asymmetric (rather than symmetric) one-phonon absorption profile. However, the discrepancy is mostly likely due to the fact that the spectral shape just to the red of the ZPH in the experimental spectrum is determined by the interplay of the negative-going pseudo-PSBH and positive-going antihole. The calculated antihole spectrum in Fig. 6 shows that the antihole increases sharply at about 15 cm^{-1} to the red of the ZPH. Thus, it is not clear that the calculated hole-burned spectrum in Fig. 6 is inaccurate in the aforementioned region. In any event, the antihole obtained using an asymmetric one-phonon profile is very similar to the one shown in Fig. 6, except that it exhibits a slightly smaller intensity near the ZPH frequency (ω_B). Both calculated antihole exhibit a contribution to lower energy (~40 cm^{-1}) of the ZPH. Its weakness, however, together with the uncertainties of the calculations, prevent us from concluding that the calculated low-energy part of the antihole is real. Nevertheless, one can confidently conclude that the NPHB predominantly creates sites whose zero-phonon transitions are shifted to higher

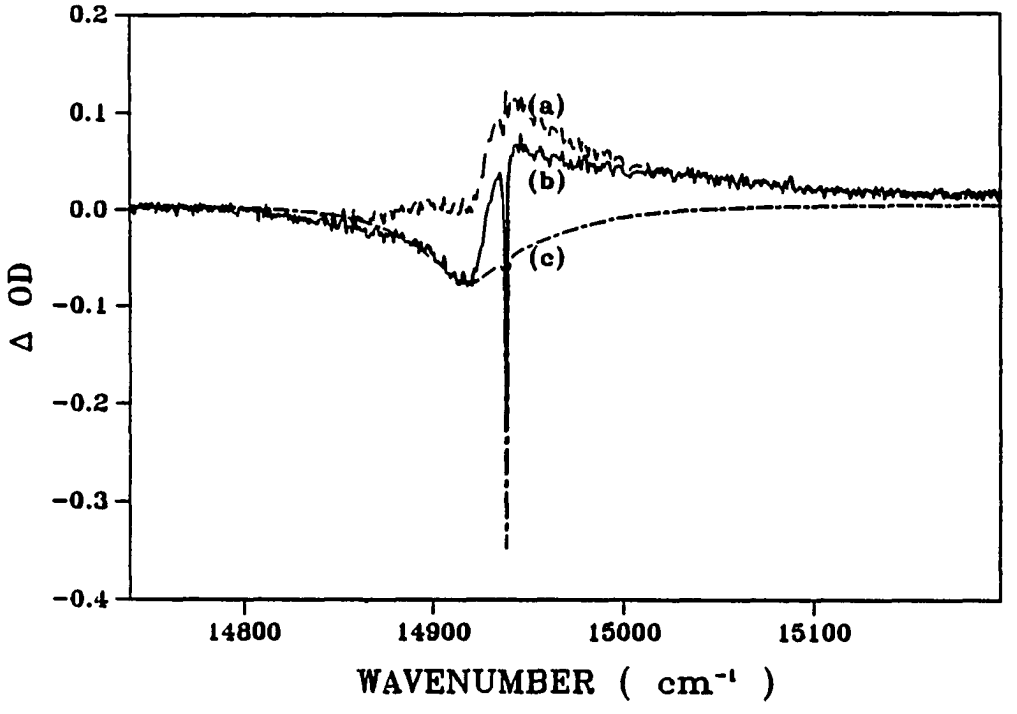

Figure 6. A comparison between (b) experimental (solid curve) and (c) calculated (dashed-dotted curve) hole spectra for PSI-200. (a) The difference (dashed curve) between the two curves approximates the antihole shape. The hole was burned at λ_B=699.5 nm for 20 min with 10 mW/cm^2. For the calculated hole S=0.8, ω_m=20 cm^{-1}, ν_m=14928.3 cm^{-1}, γ=0.04 cm^{-1}, Γ=37.5 cm^{-1}, Γ_{inh}=200 cm^{-1}, and $\sigma I \phi \tau$=26.4 cm^{-1}

energy relative to their preburn values.

Since the antihole is peaked at + 4 cm^{-1} relative to the ZPH, this shift is (on average) ~24 cm^{-1} since the antihole is primarily due to the sites associated with the pseudo-PSBH (in Fig. 6 the integrated intensity of the ZPH is weak relative to that of the pseudo-PSBH and no sharp antihole associated with the ZPH is evident). Focusing on the intense high-energy part of the antihole (which onsets at ~ 15 cm^{-1} to the left of the ZPH), it can be seen that it bears an approximate mirror symmetry relationship to the pseudo-PSBH. The tailing of the former, however, is more pronounced. The additional tailing may have its origin, in part, in the one- and higher-phonon transitions which build on the zero-phonon transitions of the sites created by NPHB. The center of the SDF for the created sites should lie close to ω_B + 4 cm^{-1} with a width of a approximately 40 cm^{-1}. For an S value of 0.8 one does expect a significant contribution from the one- through three-phonon transitions based on the Poisson distribution $\exp(-S)\, S^r / r!$. However, the absence of complete correlation between the zero-phonon excitation frequencies of the burnt and created sites (as indicated by the absence of a sharp antihole corresponding to the ZPH) may also be a contributing factor.

CONCLUDING REMARKS

The calculations of the PSBH structure presented in Section II of this paper are the most complete of any reported to date for amorphous solids. A principal finding is that there is a significant dependence of the ZPH plus PSBH structure on the location of ω_B within the inhomogeneously broadened absorption profile even for weak electron phonon coupling ($S < 1$). In retrospect, this is not surprising since even for an S value of only 0.4 the Franck-Condon factor for one-phonon transitions is about 30% of the value for the zero phonon transition. The point is that organic systems which exhibits an S value of less than 0.4 are rare so that the observations reported here for the tetraphenyl-porphin in the polystyrene system should be observable in many systems. It is clear that detailed studies of the burn time and ω_B dependences (as well as the T dependence) of the profiles for photochemical hole-burning systems can provide a complete understanding of the linear electron-phonon coupling as well as the determination of Γ_I and the center frequency of the zero-phonon site distribution function. The problem for NPHB system is more complicated due to the existence of the antihole and the dispersive kinetics of the hole burning. Provided the antihole is located primarily to higher energy of the ZPH, the problem is soluble because the linear electron-phonon coupling can be characterized and determined based on the ZPH and pseudo-PSBH. This assumes, however, that the effects of dispersive kinetics can be properly accounted for. This can be done by studying the burn time dependences of the ZPH and pseudo-PSBH, and subsequent analysis of these dependences with

the theory presented here but suitably modified for dispersive kinetics. For the case of chlorophyll *a* of PSI-200, two different approaches were used to determine a value of $S = 0.7 \pm 0.1$ from ZPH plus pseudo-PSBH profiles. Thus, we are confident that the value of 0.8 used is reasonable. For values of S close to unity the dispersive kinetics should affect the growth of the ZPH and one-phonon pseudo-PSBH to about the same extent. Thus, we feel that our neglect of dispersive kinetics for analyses of the data is justified.

The nature of the antihole determined for chlorophyll *a* of PSI-200 deserves further discussion within the context of the mechanism for NPHB since it appears to be similar to those observed in other systems (9-11, 21) Very recently, an antihole for cresyl violet in polyvinyl alcohol films was observed and is qualitatively similar to that for chlorophyll *a* (22). The fact that the sites created by NPHB possess excitation frequencies that are up-shifted relative to those of the preburn sites to carry the following implication for the NPHB mechanism of Hayes and Small (4): The two tunnel states of the TLS^{β}_{ext} for the electronically excited state β of the impurity are, on average, degenerate to within kT (~1 K) so that the aforementioned up-shifting is primarily a consequence of the fact that for the ground electronic state (α) the final populated TLS^{α}_{ext} configuration lies lower in energy than the preburn configuration. The suggestion of degeneracy to within kT is based on the notion that there should be no correlation between the relative energetic disposition of the two wells of TLS^{β}_{ext} and those of TLS^{α}_{ext}. For the preburn state of the glass there would be a preponderance of frozen-in impurity-

glass configurations that are only able to relax to lower-energy configurations by the optical excitation cycle. We note that the mixed-crystal system of thioindigo in benzoic acid is a thoroughly understood model system whose behavior is consistent with the above excited-state degeneracy argument (23).

Finally, we consider the assumptions of the model presented for the analysis of the PSBH and antihole associated with NPHB in amorphous solids. The first is the utilization of the single mean phonon frequency (ω_m) approximation for coupling of the electronic transition to the continuum of bath phonons. The single-site phonon sideband profile in absorption is governed by the product $g(\omega)S(\omega)$, where $g(\omega)$ is the phonon density of states and $S(\omega)$ is the frequency-dependent Huang-Rhys factor (20). Thus it is this product which must be reasonably sharply peaked at a single ω_m before the mean phonon frequency approximation can be made. If the short burn spectra exhibit a pseudo-PSBH that is dominated by a single maximum (at ω_m) and the assymmetry of the PSBH is consistent with the value of S (estimated from the intensity of the ZPH relative to the pseudo-PSBH), the mean phonon frequency approximation should be reasonably accurate. This was determined to be the case for TPP in polystyrene (short burn time spectra not shown) and PSI-200 (14). The type of low-energy tailing for the pseudo-PSBH shown in spectrum (b) of Fig. 6 (see also Ref. 14) is approximately that expected in the mean phonon frequency approximation for S ~ 1, as shown by the calculations reported in Ref. 18. The second approximation involves the utilization of a symmetric function for the one-phonon absorption profile. This approximation is

valid for a resonant or pseudolocalized phonon (frequency ω_m) which is rapidly damped by harmonic relaxation into delocalized bath phonons. However, it may not be valid if the one-phonon profile is due to coupling to the bath phonons themselves, since there is no physical reason to expect that $g(\omega)S(\omega)$ should be symmetric. Unfortunately, experimental spectra are often limited in the sense that they cannot be used, with any certainty, to address the symmetry question (this is the case for the systems studied in the present work). Unless the experimental spectra clearly indicate otherwise, there would seem to be little point in relaxing the above approximaitons in the model. This model assumes the low-temperature limit, $kT<<\hbar\omega_m$, which is clearly satisfied in the present work. Perhaps the most serious (and intersting) approximation for NPHB in amorphous solids is our neglect of filling of the ZPH by the antihole during the course of buring. From curve (a) of Fig. 6 for PSI-200 it is apparent that the antihole, produced by burning of sites whose zero-phonon absorption frequency lies lower than ω_B, has considerable amplitude at ω_m. Although the lower-energy sites up-shifted to ω_B can undergo subsequent burning, the intensity of the ZPH could be significantly affected by the filling process. It would be important in future studies to attempt to determine the extent of this effect. To do so would require characterization of the dispersive kinetics associated with NPHB. Such kinetics are ignored in the model.

ACKNOWLEDGMENT

The research was supported by the Division of Materials of the National Science Foundation under Grant No. DMR-8612270.

REFERENCES

1. Persistent Spectral Hole-Burning: Science and Applications, edited by Moerner, W. E., Vol.44 in Topics in Current Physics (Springer, Berlin, 1988), and references in therein.
2. Jankowiak, R.; Small, G. J. Science 1987, 237, 618.
3. Hayes, J. M.; Jankowiak, R.; Small, G. J. In Persistent Spectral Hole-Burning: Science and Applications, edited by Moerner, W. E., Vol.44 in Topics in Current Physics (Springer, Berlin, 1988), Chap. 5.
4. Hayes, J. M.; Small, G. J. Chem. Phys. 1978, 27, 115.
5. Jankowiak, R.; Shu, L.; Kenney, M. J.; Small, G. J. J. Lumin. 1987, 36, 293.
6. Berg, M.; Walsh, C. A.; Narasimhan, L. R.; Littau, K. A.; Fayer, M. D. J. Chem. Phys. 1988, 88, 1564.
7. Elschner, A.; Richert, R.; Bässler, H. Chem. Phys. Lett. 1986, 127, 105
8. Although not extensively discussed, antiholes are evident in several published spectra: see, e.g., Hirschmann, R.; Köhler, W.; Friedrich, J.; Daltrozzo, E. Chem. Phys. Rev. 1986, B34, 1.
9. Bogner, U.; Schwarz, R. Phys. Rev. B 1981, 24, 2846.
10. Childs, A. F.; Francis, A. H. J. Phys. Chem. 1985, 89, 466.
11. Fearey, B. L.; Small,G. J. Chem. Phys. 1982, 101, 269.
12. Olson, R. W.; Lee, H. W. H.; Patterson, F. G.; Fayer, M. D.; Shelby, R. M.; Burum, D. P.; Macfarlane, R. M. J. Chem. Phys. 1982, 77, 2283.

13. Walsh, C. W.; Fayer, M. D. J. Lumin. 1985, 34, 37.

14. Gillie, J. K.; Small, G. J.; Golbeck, J. H. J. Phys. Chem. 1989, 93, 1620.

15. Friedrich, J.; Swalen, J. D.; Haarer, D. J. Chem. Phys. 1980., 73, 705.

16. Friedrich, J.; Haarer, D. J. Chem. Phys. 1982, 76, 61.

17. Sapozhnikov, M. N. Chem. Phys. Lett. 1987, 135, 398.

18. Hayes, J. M.; Gillie, J. K.; Tang, D.; Small, G. J. Biophys. Biochem. Acta 1988, 932, 4928.

19. Gillie, J. K.; Fearey, B. L.; Hayes, J. M.; Small, G. J.; Golbeck,J. H. Chem. Phys. Lett. 1987, 134, 316.

20. Pryce, M. H. L. in Phonons in Perfect Lattices and Lattices with Point Defects, edited by Stevenson, R. W. H. (Oliver and Boyd, London, 1968), p.403.

21. Lee, I.-J.; Small, G. J.; Hayes, J. M. J. Phys. Chem. 1990, 94, 3376.

22. Shu, L.; Small, G. J. Chem. Phys. 1990, 141, 447.

23. Hochstrasser, R. M.; Trommsdorf, H. P. Chem. Phys. 1987, 115, 1.

PAPER II. PHOTOCHEMICAL HOLE BURNING OF PORPHYRIN IN AMORPHOUS MATRICES

70

Photochemical Hole Burning of Porphyrin in Amorphous Matrices

In-Ja Lee, Gerald J. Small, and John M. Hayes

Jounal of Physical Chemistry 1990, 94, 3376

ABSTRACT

Polarized hole and anti-hole spectra for tetraphenylporphyrin in a polystyrene matrix are presented. It is shown that, consistent with the photochemical nature of the hole, the antihole is polarized oppositely to the hole and is distributed throughout the inhomogeneous distribution of absorbers. However, there is also a pronounced asymmetry of the antihole which is interpreted as being due to the amorphous nature of the lattice. A correlation between the site energy distribution functions for the Q_x and Q_y states is also demonstrated.

INTRODUCTION

It is well known from NMR studies of porphyrin solutions that these molecules undergo facile tautomerization involving a double proton transfer (1,2). Although the dark ground state processes monitored by NMR cease at cryogenic temperatures, the tautomerization can still occur photochemically, even at temperatures <2K (3,4). That this tautomerization is the mechanism for photochemical hole burning of porphyrins and related molecules has been assumed in numerous instances (5-8) although an absorption increase due to the photogenerated tautomer has only been observed for crystalline matrices (3).

The difficulty in detecting photoproduct absorption, or an antihole, can be understood by considering that for porphins possessing D_{2h} symmetry, the tautomerization is equivalent to a 90° rotation of the molecule about a normal to the molecular plane. In the absence of environmental perturbations, the two tautomers would be energetically equivalent. In n-alkane crystals, the S_1 absorption transitions are shifted by $\lesssim 100$ cm^{-1}. This shift is less than typical inhomogeneous widths for porphyrins in amorphous matrices. In such amorphous hosts absorption widths of ~350 cm^{-1} are typical; 350 cm^{-1} is thus the range of energies over which the transition is distributed. Photoproduct absorption will occur within the same spectral region as the hole, making its detection difficult.

However, because the absorption bands of reactants and products are oppositely polarized, the anti-hole can be detected in polarized absorption spectra. Polarization properties of spectral holes have previously been discussed for

numerous systems. Among the first papers in this area were those by Romagnoli et al. (9) on NaF color centers and phthalocyanine in polyethylene and by Köhler et al. (10) on quinizarin in an alcoholic glass. Polarized spectra have also previously been used to elucidate hole burning mechanisms (11,12).

In this paper, polarized hole spectra for tetraphenylporphyrin in a polystyrene films will be used to show that although the antihole absorption is distributed throughout the inhomogeneously broadened absorption profile, there is a pronounced blue shift of the distribution of anti-hole absorption energies. In addition, a correlation between the S_1 and S_2 site energy distributions will be demonstrated.

EXPERIMENTAL

Free base 5,10,15,20-tetraphenylporphyrin and polystyrene were each dissolved in toluene and then mixed. The TPP concentration was determined by the amount of TPP solution added. The TPP/polystyrene solution was allowed to air dry from a glass surface for several days. Sections of films of uniform color were cut from the dried film and mounted in a variable temperature liquid helium cryostat (Janis, 8-DT).

Holes were burnt at 4.6K with light from a ring dye laser (Coherent 699-21, line width ~20 MHz, DCM dye). To ensure that the laser light was well polarized a Glan-Taylor polarizer was placed in the beam just before the sample. Absorption spectra were taken with a Fourier transform spectrometer (Bruker, IFS-120) using a resolution of 2 cm^{-1}. To obtain polarized spectra a Glan-Taylor polarizer was placed in the probe beam prior to the sample. Parallel and perpendicular polarizations in absorption were determined by passing the laser beam through both polarizers and adjusting the probe polarizer for maximum and null transmission, respectively. The unpolarized spectra were obtained from the polarized spectra by adding twice the perpendicular polarization to the parallel polarized spectrum (13,14). This procedure was followed to avoid polarization artifacts due to the preferential polarization of the spectrometer source arising from the orientations of mirrors and beamsplitters. It should be noted that the signal-to-noise ratio of the spectra decreases at higher frequencies. This is due to

both the increasing optical density of the sample and the decreasing detector sensitivity.

RESULTS

Figure 1 shows the unpolarized, visible absorption spectrum of TPP in polystyrene film at 4.6K. The four bands are assigned as the origin and a vibronic band of the lowest energy singlet excited state, S_1, also referred to as Q_x, and the origin and a vibronic band of the second excited singlet, S_2, or Q_y (15). The absorption width of $Q_{x,0\text{-}0}$ is about 350 cm^{-1}. From the asymmetry of the band and from the hole spectra (*vide infra*), it is known that there are several low frequency ($\omega < 300$ cm^{-1}) TPP vibrations within this width. However, since the intensities of these bands are quite weak relative to the origin absorption, inhomogeneous broadening is the major source of the observed width. The broader widths of the other bands in the spectrum reflect not only significant inhomogeneous broadening, but also contributions from multiple vibronic bands (in $Q_{x,0\text{-}1}$) and/or an increased homogeneous width ($Q_{y,0\text{-}0}$). [The width of the Q_y origin in a supersonic expansion is ~100 cm^{-1} (16).]

Figure 2 is an unpolarized spectrum showing the change in optical density throughout the spectrum following a burn at ω_B = 15508 cm^{-1}. The region about ω_B is shown more clearly in the inset. Coincident with the burn frequency there is a strong zero phonon hole (ZPH) representing a ΔOD of ~25%. Shifted 11 cm^{-1} to lower energy of the ZPH is the peak of the pseudo-phonon sideband hole (pseudo-PSBH) which arises from burning of sites at $\omega < \omega_B$ through phonon absorption (17). Important features of the spectrum are the broad antihole (absorption

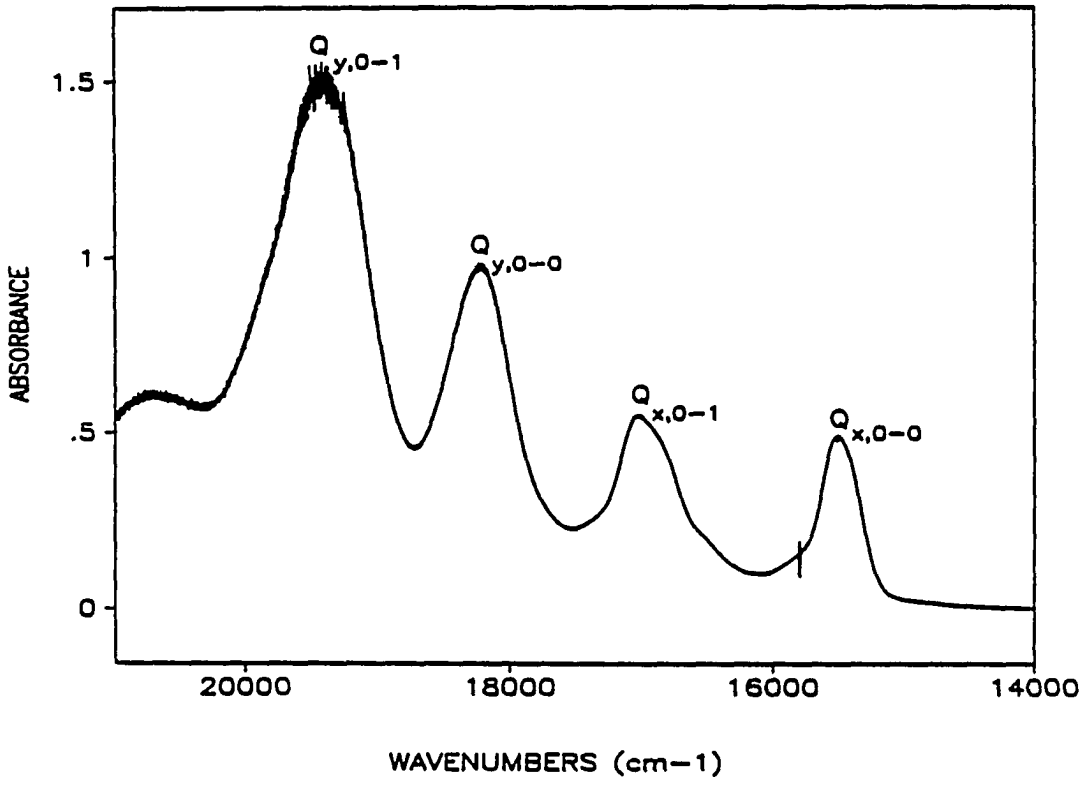

Figure 1. Unpolarized visible absorption spectrum of tetraphenylporphyrinin in a polystyrene film at 4.6 K

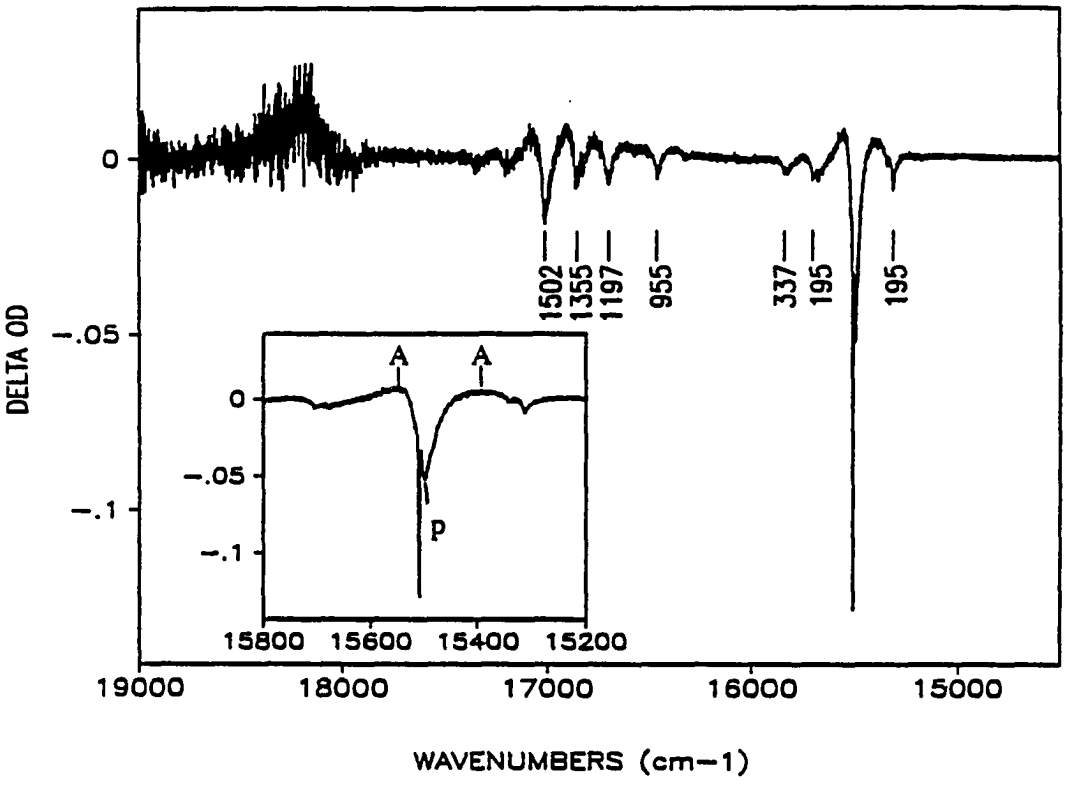

Figure 2. Unpolarized hole spectrum of tetraphenylporphyrin in polystyrene at 4.6 K. The spectrum was obtained by summing the parallel polarized spectrum with twice the perpendicular spectrum. Holes were burnt for 15 sec at 15508 cm^{-1} with 20 mW/cm^2. The numbers give the frequencies of the vibronic holes in wavenumbers. In the inset, A and P label the anti-holes and the pseudo-PSBH, respectively

increase) on either side of the ZPH and pseudo-PSBH and the broad increase in absorption of the $Q_{y,0-0}$ band. These features have not previously been noted.

Vibronic holes appear at frequencies both higher and lower than the primary burn frequency. The lower frequency vibronic holes can be referred to as pseudo-vibronic holes corresponding to sites which absorb at ω_B through a vibronic transition. The lower frequency features are then the corresponding origin holes. The higher frequency vibronic holes are real vibronic features building on the origin at ω_B. The frequency shifts relative to ω_B are labelled for some of the stronger vibronic holes. Relative to the origin hole at ω_B the depths of the real vibronic holes are directly proportional to the Franck-Condon factor for the vibronic transition. The largest Franck-Condon factor for the vibronic bands in the $Q_{x,0-1}$ is ~0.2. Thus, the intensity of the $Q_{x,0-1}$ relative to the $Q_{x,0-0}$ in the absorption spectrum is a consequence of the overlap of a large number of vibronic features rather than intrinsically higher vibronic intensity. In polarized spectra, (Fig. 3), the relative hole depths in parallel and perpendicular polarizations are useful in assigning the symmetries of vibronic bands. For the a_{1g} vibrations of TPP the holes will be deeper in parallel polarization than in perpendicular. For the non-totally symmetric vibrations, the opposite is true. These expectations are borne out for vibronic holes which are well separated from each other. However, in regions where there are multiple adjacent vibronic bands, the interference between vibronic ZPH and vibronic pseudo-PSBH can complicate assignments. In Fig. 3, for example, the band at 1502 cm^{-1} which is stronger in perpendicular polarization

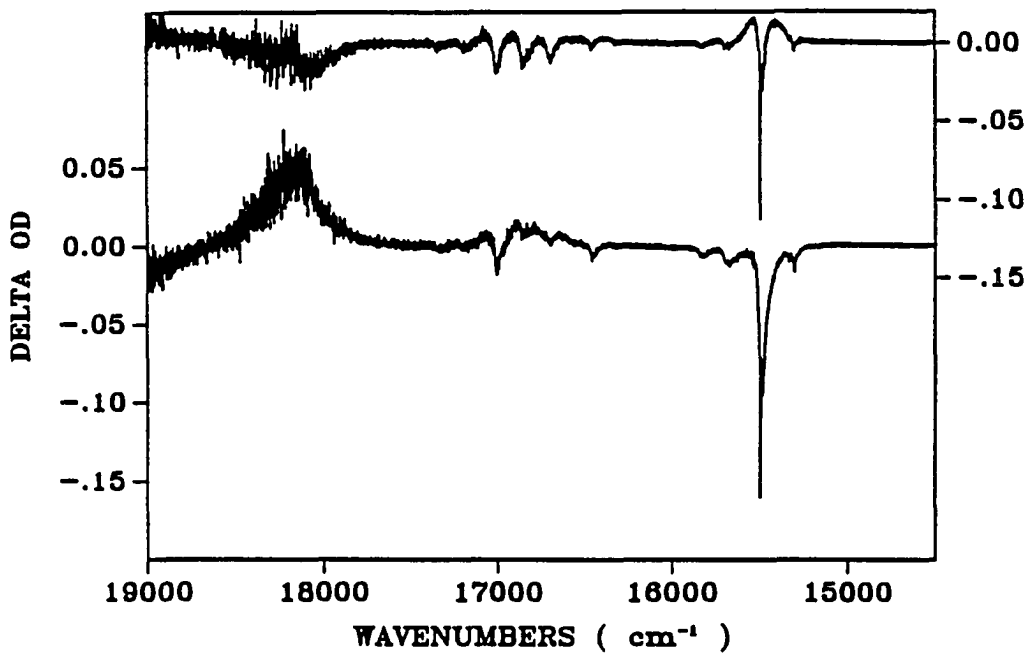

Figure 3. Polarized hole spectra for tetraphenylporphyrin in polystyrene at 4.6 K. Burn conditions as in Fig. 2. The top spectrum, associated with the right scale, is for perpendicular polarization. The bottom spectrum, associated with the left scale, is for parallel polarization

has been assigned as a_{1g} by others (5,18). From higher resolution spectra, it can be seen that there are multiple contributions to the holes in this region.

The changes in Q_y and the Q_x antihole are shown more clearly in Fig. 3 which is the ΔOD spectra measured with light polarized parallel (lower spectrum) and perpendicular (upper spectrum) to the polarization of the burn beam. From Fig. 3, it can be seen that the ZPH at ω_B and the pseudo-PSBH are much stronger for parallel polarization than for perpendicular and that the antihole in Q_x is only detectable for perpendicular polarization. Additionally, for the Q_y transition, the absorption increases for parallel and decreases for perpendicular and is broad for both orientations.

An unpolarized difference spectrum for a longer burn time is shown in Fig. 4. As in Fig. 3, ω_B = 15508 cm^{-1}, which is near the center of the inhomogeneous site distribution. The burn time was 5 min compared to 15 sec for the spectra of Figs.2 and 3. In the Q_x region of the spectrum, the main result of the longer burn time is an increase in depth of the pseudo-PSBH and pseudo-vibronic holes relative to the origin ZPH. These effects are due to burning through zero-phonon absorption being saturated more quickly than burning through phonon or vibronic absorptions (19). Fig. 4 also shows that at longer burn times, the absorption increase in the Q_y region is larger. Furthermore, as can be seen from the smoothed difference spectrum (inset A) of the Q_y region, the absorption increase is structured. On the high energy side of the Q_y antihole, there is an overtone of the 1502 cm^{-1} vibronic hole and associated low and high energy antiholes, (designated by upward- and

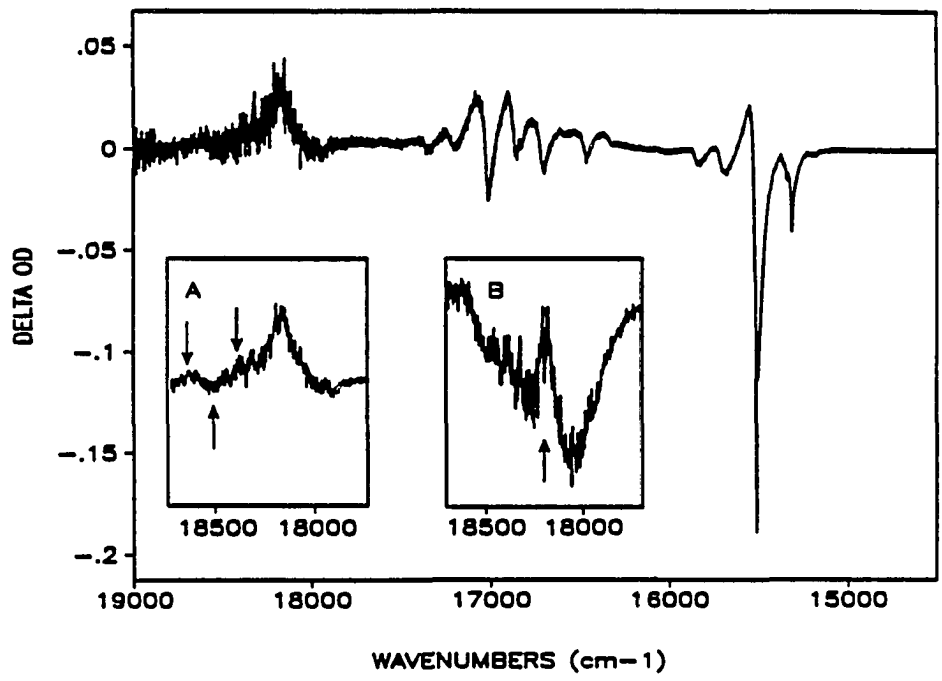

Figure 4. Unpolarized hole spectra for tetraphenylporphyrin in polystyrene at 4.6 K. Burn conditions as in Fig. 3, except burn time = 5 min. Inset A shows a smoothed trace of the Q_y transition region. The upward arrow indicates the 1502 cm^{-1} overtone hole; the downward arrows indicate the associated anti-holes. Inset B shows the perpendicularly polarized Q_y absorption. The region of no change in OD, corresponding to the Q_x hole is indicated by an arrow

downward-pointing arrows, respectively). The large absorption increase at 18090 cm^{-1} is near the center of the Q_y absorption, when ω_B is near the center of Q_x. Inset B of Fig. 4 shows the perpendicularly polarized Q_y absorption.

DISCUSSION

Consider first, that hole burning in porphyrins is a special case of PHB in which proton tautomerization yields a photoproduct that is identical to the photoreactant molecule. The absorption spectrum of the product will be the same as that of the reactant except that the transition dipole moment is rotated 90° and the excitation frequency will be shifted due to the site symmetry being lower than the D_{2h} molecular symmetry. The frequency shifts are expected to be distributed throughout the inhomogeneous width of the absorption, i.e., ~300 cm^{-1} in the present case. As a result, one can expect that there should be no net change in integrated absorption intensity, but rather a redistribution of absorbers throughout the spectrum. That this is so is not obvious from Fig. 2. Considering the region about the $Q_{x,0\text{-}0}$ band, the unpolarized hole spectrum shows antiholes on both sides of the ZPH. The integrated intensity of these, however, is a factor of ~4 less than the intensity of the negative-going ZPH plus pseudo-PSBH. A part of the discrepancy is due to the interference of vibronic holes (both low and high energy) with the expected antiholes. However, integration of the absorption over a region which would include holes and antiholes due to both the origin band and the low frequency ($\omega \lesssim 300$ cm^{-1}) vibrations still does not result in conservation of the total absorption strength. For example, the range from 15000 cm^{-1} to 16100 cm^{-1} encompasses ~500 cm^{-1} below ω_B to ~600 cm^{-1} above ω_B. Thus this region includes all the low frequency TPP vibrations and their inhomogeneous broadening contributions. Integrating the pre- and post-burn absorptions throughout this

range reveals a small, but significant loss of integrated absorption intensity which increases for longer burn times. In order to obtain quantitative agreement between integrated absorption intensity for pre- and post-burn spectra, it is necessary to integrate over the entire Q_x absorption, i.e., from 15000 cm^{-1} to 17550 cm^{-1}. As expected, the total absorption intensity is conserved and the antihole is within the original band. From the polarized spectra, Fig. 3, it is clear that the antihole is only present in the perpendicular polarization, confirming the proton tautomerization mechanism.

However, the integration range required to obtain the conservation of absorption intensity is surprising. That the intensity is not conserved over the ~1100 cm^{-1} range encompassing the inhomogeneously broadened origin band and the low frequency vibrations indicates that there is a shift of a substantial number of absorbers toward the blue and this shift extends over a range in excess of the inhomogeneous width of the band. In addition, the blue shift increases with burn time. This effect can be seen by comparing the intensity of the antihole on the low energy side of ω_B in Figs. 3 and 4. In Fig. 4, the intensity of the low energy antihole has been reduced by an increase in the pseudo-PSBH. However, the large integration range necessary to obtain conservation of absorption intensity should not be taken to imply that the absorption energies are actually shifted by more than 2000 cm^{-1}. Because the vibronic holes and vibronic antiholes are also shifted, it is difficult to determine the actual extent of tailing of the antihole absorption. Nevertheless, a clear qualitative picture of the antihole does emerge: it is sharply

peaked about ω_B but has a very broad tail that extends by more than Γ_{inh} to the blue of ω_B. It has recently been noted that similar broad shifts of the absorption, predominantly to higher energies, are a general characteristic of nonphotochemical hole burning, (NPHB), in π-π^* absorptions of molecules in amorphous matrices (20). To explain that observation a new model for NPHB based on a hierarchy of constrained configurational tunneling events that proceed from the outer solvent sphere inward to the absorbing species was proposed. That the hole burning mechanism in TPP is photochemical is certain based on the perpendicularly polarized anti-hole near ω_B; however, it is not surprising that the amorphous polystyrene matrix should exert an influence similar to that observed in NPHB, since it is precisely site energy differences which allow the tautomerization to be detected optically.

In the Q_y region of the spectrum, if there is no correlation between the site distributions for $Q_x$and Q_y, one would expect that the holes and antiholes will both be distributed throughout the absorption band resulting in no change in the unpolarized spectra. That this expectation is not fulfilled is clear from examining Fig. 2. In the spectrum (Fig. 2), there is clearly a slight increase in absorption in the Q_y region, which becomes more pronounced at longer burn times. This increase is one manifestation of site energy correlation between Q_x and Q_y. Because the antihole in Q_x region is distributed over a much broader range than the hole, in Q_y region the decrease in absorption is also more broadly distributed than the corresponding absorption increase, *if there is positive correlation between*

Q_x and Q_y transitions. In polarized spectra, since the transition dipole moments for Q_x and Q_y are orthogonal, holes in Q_x appear as antiholes in Q_y and vice versa. In the polarized spectra, particularly at long burn times (Fig. 4, inset B), there is structure in the Q_y region of the perpendicularly polarized difference spectrum. This structure appears as a region of no change in optical density surrounded by regions of decreased optical density, i.e., holes in Q_y which correspond to antiholes in Q_x. As the burn wavelength is varied from low to high energy within the Q_x band, the Q_y peak in the unpolarized spectrum also shifts from low to high energy as does the region of no change in optical density in the perpendicularly polarized spectra. The region of no OD change in Q_y corresponds to the hole at ω_B in Q_x, homogeneously broadened by the short lifetime of this state, while the surrounding decreases in absorption are the Q_y analog of the Q_x antiholes. These effects, as well as the tracking of the Q_y peak in the unpolarized spectra with ω_B, are clear evidence of correlation between the Q_x and Q_y site distributions.

Such correlation between different electronic states is not common (21) and is remarkable for electronic transitions in which the the transition dipole moments are orthogonal to each other. The observation of site energy correlation indicates that the polarization induced in the solvent sphere about the TPP molecule by the transition dipoles for the two states is the same for any one molecule. Nevertheless, the width of the inhomogeneous site distribution (~300 cm^{-1}) indicates that there is a large range of interactions between the TPP molecules and their associated solvent spheres. It should be noted that the gas-to-solid shifts of

the Q_x and Q_y transition energies (~125 and ~550 cm^{-1}, measured from the absorption maxima) are consistent with there being isotropic solvent interactions within the molecular xy plane. That is the ratio of the Q_y to Q_x shift scales very nearly as ratio of their oscillator strengths squared, as expected by a model in which the solute-solvent interactions are considered isotropic (22).

ACKNOWLEDGMENT

This research was supported by the Division of Materials research of the National Science Foundation under Grant No. DMR-8612270.

REFERENCES

1. Storm, C. B.; Teklu, Y.; Sokoloshi, E. A. Ann. N. Y. Acad. Sci. 1973, 631, 206.
2. Abraham, R. J.; Hawkes, G. E.; Smith, K. M. Tetrahedron Lett. 1974, 16, 1483.
3. Völker S.; van der Waals, J. H. Mol. Phys. 1976, 32, 1703.
4. Völker, S.; Macfarlane, R. M.; Genack, A. Z.; Trommsdorff, H. P.; van der Waals, J. H. J. Chem. Phys. 1977, 67, 1759.
5. Dick, B. Chem. Phys. 1989, 136, 429.
6. Kishii, N.; Asai, N.; Kawasumi, K.; Tamura, S.; Seto, J. Appl. Phys. Lett. 1988, 52, 16.
7. Hori, K.; Mori, T.; Naito, T.; Mita, I. Appl. Phys. Lett. 1988, 53, 935.
8. van den Berg, R.; Visser, A.; Völker, S. Chem. Phys. Lett. 1988, 144, 105.
9. Romagnoli, M.; Levenson, M. D.; Bjorklund, G. C. J. Opt. Soc. Am. B 1984, 1, 571.
10. Köhler, W.; Breinl, W.; Friedrich, J. J. Phys. Chem. 1985, 89, 2473.
11. Spitzer, R. C.; Ambrose, W. P.; Sievers, A. J. Optics Lett. 1986, 11, 428.
12. Ambrose, W. P.; Sievers, A. J. Chem. Phys. Lett. 1988, 147, 608.
13. Perrin, F. Ann. Phys. 1929, 12, 169.
14. Vermeglio, A.; Breton, J.; Paillotin, G.; Cogdell, R. Biochim. Biophys. Acta 1978, 501, 514.
15. Gouterman, M. J. Mol. Spectrosc. 1961, 6, 138.

16. Even, U.; Magen, J.; Jortner, J.; Friedman, J.; Levanon, H. J. Chem. Phys. 1982, 77, 4374.

17. Details regarding hole shapes may be found in: W. E. Moerner, Ed., Persistent Spectral Hole Burning: Science and Applications, Springer-Verlag: Berlin, 1988.

18. Tamkivi, R.; Renge, I.; Avarmaa, R. Chem. Phys. Lett. 1983, 103, 103.

19. Lee, I.-J.; Hayes, J. M.; Small, G. J. J. Chem. Phys. 1989, 91, 3463.

20. Shu L.; Small, G. J. Chem. Phys. in press.

21. Lee, H. W. H.; Walsh, C. A.; Fayer, M. D. J. Chem. Phys. 1985, 82, 3948.

22. McRae, E. G. J. Phys. Chem. 1957, 61, 562.

CONCLUSIONS

The theory proposed to simulate hole profiles for arbitrary strong electron-phonon coupling in short burn time limit was extended to examine the hole profiles at arbitrary burn time. The shapes of real- and pseudo-PSBH in the hole burned spectra in amorphous solids strongly depend on burn time and burn wavelength. As the burn time increases, hole burning through the PSB becomes more important. At shorter wavelengths, the pseudo-PSBH dominates the real-PSBH. This results from the strong dependence of the hole burning selectivity on the burn frequency and burn time.

The antihole spectrum was deconvolved from the hole spectrum by using the simulated hole spectrum. From the deconvolved antihole profile, we concluded that NPHB of the antenna complex of PSI-200 predominantly creates sites whose zero-phonon transitions are shifted to higher energy relative to preburn sites.

The first observation of the antihole of porphyrin in amorphous solids was presented. The antihole was polarized oppositely to the hole and distributed throughout the inhomogeneous absorption band. Vibronic frequencies and Franck-Condon factors were measured. A positive correlation between the site distributions for Q_x and Q_y was observed.

REFERENCES

1. Völker, S.; van der Waals, J.H. Mol. Phys. 1976, 32, 1703.
2. Olson, R.W.; Lee, H.W.H.; Patterson, F.G.; Fayer, M.D.; Shelby, R.M.; Burum, D.P.; Macfarlane, R.M. J. Chem. Phys. 1982, 77, 2283.
3. Kharlamov, B.M.; Bykovskaya, L.A.; Personov, R.I. Chem. Phys. Lett. 1977, 50, 407.
4. Dick, B. Chem. Phys. 1989, 136, 429.
5. Friedrich, J.; Wolfrum, H.; Haarer, D. J. Chem. Phys. 1982, 77, 2309.
6. Hayes, J.M.; Gillie, J.K.; Tang, D.; Small, G.J. Biochim. Biophys. Acta 1988, 932, 287.
7. Friedrich, J.; Swalen, J.D.; Haarer, D. J. Chem. Phys. 1980, 73, 705.
8. Personov, R.I.; Kharlamov, B.M. Laser Chem. 1986, 6, 181.
9. Friedrich, J.; Haarer, D. Angew. Chem. Int. Ed. Engl. 1984, 23, 113.
10. Sapozhnikov, M.N. Chem. Phys. Lett. 1987, 135, 398.
11. Friedrich, J.; Haarer, D. In Optical Spectroscopy of Glasses, Zechokke, I., Ed.; D. Reidel Publishing Company: Dordrecht, 1986.
12. Seybold, P.G.; Gouterman, M. J. Mol. Spectrosc. 1969, 31, 1.
13. Gurinovich, G.D.; Sevchenko, A.N.; Solov'ev, K.N. Soviet Phys. Uspekhi 1963, 6, 67.
14. The Porphyrins, vol. 1-7; Dolphin, D., Ed.; Academic Press: New York, 1978.

15. Porphyrins: Excited States and Dynamics; Gouterman, M.; Rentzepis, P.M., Straub, K.D., Eds.; American Chemical Society: Washington, D.C., 1986.

16. Almöf, J., Intern. J. Quantum Chem. 1974, 3. 915.

17. Radziszewski, J.G.; Waluk, J.; Michl, J. Chem. Phys. 1989, 136, 165.

18. Chen, B.L.L.; Tulinsky, A. J. Am. Chem. Soc. 1972, 94, 4144.

19. Silvers, S.J.; Tulinsky, A. J. Am. Chem. Soc. 1967, 89, 3331.

20. Storm, C.B.; Teklu, Y.; Sokoloshi, E.A. Ann. N. Y. Acad. Sci. 1973, 631, 206.

21. Abarham, R.J.; Hawkes, G.E.; Smith, K.M. Tetrahedron Lett. 1974, 16, 1483.

22. van den Berg, R.; Visser, A.; Völker, S. Chem. Phys. Lett. 1988, 144, 105.

23. Horie, K.; Mori, T.; Naito, T.; Mita, I. Appl. Phys. Lett. 1988, 53, 935.

24. Zallesskii, I.E.; Kotlo, V.N.; Sevchenco, A.A.N.; Solov'ev, K.N.; Shkirman, S.F. Soviet Phys.-Dokl. 1973, 17, 1183.

25. Sarai, A. J. Chem. Phys. 1982, 76, 5554.

26. Schlabach, M.; Rumpel, H.; Limbach, H.H. Angew. Chem. Int. Ed. Engl. 1989, 28, 76.

27. Limbach, H.H.; Hennig, J. J. Chem. Phys. 1979, 71, 3120.

28. Smedarchina, Z.; Siebrand, W.; Zerbetto, F. Chem. Phys. 1989, 136, 285.

29. Butenhoff, T.J.; Moore, C.B. J. Am. Chem. Soc. 1988, 110., 8336.

30. Wehrle, B.; Limbach, Köcher, M.; Ermer, O.; Vogel, E. Angew. Chem. Int. Ed. Engl. 1987, 26, 934.

31. Völker, S.; Macfarlane, R.M.; Genack, A.Z.; Trommsdorf, H.P.; van der Waals, J.H. J. Chem. Phys. 1977, 67, 1759.

32. van Dorp, W.G.; Soma, M.; Kooter, J.A.; van der Waals, J.H. Mol. Phys. 1974, 28, 1551.

33. Silvers, S.; Tulinsky, A. J. Am. Chem. Soc. 1964, 86, 927.

34. Hoard, J.L.; Hamor, M.J.; Hamor, T.A. J. Am. Chem. Soc. 1963, 85, 2334.

35. Even, U.; Magen, J.; Jortner, J.; Friedman, J.; Levanon, H. J. Chem. Phys. 1982, 77, 4374.

36. Bykovskaya, L.A.; Personov, R.I.; Romanovskii, Yu, V. J. Appl. Spectrosc. 1979, 31, 1437.

37. Tamkivi, R.; Renge, I.; Avarma, R. Chem. Phys. Lett. 1983, 103, 103.

SECTION II.

SPECTRAL DIFFUSION AND HOLE BURNING WITH CONSTANT FLUENCE

INTRODUCTION

It is well known that the thermal and acoustic properties of guest molecules in amorphous solids at very low temperatures are remarkably different from those in crystalline solids (1). These anomalous properties have been at least qualitatively explained by Phillips (2) and Anderson et al. (3). Their model was based on tunneling of glassy bistable configurations which are often referred to as two level systems (TLS). Not only thermal and acoustic properties but also photophysical properties such as optical dephasing are anomalous in amorphous media. In the amorphous solids the optical dephasing is 10-100 times faster than in crystals and has a T^{α} ($1<\alpha<2$) dependence on the temperature compared to a T^{7} dependence in crystals.

A number of different techniques have been used to measure the electronic optical dephasing by extracting the homogeneous line shape from the inhomogeneously broadened line shape. Examples are picosecond photon echo (4-8) and hole burning (9-20) which have been applied to both organic and inorganic systems. The temperature dependence of linewidth studied by PHB has most frequently shown a T^{α} ($\alpha=1.3$) power law within the experimental error over an extended temperature range (0.3-20 K). Many organic systems, including free base porphyrin in various glasses (9-11), chlorin in polymethacrylate (PMMA) and polystyrene (10,12), dimethyl-s-tetrazine in PMMA (10) and quinizarin in ethanol-methanol (3:1) (13) have been studied. etc. However, protonated phthalocyanin in concentrated sulfuric acid glasses (14) was an exception, showing a T^{α} ($\alpha=1.8$) power law. Temperature dependent NPHB data for cresyl violet perchlorate in ethanol and PMMA (11,15), resorufin in ethanol and PMMA (11), pentacene in

PMMA (16) and tetracene in glasses (17,18) also showed a T^{α} (α=1.3) power law. Thus a T^{α} (α=1.3) power law of the linewidth has been observed for a substantial number of organic systems regardless of the nature of the guest molecules (21). Furthermore, a $T^{1.3}$ extrapolation to lower temperature has yielded a lifetime limited value of the homogeneous linewidth for several systems (9,10,19).

Agreement between the NPHB (11,16) and the photon echo data (4) showing a $T^{1.3}$ power law of linewidth for pentacene in PMMA has been achieved. Shortly before this, similar agreement was observed by Macfarlane and Shelby (20) in their study of the Pr^{3+}/silicate glass system.

On the other hand, Fayer and his group have reported that there are discrepancies in the optical linewidths as measured by NPHB as opposed to photon echo measurement (8,22,23). The homogeneous linewidths of resorufin in ethanol glasses measured by NPHB, although showing a T^{α} (α=1.3) dependence (in agreement with ref. 14), were four times broader than those measured by the photon echo method (8,22). For resorufin in glycerol glass (23) and cresyl violet in ethanol and deuterated ethanol (24), the low temperature optical linewidths obtained from NPHB were also eight times broader than those measured by the photon echo method. These workers attributed the discrepancies of the linewidths measured by the two different techniques to spectral diffusion because, while the photon echo is only sensitive to the homogeneous dephasing, the hole burning experiment is sensitive to both homogeneous dephasing and slow spectral diffusion. Since the two techniques operate on very different time scales (psec for photon echos and seconds to minutes for hole burning experiments), the holes can be broadened by slow dark ground state relaxation processes of TLS_{int}.

More recently, in Ref. 25 Fayer's group measured time dependent hole width for cresyl violet in ethanol in the time range from 100 msec to 3000 sec at 1.3 K. The hole width increased linearly by a factor of two on this time scale, changing most rapidly in the range around 20 sec. They interpreted the hole broadening as being due to the broad distribution of TLS relaxation rates in the glass. Shortly after this, they also performed a transient hole burning experiment for cresyl violet in deuterated ethanol in the 10 μsec to 50 msec time range at 1.3 K (26). They observed the hole width to increase logarithmically with time.

However, in Refs. 16 and 19 Völker and her group attributed the above discrepancy to the sample preparation and burning and detection methods. For pentacene in PMMA (16) and resorufin in ethanol (19), they observed that hole widths measured in transmission are larger than those measured in fluorescence excitation because lower laser intensity can be used in fluorescence detection. Furthermore, they observed that holes probed by fluorescence excitation do not show any broadening by spectral diffusion over several hours, while holes observed in transmission show hole broadening with time (16,19). They suggested that when molecules are probed at the surface of the sample (as in fluorescence excitation), there is no spectral diffusion because they are in thermal contact with liquid helium. However, in the bulk of the glass, (which has a poor thermal conductivity), which is pertinent to the transmission mode, they suggest that strain from a thermal gradient probably causes structural relaxation of the glass (19). They concluded that hole burning experiments, if properly designed, e.g., very shallow holes (≤5% hole depth) burned with very low burn intensities and

probed with fluorescence detection, yield the correct optical dephasing times in glasses.

Recently, in Ref. 27 Völker's group performed transient hole burning on free base porphyrin in polyethylene with 5 msec time resolution. They obtained the homogeneous linewidth by extrapolating to the zero burn intensity. The optical dephasing measured by the transient hole burning on a 5 msec time scale was identical to that obtained by PHB on a 100 sec time scale. Thus, again they concluded that the hole width is not influenced by spectral diffusion.

Breinl et al. (28) have observed that the hole width of quinizarin in ethanol/methanol glass increases logarithmically in a time range between minutes and about 10^4 min. They interpreted this result as due to spectral diffusion in amorphous solids. Meiler and Friedrich (29) observed similar trends for dimethyl-s-tetrazine in ethanol/methanol glass and concluded that spectral diffusion processes are slow and occur on the experimental time scale.

Rebane (30) has measured the evolution of the hole width of free base octaethylporphyrin in polystyrene at times from 10 μsec to 3 sec. A considerable hole broadening was observed with the hole width varying from 0.004 cm^{-1} at t_w=10 μsec to 0.03 cm^{-1} at t_w=3 sec, where t_w is the time difference between the burn and the probe. Gorokhovskii and Rebane (31) have observed that for H_2-tetra-4-tert-butylphthalocyanine in alcohol glass, spectral diffusion occurs on 10^3 sec or longer time range but not in a time range from 10 msec to 100 sec.

Recently, Nakatsuka et al. (32) have measured the time evolution of the hole of 1,3,3,1',3',3'-hexamethyl-2,2'-indotricarbocyanine iodide in polyvinyl alcohol in the time range of from 10 msec to 5000 sec after burning. Although there was a

considerable decrease of the hole depth from 10 msec to 5000 sec, the hole width did not change appreciably. However, the hole width measured in transmission was about three times broader than the homogeneous width measured by photon echo. Thus, the hole apparently broadens by a factor of three between 5 nsec and 10 msec, possibly due to spectral diffusion. Hole broadening from 10 msec to 5000 sec was negligible.

Although many different authors have indicated that spectral diffusion does affect the time dependence of the hole width, the question is still controversial and unresolved.

As discussed in the general introduction of this dissertation, there is a distribution of the tunnel parameter λ with average value λ_0 and varience σ_2, resulting in a distribution of TLS relaxation rates ($R = \Omega_0 \exp(-2\lambda)$) (33, 34). Ω_0 is defined by the type of the experiment, i.e., spontaneous hole filling or hole growth. For spectral diffusion one has to consider the number of TLS states which relax into the thermal equilibrium in a time from t_{min} ($= 1/R_{max}$) to t where R_{max} is the maximum rate corresponding to the fastest relaxation processes and t is the obervation time (35). Similar arguments have been used to explain the time dependent specific heat data (1,35). Therefore, the same time dependence for both specific heat and spectral diffusion is expected if the same TLS ensemble determines the thermodynamic and the optical relaxation processes. Knaak et al. (36) and Loponen (37) have measured the time dependence of the heat capacity of vitreous silica between 0.35 and 1.6 K on a time scale from 2 μsec to 0.5 msec. They observed that specific heat increases nearly logarithmically with time for measurement times of the order of 10 μsec and that the time dependence becomes

more complex at longer times. Jankowiak et al. (38) calculated time-dependent specific heat considering the contributions from both weakly coupled (internal) and strongly coupled (external) tunneling states. Their calculation is consistent with experimental data of refs. 36 and 37.

The primary goal of this section of this dissertation was the study of optical dephasing as a function of the time. From the above mentioned time dependent specific heat data (36-38), it was expected that there may be large hole width change in the 1 μsec to 1 msec range. Spectral diffusion would affect the hole width but not hole area. With this in mind, an experiment was designed and tested. Unfortunately, this experiment has not yet yielded the desired information. Possible reasons for this are discussed and future spectral diffusion experiments are suggested in the second part of this section.

Using the same experimental apparatus with small modification, hole burning experiments were performed to investigate the burn intensity dependence of the hole at fixed burn fluence. These results are relevant to understanding the difficulties involved in hole burning on a μsec time scale. The results are discussed in terms of kinetic models and the hole broadening mechanism.

EXPERIMENTAL METHODS

Sample Preparation

The sample used in this study was oxazine 720 perchlorate (Ox720) in a hydrogen bonding polymer, polyvinyl alcohol (PVOH). Ox720 ($C_{21}H_{22}ClN_3O_5$) was purchased from Exciton Chemical Company and used without further purification. PVOH with an average molecular weight of 14,000 was purchased from Aldrich Chemicals. PVOH was dissolved in distilled hot water until a syrupy solution was attained. Because Oxazine 720 has very large extinction coefficient (9.2×10^4 liter $mole^{-1}$ cm^{-1}, the dye was added to polymer solution in small increments until the desired concentration was approximately obtained. The well-mixed solution was poured onto a glass plate (3" x 1") to a liquid thickness of 2~3 mm. The samples were allowed to air dry for 2~3 days. Sections of polymer with clear surface and uniform color were selected and used as samples. This procedure is basically the same as that used in ref. 39.

Cryogenic Equipment

The polymer samples were mounted between two brass plates which allowed for thermal conduction and optical access to the sample. The samples were cooled to 4.2 K in a Janis model 8-DT Super Vari-Temp liquid helium cryostat. Lower sample temperatures (down to 1.6 K) were obtained by reducing the vapor pressure above the liquid helium by pumping. The sample temperature was measured using a calibrated (1.4 K to 300 K) silicon diode thermometer (Lake Shore Cryogenic model DT-500K) with a cryogenic temperature controller (Lake Shore

Cryogenic model DTC-500). All the experiments described in this section were performed at 1.6 K.

Lasers

Hole burning experiments were performed using an actively stabilized single frequency ring dye laser (Coherent model CR-699-21) pumped by a 6 W cw argon ion laser (Coherent model Innova 90-5). The Argon ion laser has a linewidth of 10 GHz and the ring dye laser has a linewidth ≤1 MHz. In the ring dye laser, a vertex mounted Brewster angle plate is used to vary the effective cavity length and therefore single frequency scans of up to 30 GHz could be made.

The laser dye used was DCM (Exciton).

To increase the ring dye laser output energy, the frequency doubled output of a Q-swiched Nd:YAG laser (Quantel model 480) was used to pump a two stage amplifier. The Nd:YAG laser has 15 nsec pulse duration and ~4 cm^{-1} bandwidth.

Apparatus

Figure 1 shows the configuration of the apparatus used for the hole burning studies with variable burn intensity at fixed burn fluence. The solid lines indicate the optical path and dotted lines, the electrical signal path. The ring dye laser was used for both hole burning and reading. Depending on the power levels required in the experiment either leg 1 or leg 2 was used.

The configurations of leg 1 will be discussed first. Using beam splitter BMS_2, a part of the ring dye laser output was diverted into a confocal spectrum analyzer,

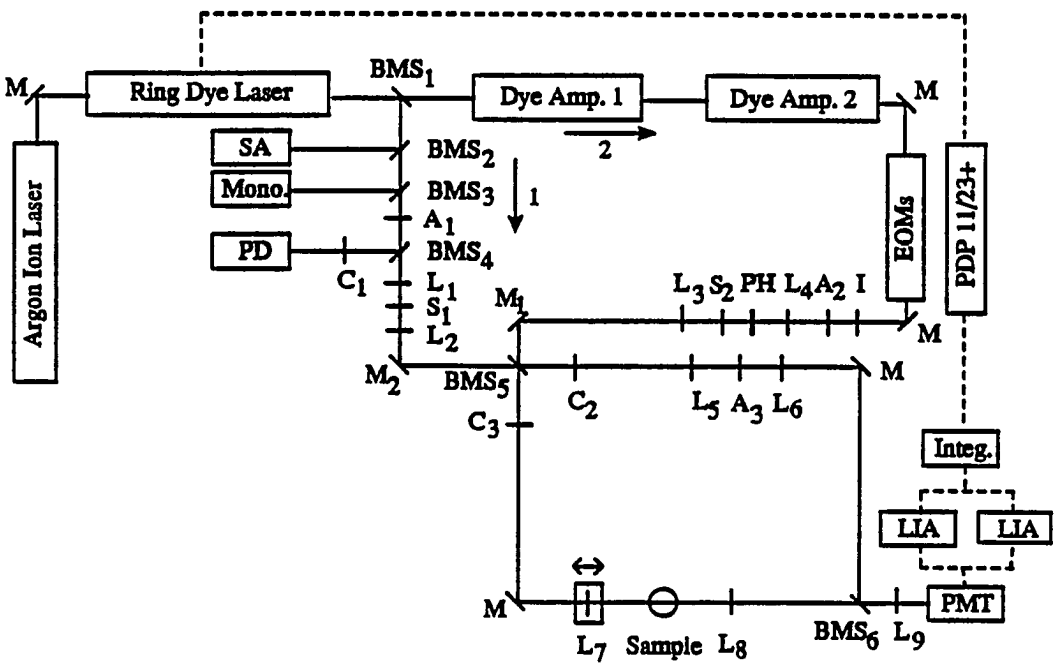

Figure 1. Experimental apparatus used to study burn power dependent hole depth with constant fluence. M; mirror, BMS; beam splitter, A: attenuator, L;lens, S; shutter, C; chopper, PH; pinhole, EOM; electro-optic modulator, PMT; photomultiplier tube, LIA; lock-in amplifier, Integ;integrator. Dye amplifier part is described in detail in Fig. 2

SA (Spectra-Physics model 470-04, free spectral range = 8 GHz) to monitor the laser frequency stability. The output of the spectrum analyzer was amplified and displayed on an oscilloscope. The laser wavelength was determined by splitting the beam into a 1 / 3 meter monochromator (McPherson model 218) by using BMS_3. The laser intensities were adjusted to appropriate values for hole burning and reading using a variable attenuator (NRC model 925B) and neutral density filter A_1. In order to measure the intensity after attenuation, part of the attenuated beam was split by BMS_4, modulated by mechanical chopper C_1 (PAR model 125) and monitored using a photodiode detector PD (Molectron model LP-141) and lock-in amplifier. Sample irradiation times were controlled using shutter S_1 (Uniblitz model 12X with a Uniblitz model SD-1000 shutter drive / timer), capable of producing exposure time from 900 μsec upwards. Two lenses, L_1 and L_2 were located before and after the shutter to minimize the rise and fall time of the shutter opening and to collimate the laser beam. The laser beam then enters a double beam apparatus (40,41) by a mirror M.

After reaching the double beam apparatus, the laser beam is split into reference and sample beams by BMS_5. Both reference and sample beam paths contain identical optics but are modulated at different frequencies using mechanical choppers C_2 and C_3 (Laser Precision CTX-534). Attenuator A_3 (NRC model 935-3) was used in the reference beam to match the light intensity loss on the sample beam caused by scattering from the sample and cryostat windows. Each beam was focused and recollimated using lenses. The sample in the cryostat

is located near the focal point of L_7. The beam diameter at the sample could be adjusted using a translational stage to vary the position of L_7. The beam diameter was limited by a pinhole on the sample. Sample and reference beams are recombined and focused into a photomultiplier tube PMT (EMI 9558QB in a Product For Research TE-104-RF thermoelectrically cooled housing).

The output of PMT was sent to each of two lock-in amplifiers (Ithaco model 97EO) referenced to the two mechanical choppers C_2 and C_3. An integrator / coupler (Ithaco model 385EO-2) was used to digitize and integrate the analog signal (at 60 Hz). The output of the integrator / coupler was sent to a microcomputer (Digital Equipment Corporation Micro PDP-11 / 23+ with RT11 operating system), which calculates and stores the sample absorbance data. This computer also provides -5 V to +5 V dc voltages that scan the ring dye laser externally. With this apparatus, the burn and probe beams have identical paths. Burning is accomplished by disabling C_3 after setting the appropriate laser power.

In order to provide ~15 nsec burn pulses with narrow linewidth (≤1 MHz) and high peak powers (≥1 W), the output of the ring dye laser was amplified and then passed through two electro-optic modulators (EOMs) in series in leg 2 of Fig. 1. In order to monitor the beam quality and wavelength, leg 1 in Fig. 1 was also used with S_1 closed and with a quartz plate for BMS_1. Figure 2 shows a schematic of leg 2 in detail. For the dye amplification stages, the frequency doubled output of a Q-switched Nd:YAG laser (Quantel model 480) was used to pump a system that

amplifies the output of cw ring dye laser. The basic design is similar to that of Drell and Chu (42) but with two (not three) amplification stages.

Concentrations of approximately 10^{-3} M of DCM proved appropriate for the transversely pumped dye cells. The lenses (10 cm focal length) obtained from Newport Corporation were antireflection coated. The ring dye laser had to be optically isolated from the amplifier system since the intense back reflection from the first amplification stage to the ring dye laser could disturb its frequency locking mechanism. Two irises were placed between the ring dye laser and first amplification stage for this reason. Two flowing dye cells (NSG Precision Cells model T-3FL) were tilted with respect to the cw laser beam to minimize back scattering to the laser reference cavity. Also, some of the lenses were tilted in the same manner for the same reason. Separate dye reservoirs and pumps were used for each stage, but the dye concentrations were equal. A filter between the dye cell and reservoir eliminated air bubbles in the flow.

The two amplification stages are very similar and are described below. To focus the ring dye laser beam (~200 mW) into the dye cell and recollimate the beam behind it, two 10 cm lenses were used with the dye cell at the common focal point. A 10 cm cylindrical lens was used to focus a part (~4%) of the output of the Nd:YAG laser into the first dye cell. For efficient amplification, the output of the ring dye laser and Nd:YAG laser had to be maximally overlapped by rotating the cylindrical lens about the axis of propagation of the Nd:YAG laser. To minimize the

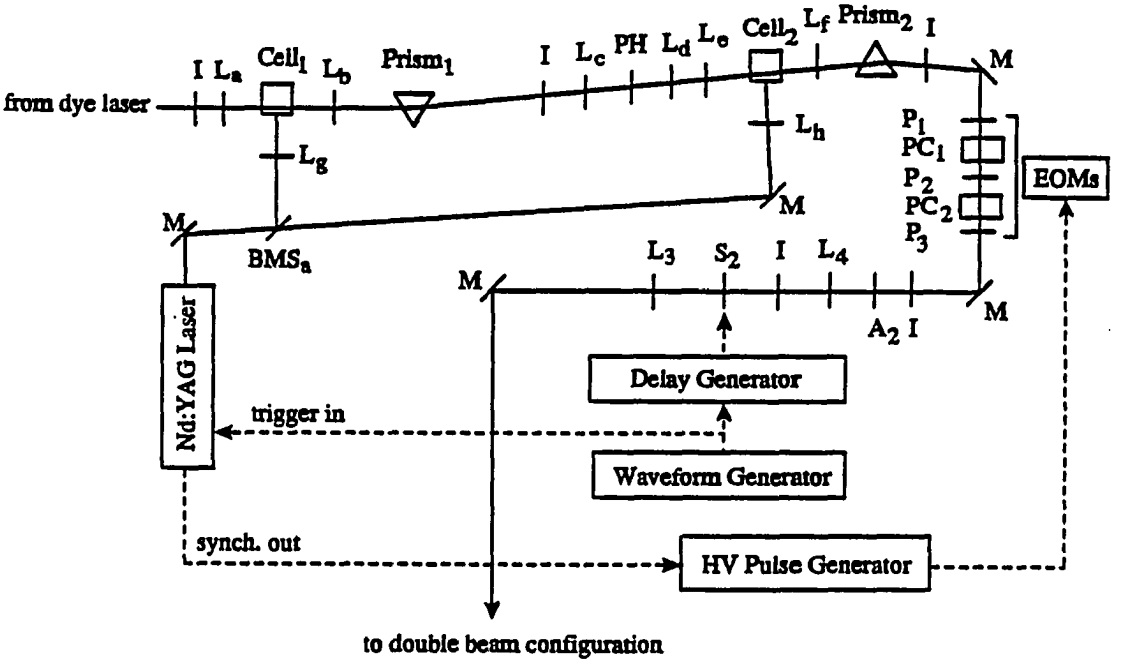

Figure 2. Dye amplification stages used in this experiment. I; iris, L; lens, PH; pinhole, M; mirror, P; polarizer, PC; pockel cell, A; attenuator, S; shutter

background, spontaneous emission after the first amplification stage was spatially filtered. This was achieved using a prism and spatial filter comprised of two 10 cm achromatic lenses (separation ~20 cm) with a 100 μm pinhole at the common focal point. The second amplification stage is identical to the first, except that the dye laser beam is focussed in front of the dye cell in order to use a larger volume for amplification. The remaining part (~96%) of the output of the Nd:YAG laser was used to pump the second stage. The gains were ~200 and ~10 at the first and second amplification stages, respectively.

Because of space limitation of the optical table, the amplified beam built on top of the cw laser beam was first modulated by the EOM and then spatially filtered. The output of the second amplifier was a 15 nsec pulse built on the unamplified cw output of the ring laser. The unamplified part of the output from the second stage, which had ~tens of mW of power and could burn holes easily, had to be temporally filtered. The shortest exposure time of commercially available mechanical shutters was ~0.9 msec, was too long for this experiment. Therefore, a series of two EOMs (two Lasermetrics model 1071FW controlled by a Lasermetrics model 8612C high voltage pulse generator) were introduced in the beam path for providing the shutter action. The EOMs consist of three polarizers and two crystals. Input polarizer, P_a, and second analyzing polarizer, P_c, were aligned with the polarization parallel to the EOM crystal x (or y) axis, which was parallel to the polarization of the incoming laser beam. The first analyzing polarizer, P_b, was rotated by 90°. This combination produces an intensity minimum with no

voltage applied to crystals. When a halfwave voltage (~9 KV) is applied, the transmitted intensity becomes maximum. Two EOMs were used instead of one to get a higher extinction ratio. The Lasermetrics model 1071FW EOM has a specified extinction ratio of 800:1, which means that the minimum output (~0.1 mW) of one EOM could still burn a hole. With a series of two EOMs, an extinction ratio of greater than 10^5 was obtained. The rise time of the output from the EOMs was $\leq$ 1 nsec and the output pulse width was 100 or 300 nsec. The output from the EOMs was spatially filtered using irises and a pinhole. Burn intensity was controlled using a variable attenuator (NRC model 925B) and neutral density filters, A_2. An energy meter was used to measure the pulse energy from the EOMs. Although the EOMs had a high contrast ratio, there was still leakage of light from the EOMs with no voltages applied. This leakage was used to probe holes as it had high enough intensity for hole reading and the same beam path as the burn pulse did. The number of burn pulses was controlled using a shutter S_2 (Uniblitz model 26L with Uniblitz model SD-122B shutter drive control), capable of producing exposure time from 1 msec to longer times. The laser beam was then sent to the double beam configuration, which was discussed above.

The opening time of the two EOMs results in a temporal window of 300 nsec. For the amplified pulse to always be contained in this time window, the triggering of the EOMs must be synchronized with the triggering of the Nd:YAG laser. A 5 MHz waveform generator (Wavetek model 184) was used as a source for providing the triggering pulses. The Nd:YAG laser was triggered externally using a pulse

from the waveform generator. The synchronising output from the Nd:YAG laser was then used to trigger the EOMs since this pulse precedes the Nd:YAG laser output pulse by 180 nsec. A home made delay generator was used to introduce a delay between the synchronizing pulse and the shutter control unit of S_2 in order to precisely control the number of burn pulses. In this way, the amplified part of the dye laser output will always pass through the EOMs and S_2. The opening time of S_2 was 1 msec.

Figure 3 shows the development of the beam intensity as it passes through the optical elements in the beam path. As shown in Fig. 3-(a), the beam intensity just before the dye amplifiers is constant but after the amplifiers a 15 nsec light pulse is built on top of the dc level (Fig. 3-(b)). Only the amplified part of the beam had higher intensity (15 nsec width) while the intensity of the unamplified part of the beam was unchanged. The beam intensity profile after the EOMs is shown in Fig. 3-(c) and consists of 15 nsec pulse built on the top of the 300 nsec pulse. Because of the high contrast ratio of EOMs, the dc level is suppressed to zero except during 300 nsec open time.

In the same manner as for hole burning with weak to moderate burn intensities, chopper C_3 was turned off while burning a hole. While reading holes, the Nd:YAG laser and EOMs were not triggered and shutter S_2 stayed open.

For the spectral diffusion experiment, the experimental set-up was slightly modified. First, only one pulse is extracted for hole burning and also one for probing. For hole burning with moderate burn intensities 96% of the output of

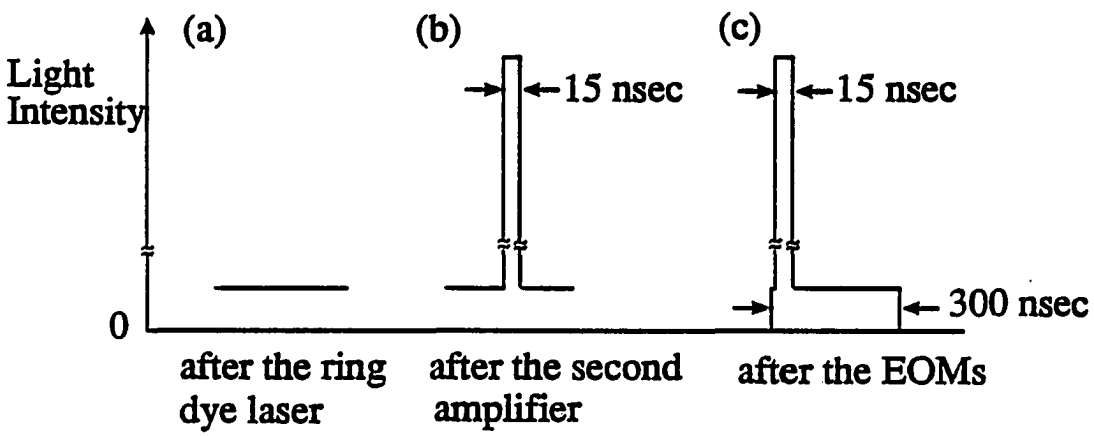

Figure 3. Beam shapes at each stage. (a) There is only dc light just after the ring dye laser. (b) After the second amplifier, 15 nsec high intensity light builds on top of the dc light. (c) After the EOMs, the dc light has a 300 nsec pulse width. Therefore, the 15 nsec pulse is superimposed on top of the 300 nsec pulse

the ring dye laser was extracted using BMS_1 and pulsed by the EOMs to limit pulse widths to 100 nsec or 300 nsec. The amplification stage is used for high peak burn intensities. In the double beam configuration, the burn beam from leg 2 does not have same beam path as the probe beam, rather, the beams cross each other at the sample position. The burn beam after the sample was blocked. However, the intensity of the burn beam in this experiment is at least 5 orders of magnitude larger than that of the probe beam, hence the scattered light from the burn beam interferes with the signal of interest. This interference was overcome using polarizers. The polarization direction of the burn beam is determined by P_3 of the EOMs in leg 2. However, in order to ensure a higher degree of polarization, a second polarizer (same polarization direction as P_3) was located between lens L_3 and M_1. A polarization rotator (45° to the polarization direction of the P_3) was inserted into leg 1 between L_2 and M_2. Then another polarizer (90° to the burn beam and 45° to the probe beam) is inserted between L_8 and BMS_6. Thus the scattered burn beam is prevented from entering the PMT while the probe beam does. The signal from the PMT is directly sent to a digital oscilloscope (LeCroy model 9600A) triggered by the same waveform generator which controls the Nd:YAG laser and S_2. For the spectral diffusion experiment, the probe beam provided by leg 1 must be synchronized with burn beam. This is achieved by having S_1 controlled by the same delay generator as S_2. The resulting time relationship between the burn and probe beam is shown in the Fig. 4. The probe beam has a 3 msec opening time and the burn beam reaches the sample 1 msec

after the opening of the S_1. In this way, the transmission of the sample can be detected between 1 msec before and 2 msec after the burn.

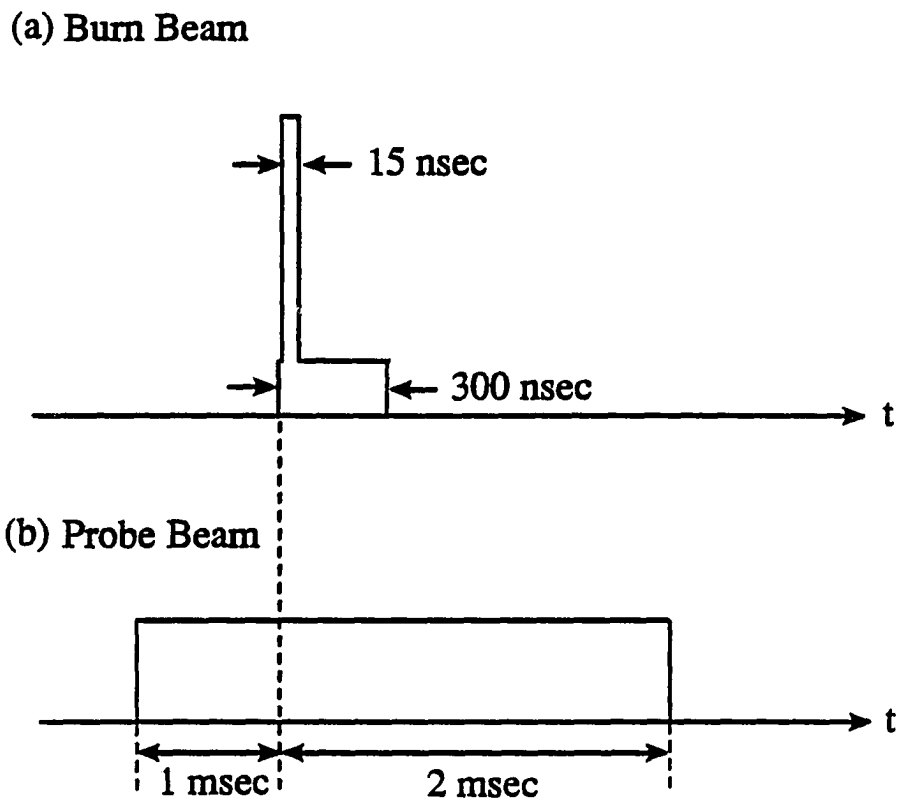

Figure 4. Time relationship between the burn and probe beam. 1 msec after the probe beam reaches the sample, the burn beam irradiates the sample. The probe beam irradiates the sample for 3 msec

RESULTS AND DISCUSSION

Figure 5 shows the difference hole burned spectra of Ox720 in PVOH at 1.6 K for λ_B=645 nm. Each hole was burned with the cw laser and a constant fluence of 2.2 mJ/cm^2 but with different burn intensities. Burn intensities used were (a) 2.2 W/cm^2, (b) 220 mW/cm^2, (c) 22 mW/cm^2, (d) 2.2 mW/cm^2, (e) 220 μW/cm^2 and (f) 22 μW/cm^2, respectively. Although the burn fluence is kept constant, both hole depth and hole area are not conserved. The hole depth clearly increases as the burn time increases over several decades while the hole width slowly increases with burn time. Significent hole broadening is particularly evident in (a).

The relative hole depths (as percent change in optical density) represented in Fig. 5 are plotted as a function of burn time in Fig. 6. The data points plotted as x's (curve (a)) correspond to a constant burn fluence of 2.2 mJ/cm^2 at the sample. The hole depths were proportional to the log of burn time for the burn times used. This trend continues even as the burn intensities were decreased by 5 orders of magnitude. Moerner (43) and Romagnoli et al. (44) have observed similar trends, hole depth burned with constant fluence decreased for burn times between 10 msec and 100 μsec, for free base phthalocyanine in a polyethylene film. They interpreted this as a hole burning bottleneck due to population build up in the triplet state. Walsh and Fayer (45) also reported the results of constant fluence hole burning experiments for pentacene in benzoic acid and analyzed the results in terms of a rate equation model showing hole burning originates from the S_1 state. The data represented by open circles (curve (b)) in Fig. 6 correspond to a constant burn fluence of 22 mJ/cm^2 at the sample. It should be noted that the two data sets fall on the same curve although the burn fluences differed by an order of

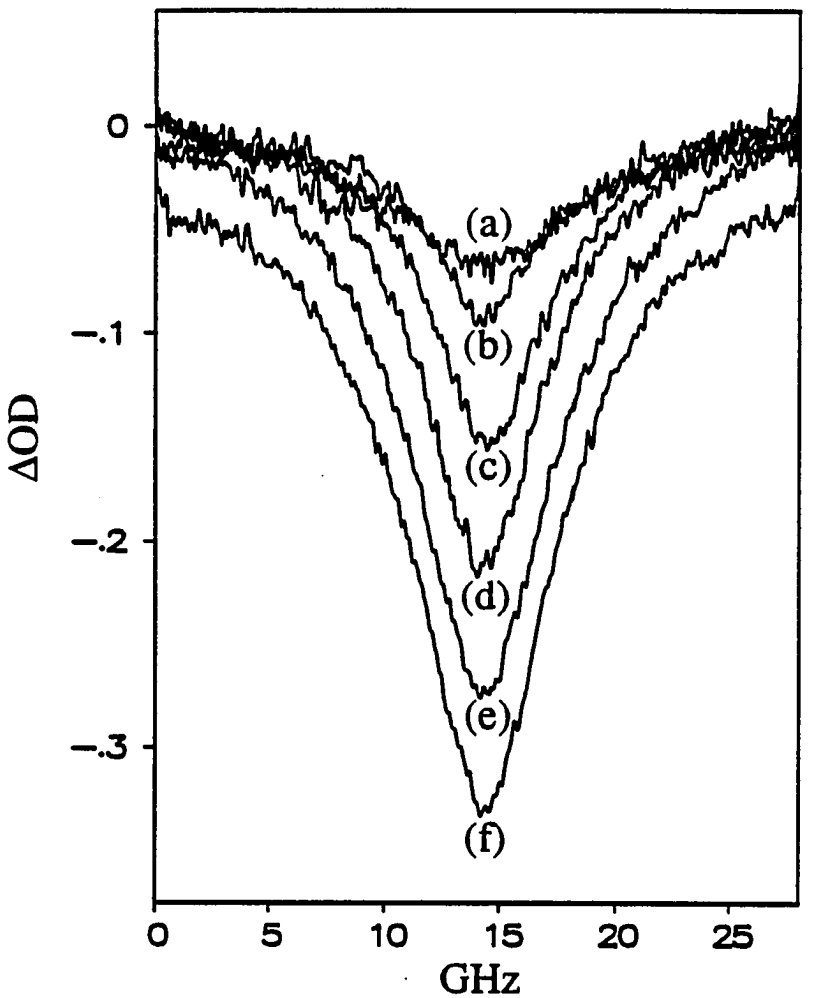

Figure 5. The difference hole burned spectra of Ox720 in PVOH at 1.6 K for λ_B=645 nm. Burn fluence was 2.2 mJ/cm^2 for every hole. Burn intensities used were (a) 2.2 W/cm^2, (b) 220 mW/cm^2, (c) 22 mW/cm^2, (d) 2.2 mW/cm^2, (e) 220 μW/cm^2 and (f) 22 μW/cm^2, respectively

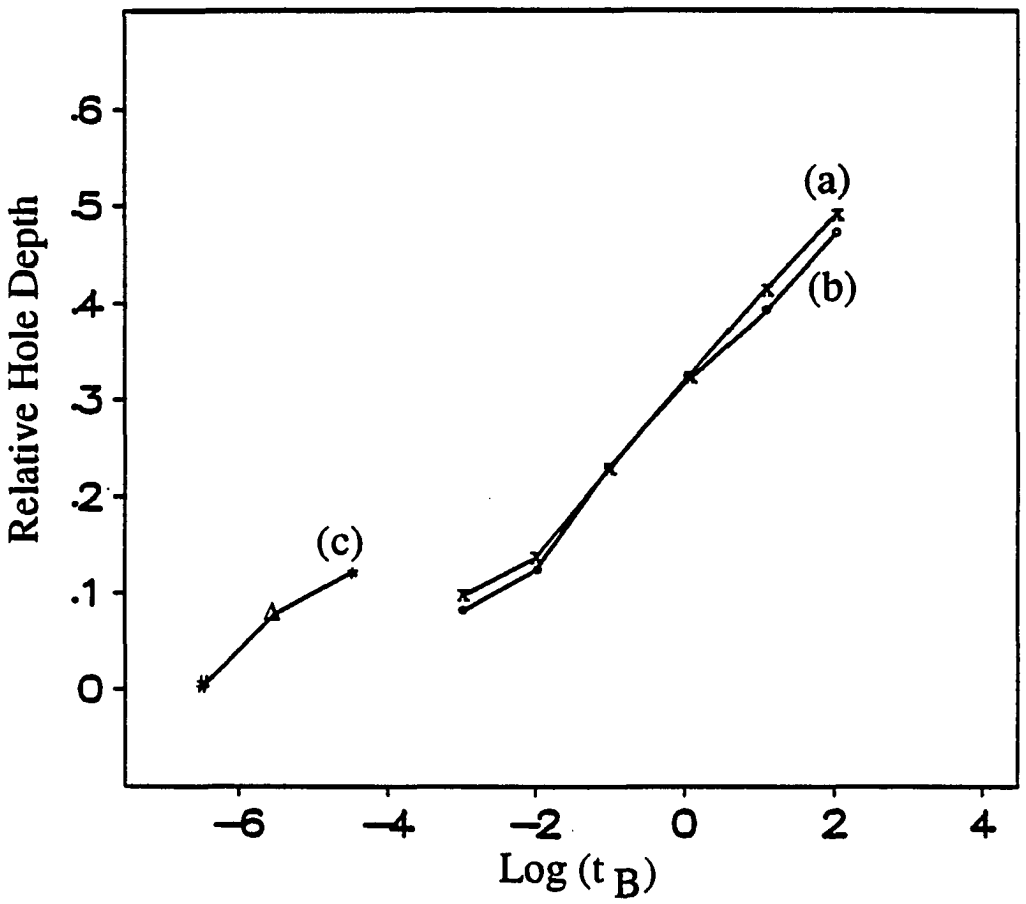

Figure 6. Relative hole depth as a function of the burn time. Burn fluence is 2.2 mJ/cm^2 for (a) and 22 mJ/cm^2 for (b) and (c). (a) and (b) were burned with cw light and (c) were burned with 15 nsec pulses

magnitude. The data for holes burnt with the same fluence, 22 mJ/cm^2, but higher peak intensities is plotted as #, Δ and * (curve (c) in Fig. 6) corresponding to 84000 (#), 8400 (Δ) and 840 (*) W/cm^2, respectively. Amplified burn pulses were used to obtain these data and the number of burn pulses were controlled to give the same burn fluence. These 3 points also show a hole depth proportional to the log of burn time. However when compared to the holes (open circles) burnt with cw light at the same fluence, there is a discontinuity between the data sets. The solid lines in (a), (b) and (c) are linear connections between the points in each set.

The rest of this subsection deals with the following questions: [1] Why is there a slope present in the constant fluence curve (the plot of relative hole depth versus log of burn time for constant burn fluence) and what determines the magnitude of the slope? [2] What does the position of the slope mean in the constant fluence curve? [3] Why is there a discontinuity between the curve (b) and (c) in the Fig. 6 while the burn fluences are same for both? In order to answer these questions, simple rate equation models were considered and tested. In this dissertation two of those models are presented and discussed.

Model 1

This model assumes a three-level system, as shown in Fig. 7-(a). A similar model has been used by others to determine the required photophysical properties for a frequency-domain optical storage system based on hole burning (46) or to find the relaxation rates of nonradiating levels of guest molecules (47). An absorbed

photon excites the system from the ground state $|0\rangle$ to the first excited singlet state $|1\rangle$. There are then these possibilities: decay back to the ground state by stimulated emission with rate $P\sigma$, or by spontaneous emission with decay rate k_1, or hole burning to the product state $|2\rangle$ with rate constant k_2. Here P is the photon flux and σ is the absorption cross section. For this model, the differential changes of the ground-, excited- and product state populations with time are

$$dN_0/dt = P\sigma(N_1-N_0) + k_1N_1 \quad (1)$$

$$dN_1/dt = -P\sigma(N_1-N_0) - (k_1+k_2)N_1 \quad (2)$$

$$dN_2/dt = k_2N_1 \quad (3),$$

where N_0, N_1 and N_2 are the fractional occupations of levels $|0\rangle$, $|1\rangle$ and $|2\rangle$. The solutions to equations (1), (2) and (3) for the initial conditions $N_0(0)=1$ and $N_1(0)=N_2(0)=0$ are:

$$N_0(t) = \exp(-P\sigma k_2t/(2P\sigma+k_1) - N_1(t) \quad (4)$$

$$N_1(t) = [\exp(-P\sigma k_2t/(2P\sigma+k_1)) - \exp(-(2P\sigma+k_1)t)]\, P\sigma/(2P\sigma+k_1) \quad (5)$$

$$N_2(t) = k_2\,[-\{\exp(-P\sigma k_2t\,/(2P\sigma+k_1))\}/k_2 + \{\exp(-(2P\sigma+k_1)t)\}P\sigma/(2P\sigma+k_1)^2 + 1/k_2 - P\sigma/(2P\sigma+k_1)^2] \quad (6)$$

where the approximation $k_2<<k_1$ has been made. The hole burning quantum efficiency is given by $\phi_{HB} = k_2 / (k_1+k_2)$. With the approximation $k_2<<k_1$, k_2 ~

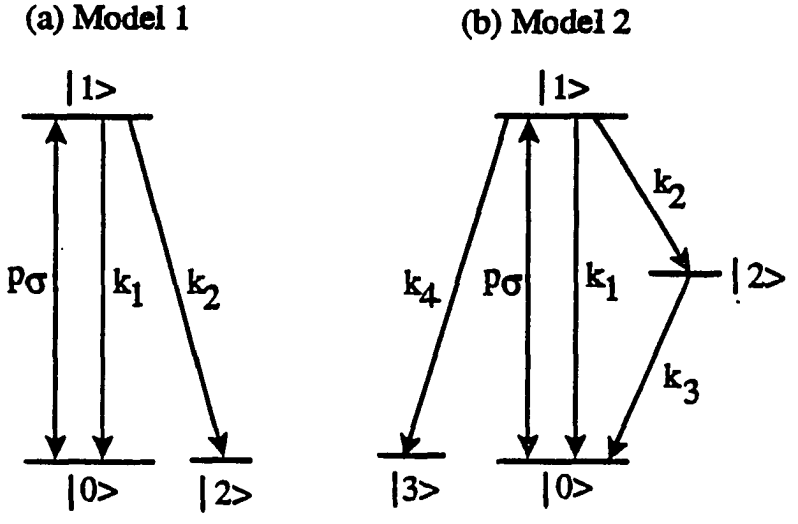

Figure 7. Hole burning kinetic models.

(a) Three-level system consists of the ground state $|0\rangle$, excited electronic state $|1\rangle$ and hole state $|2\rangle$. Hole is produced from $|1\rangle$.

(b) Four-level system consists of the ground $|0\rangle$, excited $|1\rangle$, triplet state $|2\rangle$ and hole state $|3\rangle$. Hole is produced from $|1\rangle$

$\phi_{HB}\, k_1$. After burning a hole for a time, t_B, the hole depth is $H = N_2(t_B) + \phi_{HB} N_1(t_B)$. Here the contribution from the second term is negligible since ϕ_{HB} (10^{-3}~10^{-6}) <<1. Therefore, the hole depth H is given by

$$H \sim N_2(t_B) \sim 1 - \exp(-P\sigma k_1 \phi_{HB} t_B/(2P\sigma+k_1)) \qquad (7)$$

because $P\sigma/(2P\sigma+k_1)^2 << 1$. As this is the simplest model used, it will be discussed in detail to illustrate qualitatively how the hole depth depends on burn intensity at constant burn fluence.

Figure 8 shows calculated hole growth curves (percent hole depth versus log of burn time at a given burn intensity) using Eq. (6) with the inclusion of dispersive kinetics. The effect of the Huang-Rhys factor was not considered in this model calculation. The burn intensities used were (a) 120000 W/cm^2, (b) 1200 W/cm^2, (c) 320 mW/cm^2, (d) 320 μW/cm^2 and (e) 3.8 μW/cm^2, respectively. The other parameters are given in the figure caption. The shapes of the curves are all the same but are displaced in time as the burn intensity is varied. The hole growth curves with the two highest burn intensities ((a) and (b)), however, are identical even though there is a 2 order of magnitude difference in the burn intensities. For these two curves, the stimulated emission rate, $P\sigma$, is $1.4*10^{13}$ s^{-1} and $1.4*10^{11}$ s^{-1}, respectively, which are much larger than k_1. For the hole growth curves (c),(d) and (e), the hole depths are identical for the same burn fluence. These observations can be explained using Eq. (7). When $P\sigma \gg k_1$, as is the case for (a)

and (b) in Fig. 8, the hole depth is $H \sim 1 - \exp(-k_1\phi_{HB}t_B/2)$. Therefore, when $P\sigma \rangle\rangle k_1$, the hole depth will be independent of burn intensity and will be determined only by the burn time. Thus as in Fig. 8, the hole growth curves will be coincident regardless of the burn power, when $P\sigma\rangle\rangle k_1$. This explains the reason why there is a slope present in the constant fluence curve. For $P\sigma << k_1$, as is the case for (c), (d), and (e), the hole depth $H \sim 1 - \exp(-P\sigma\phi_{HB}t_B)$. Thus as the burn intensity changes, the hole growth curve shifts but the same hole depths are expected when the burn fluences are the same. This is often observed in hole growth experiments (48). Other hole growth kinetic models also predict that constant hole depth will result when burn fluences are equal (49,50).

Figure 9 shows the constant fluence curves calculated using Eq. (7) for k_1 variation (Fig. 9-(A)), for ϕ_{HB} variation (Fig. 9-(B)) and for burn fluence variation (Fig. 9-(C)). It is clear from Eq. (7) that for different values of ϕ_{HB} and k_1, the constant fluence curves will shift along the time axis in a manner dependent on their values. From Fig. 8 and Eq. (7), it is expected when $Pt_B \rangle\rangle (\sigma\phi_{HB})^{-1}$, the constant fluence curve for a given system will be identical regardless of fluence and have maximum 100% hole depth at low burn intensities. However, when $Pt_B << (\sigma\phi_{HB})^{-1}$, the maximum hole depth will be smaller than 100% depending on the burn fluence but the slope onsets at the same position. This is shown in Fig. 9-(C).

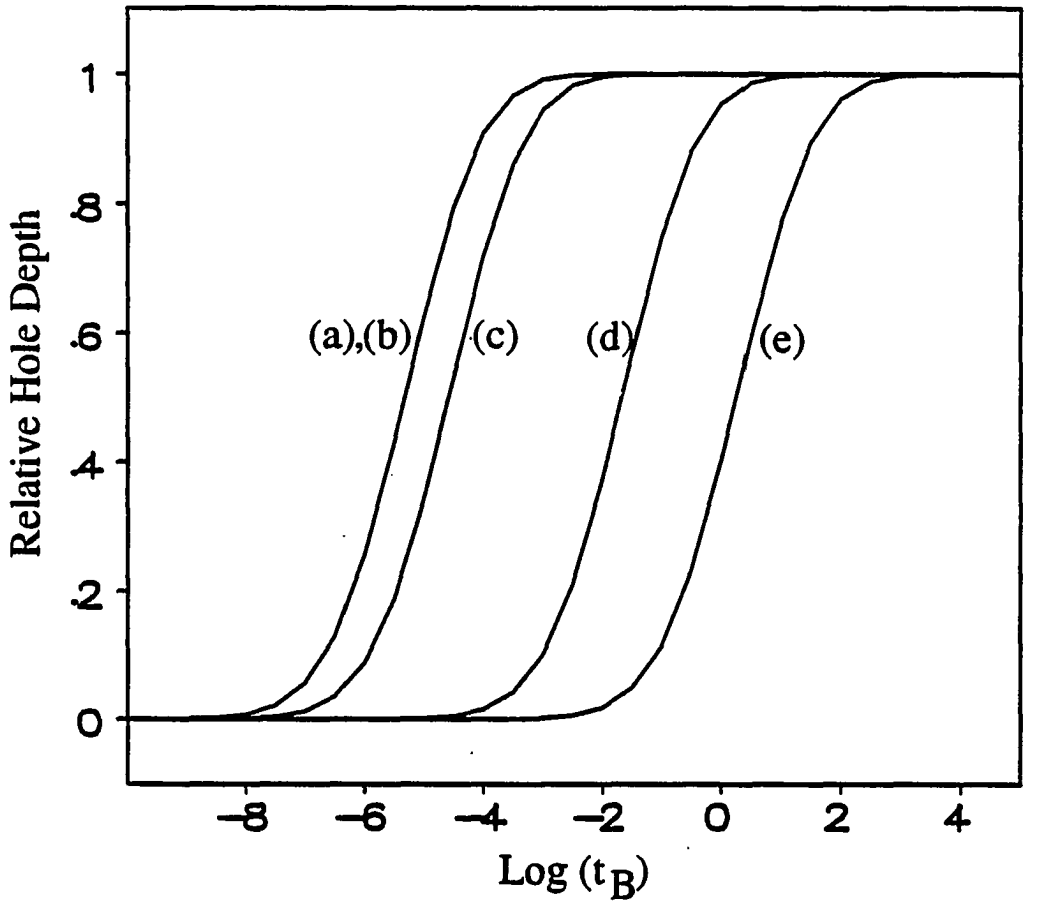

Figure 8. Calculated hole growth curves with different burn intensities. The curves are calculated for model 1. Dispersive kinetics are accounted for: average value of the tunnel parameter λ_0=7.6, width of the distribution σ_2=1.0 and $\Omega_0=10^{12}$ s^{-1}, where Ω_0 is defined by the TLS relaxation rate $R=\Omega_0 \exp(-2\lambda)$. Parameter used were k_1 used was $k_1=3.7*10^8$ s^{-1} and $\sigma=4*10^{-11}$ cm^2. The burn intensities used were (a) 120000 W/cm^2, (b) 1200 W/cm^2, (c) 320 mW/cm^2, (d) 320 μW/cm^2, and (e) 3.8 μW/cm^2

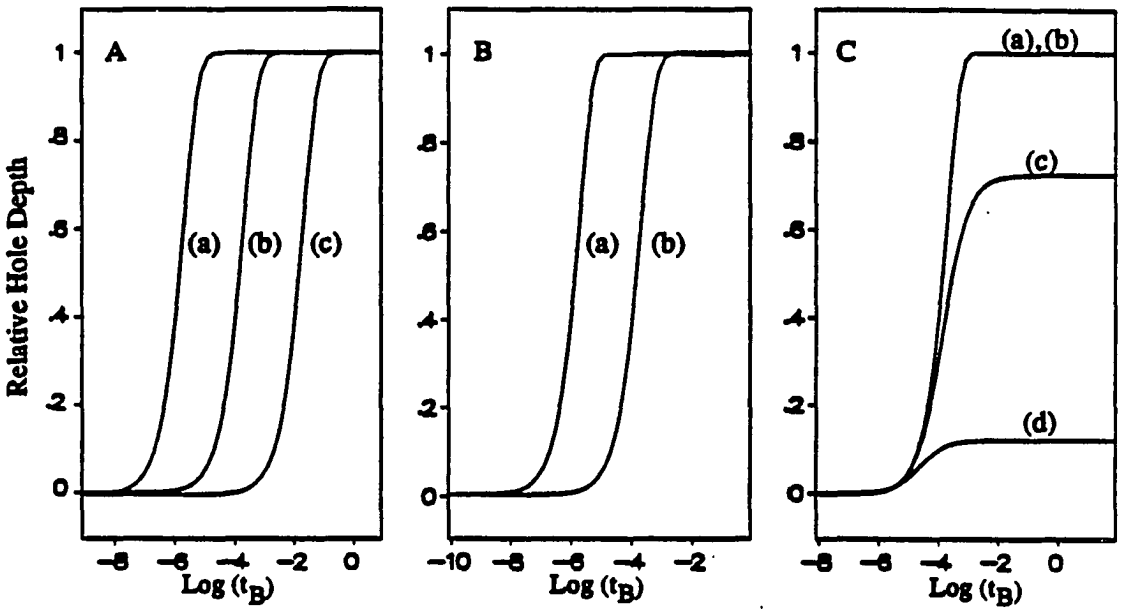

Figure 9. Relative hole depth as a function of time (for constant fluence) in the logarithmic time scale for different k_1 values (A); ϕ_{HB} (B); and for different burn fluences (C). The curves are calculated for model 1. (A) For ϕ_{HB} equal to 0.0001, burn fluence equal to 0.001 W/cm^2, k_1 equals to (a) 10^{10}, (b) 10^8 and (c) 10^6 s^{-1}, respectively. (B) $k_1=10^8$ s^{-1}, burn fluence equal to 0.001 W/cm^2, ϕ_{HB} equals to (a) 0.01 and (b) 0.0001. (C) $k_1=10^8$ s^{-1}, $\phi_{HB}=0.0001$, burn fluence equals to (a) 1.0 J/cm^2, (b) 10 mJ/cm^2, (c) 100 μJ/cm^2 and (d) 10 μJ/cm^2, respectively

Model 2

This model assumes a four-level system, as shown in Fig. 7-(b). Here the hole is again produced from the first excited singlet state, but decay into a metastable (triplet) state is also included. An absorbed photon excites the system from the ground state $|0\rangle$ to the first excited state $|1\rangle$. The state $|1\rangle$ can decay to the metastable triplet state $|2\rangle$ with decay rate, k_2, and then back to the ground state with decay rate, k_3, or can decay to the product state $|3\rangle$ with decay rate, k_4. Or state $|1\rangle$ may also return to the ground state through stimulated emission with rate of $P\sigma$ or through spontaneous emission with a rate of k_1. The hole burning quantum yield is expressed as $\phi_{HB} = k_4 / (k_1+k_2+k_4)$ and triplet quantum yield as $\phi_T = k_2 / (k_1+k_2+k_4)$. Under the approximation of $k_1 \rangle\rangle k_2$ and $k_1 \rangle\rangle k_4$, k_4 is expressed as $k_4 \sim \phi_{HB} k_1$ and k_2 as $k_2 \sim \phi_T k_1$.

The rate equations are as follows:

$$dN_0/dt = -P\sigma N_0 + (P\sigma+k_1)N_1 + k_3N_2 \quad (8)$$

$$dN_1/dt = P\sigma N_0 - (P\sigma+k_1+k_2+k_4)N_1 \quad (9)$$

$$dN_2/dt = k_2N_1 - k_3N_2 \quad (10)$$

$$dN_3/dt = k_4N_1 \quad (11),$$

where N_0, N_1, N_2 and N_3 are the fractional occupations of levels $|0\rangle$, $|1\rangle$, $|2\rangle$ and $|3\rangle$. Here the initial conditions are $N_0(0)=1$ and $N_1(0)=N_2(0)=N_3(0)=0$. In this system, the triplet state, $|2\rangle$, serves as a population bottleneck. Similar models

have been presented by de Vries and Wiersma (51) to find T_2, the dephasing time, in the steady state approximation and by Walsh and Fayer (45) to explain the hole depth dependence on the burning time at constant fluence. The time dependent solution of these equations is obtained using the Laplace transform technique and theory of partial fractions. In applying this technique, the roots of the third order equation were calculated using Cardan's formular (54). Because the solutions of the third order equation are not obtained in analytic form, this model is not analysed in detail here. However, the model calculations (not shown) show trends similar to model 1 when ϕ_{HB}, k_1, k_2, burn intensity and burn fluence are varied.

In addition to these two models, a third model in which the persistent hole burning occurs from the triplet state instead of singlet was considered. This model shows results similar to model 2 but the saturation of the first excited state does not effect the hole burning. A similar model has been analyzed by Romagnoli et al. (49). In their model it was assumed that direct decay from the excited state to the ground state is negligible and the triplet quantum yield is 1. However for the present experimental system, stimulated and spontaneous emission can not be neglected because of the relatively small triplet quantum yield of Ox720 and the high burn intensities used here. Therefore this model was not considered in analyzing the experimental data. Julmukhambetov and Osad'ko (53) and Gorokhovskii and Kikas (54) have reported a more complicated model which includes hole burning from every possible level to analyze the effect of the intensity of the burning light on the kinetics and shape of the holes. The theories are

restricted by the intensity of a cw source at which stimulated transitions are less probable than spontaneous transitions.

It is known that the measured fluorescent decay constant from the first excited state singlet state of Oxazine 720 is $3.7*10^{8}$ s^{-1} (55), the absorption cross section is $4*10^{-11}$ cm^2, the Huang-Rhys factor is 0.45 and the average hole burning quantum efficiency is 0.005 (48). The triplet quantum yield and triplet state lifetime of Ox720 are not known. However, it is known that the triplet quantum yield of cresyl violet and nile blue in ethanol at room temperature are both 0.04±0.02 (56). Because of their structural similarities to Ox720, it is assumed that the triplet quantum yield of Ox720 in PVOH is also ~0.04. Therefore $k_1 \sim (1-\phi_T-\phi_{HB})K \sim 3.55*10^{8}$ s^{-1} and $k_2 \sim \phi_T k_1 \sim 1.5*10^{7}$ s^{-1}. The only unknown parameter is the lifetime of the triplet state $|2\rangle$.

The constant fluence (2.2 mJ/cm^2) curves calculated with above parameters are shown in Fig. 10. It is assumed that cw light is used to burn holes. The effect of the Huang-Rhys factor was included. The constant fluence curves (a) and (b) were calculated to compare with the experimental curve (c) using the models 1 and 2, repectively. The dispersive kinetics were not included in these calculations because computation time required was prohibitive. Curve (a) in Fig. 10 is shifted far to the left compared with (c). In model 1, there is no parameter that could be varied to make the curve shift to the right. Thus it seems this model is too simple to explain the observed experimental data. Curve (b) in Fig. 10 consists of 3 plateaus, one at very high burn intensity (very short burn time), one at moderate

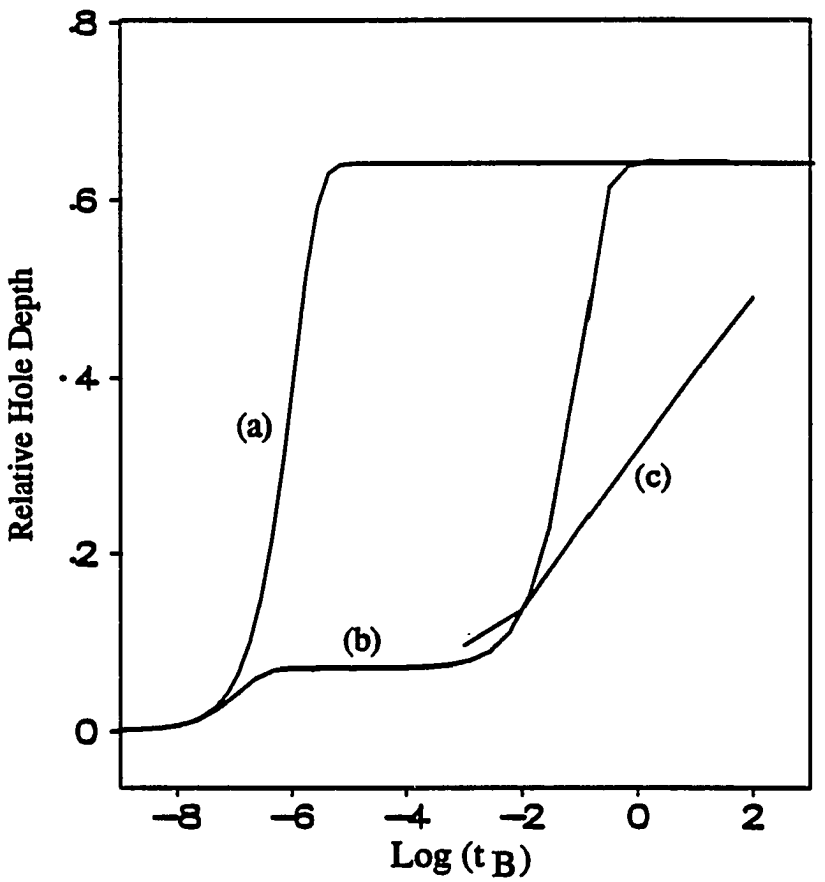

Figure 10. Constant fluence curves. The constant fluence curves (a) and (b) were calculated for comparison with the experimental curve (c) using the models 1 and 2 in Fig. 7, respectively. Parameters used were Burn fluence 2.2 mJ/cm^2, $k_1 = 3.7*10^8$ s^{-1}, ϕ_{HB}=0.005, ϕ_T=0.04 and $\sigma=4*10^{-11}$ cm^2. The triplet lifetime 10 msec was obtained from the fit

burn intensity and one at low burn intensity (long burn time). The plateau in the very short burn time ranges ($t_B < 1/K$, where $K = (k_1+k_2+k_4)$) results from the saturation of the excited state. After a time 1/K, the excited state starts relaxing to either of the triplet state or hole state. For t_B longer than 1/K, the hole and triplet state populations begin to build-up. The plateau at the middle results from the saturation of the triplet state and the ratio of the hole depth to the triplet state population at the end of the burning is governed by the ϕ_{HB}/ϕ_T in this region. Although ϕ_T~0.04, the bottleneck effect is very large when the burn intensity is large. The duration of the second plateau depends most strongly on the relative lifetime of the states, $|1\rangle$ and $|2\rangle$. As the burn intensities get weaker, the triplet build-up is smaller. Thus the probability of burning a hole is larger until finally a 100% hole results. This is the reason for the third plateau.

As far as the position of the curves is concerned, model 2 is consistent with the experimental data (c) if a triplet lifetime of 10 msec is used. Littau and Fayer (27) reported lifetimes for the individual triplet sublevels of cresyl violet in deuterated ethanol which were 80 μsec, 1.5 msec and 60 msec with relative populations of 4:2:5. In the hole burning experiment, the triplet state with longest lifetime (e.g., 60 msec for cresyl violet) should dominate the bottleneck effect. Therefore the value of the triplet state lifetime of the Ox720 in PVOH, used in the calculations does not seem to be unreasonable given the similarity of the chemical structures of Ox720 and cresyl violet.

From Fig. 10, it is seen that slope of the experimental constant fluence curve (c) is very small relative to the calculated slope. This difference in the slopes may be explained by considering dispersive kinetics (48,49). Because there is a distribution of the TLS relaxation rates, the hole burning rate also has a distribution. This will result in the hole growth starting earlier and lasting longer than in the nondispersive case. As the distribution of the relaxation rate becomes larger, the slope of the constant fluence curve will be smaller. In ref.(48), the dispersive kinetic parameters for Ox720 in PVOH were obtained. The parameters were λ_0=7.6 (average of the tunnel parameter λ), σ_2=1.0 (width of the distribution of λ) and Ω_0 =10*10^{12} s^{-1} where the Ω_0 is defined by TLS relaxation rate R = Ω_0 exp(-2λ) (48,49).

Another explanation of the differences in the slopes is the hole saturation broadening. As the hole gets deeper, hole burning through ZPL becomes saturated and molecules which absorb light through the tail of their ZPL start to burn. This results in broadening of the hole and slowing down of the hole growth rates. In Fig. 5, it is shown that the hole width (except (a)) slowly increases as hole depth becomes larger. However, this effect was not included in the calculations. Thus hole saturation broadening may partly explain the differences between the experimental and calculated slopes.

When a hole is burnt with high intensity, the hole can be broadened by several mechanisms: thermal broadening by local heating, power broadening and broadening by population of the bottleneck triplet state. However, these types of

hole broadening would make the differences in slopes larger because normally these effects are accompanied by reduction of hole depth at short burn times (high burn intensity) on the constant fluence curves. In Fig. 5, it is shown that the hole burned with 2.2 W/cm^2 is broader than the hole burned with 220 mW/cm^2 while the hole depth is smaller. This clearly indicates that burn intensity of 2.2 W/cm^2 results in significant hole broadening by one or a combination of these mechanisms. These hole broadening processes are further discussed below.

With typical power levels on the order of ~mW focussed in small spots, large temperature increases can occur, depending on the thermal conductivity of the medium. If it is assumed that the specific heat, density and thermal conductivity of PVOH is similar to polyethylene, then the the final temperature of the sample irradiated with 84,000 W/cm^2 for 15 nsec is expected to be ~6 K according to Schellenberg's calculations (57). Here it is assumed that 90% of the absorbed energy is radiated by the fluorescence, the OD of the sample is 0.7 and initial temperature was 1.6K. From a T^{α} (α=1.3) power law it is expected that the hole will be broadened by about a factor of 6 due to local heating. From the magnitude of broadening observed, it is concluded that thermal broadening is negligible for hole burning with the cw laser intensities used in this experiment.

Hole broadening due to power broadening and to triplet state population becomes significant as burn intensities become larger. When the burn intensity is 84,000 W/cm^2 (the highest intensity used in this experiment), the corresponding Rabi frequency ($\chi=\mu E_0/\hbar$) is ~30 GHz. Here μ is the electric transition dipole

moment and E_0 is the magnitude of the electric field. $1/\chi$ is considered as the characteristic time of the coupling between the molecule and the field. For a three-level system such as model 2 in Fig. 7 without a persistent hole state (level $|3\rangle$), the full width at half maximum (FWHM) of a hole due to population bottleneck hole burning would depend on the light intensity (51) as

$$\Gamma_{hole} = (\pi T_2)^{-1} [\, 1 + \sqrt{(1 + K^2 T_2^2)}\,] \qquad (12)$$

where K is defined as $K^2 = \chi^2 (2+A) / 2T_2K_2$ and includes effects of both power saturation and triplet bottleneck hole burning. Here K_2 is the fluorescence decay time ($K_2 = k_1 + \Sigma(k_2)_i$), T_2 is the dephasing time and i labels the spin level of the triplet state. A is defined by $A = \Sigma(k_2/k_3)_i$. Thus the power dependence of the width of a three-level bottleneck hole is much stronger than that of a two-level population hole by a factor of $\sqrt{((2+A)/2)}$ when high intensity light is used. By extrapolating the hole width to zero power, the result that $\Gamma_{hole} = 2 / \pi T_2 = 2\gamma$ is obtained.

From Eq. (12), one can determine that for Ox720 in PVOH holes will be broadened by a factor of ~10 when the burn power is larger than ~50 W/cm^2 which corresponds to hole burning with amplified pulses (curve (c) in Fig. 6). The combined effects of this and thermal broadening predict that no narrow hole will be observed. However, narrow holes were observed (not shown) when 8400 and 840 W/cm^2 were used to burn holes. These narrow holes resulted from burning by the

300 nsec pulses on which the amplified pulses are built as shown in Fig. 3-(c). The intensity of these 300 nsec pulse is near by 5 orders of magnitude smaller than those of the amplified pulses, and the fluences are a factor of 5000 smaller. However, the fluences for burning with 300 nsec were also kept constant. With these burn intensities and burn fluences the model calculations using model 2 have been performed. The calculation shows hole depth trends very similar to those in Fig. 6-(c).

To study the optical dephasing as a function of the observation time using persistent hole burning, experiments were performed by varying the burn intensities from the 10 mW/cm^2 to 84000 W/cm^2. Burn times of 15 nsec, 100 nsec, 300 nsec were used. However none of the combinations used produced observable persistent holes. As mentioned before, when hole is burned with amplified pulses significant hole broadening occurs. Thus population bottleneck, thermal and power broadening prevented observing spectral diffusion when holes are burned with the high burn intensities ($\geq$100 mW/cm^2). For burn intensities smaller than 100 mW/cm^2, the longest burn time used was 300 nsec which is limited by the opening time of the EOMs. This gives the maximum fluences of 30 nJ/cm^2 which is much smaller than the burn fluence (~170nJ/cm^2) required to burn a ~5% persistent hole with ~40 nW/cm^2 (48). This explains why spectral diffusion in the ~μsec range was not observed in this system using the persistent hole burning. However using the persistent hole burning technique,.spectral diffusion in the ~msec range can be observable by burning a hole with ~100 μsec pulses. Burning a hole with 100

mW/cm^2 for 100 μsec gives a fluence of 10 $\mu J/cm^2$ which would result in ~30% hole depth when hole is produced with same fluence but with 400 nW/cm^2 (48). However, from Fig. 6 it is noted that the burn time 100 μsec is located near the lower end of the slope. From the Figs. 5, 6 and 9-(c), it is easily seen that hole depth will not be very deep (≤10%).

Spectral diffusion in the ~μsec range can be observable using the transient hole burning. However in this case burn intensities low enough to avoid hole broadening should be used. Preliminary calculations using model 2 predict that the transient hole depth of Ox720 in PVOH will be ~10% when hole is burned with 50mW/cm^2 for 300 nsec.

Spectral diffusion experiment in a time range from 300 nsec to 10 μsec will be continued by this group.

CONCLUSIONS

The extent of hole burning of Ox720 in PVOH has been studied as a function of burn intensity for fixed burn fluences. It was shown that the hole depth increased logarithmically with burn time over several decades. Although the triple quantum yield of Ox720 is as low as 0.04, it is observed that the triplet bottleneck effect plays an important role in hole burning (both on hole broadening and hole growth) when burn intensity becomes large. By comparing the calculated and measured constant fluence curves, the longest lifetime of the spin sublevel in the triplet state was obtained.

The large differences in the magnitude of the slopes between the measured and calculated constant fluence curves may be explained mostly by the effect of dispersive kinetics and partly by hole saturation broadening.

The discontinuity of the constant fluence curves between (b) and (c) in the Fig. 6 resulted from the hole burning by the 300 nsec pulses on which the amplified pulses build. The holes burned with the amplified pulses were not observed because of the significant broadening by the local heating and power broadening.

Spectral difussion in ~μsec range using the persistent hole burning was not observed in the Ox720 in PVOH. However it may be observed when the transient hole burning is used.

REFERENCES

1. Phillips, W.A., Ed., Amorphous Solids, Springer-Verlag: Berlin, 1981.
2. Phillips, W.A. J. Low Temp. Phys. 1972, 7, 351.
3. Anderson, P.W.; Haperin, B.I.; Varmar, C.M. Phil. Mag. 1972, 25, 1.
4. Molenkamp, L.W.; Wiersma, D.A. J. Chem. Phys. 1985, 83, 1.
5. Patterson F.G.; Wilson, W.L.; Lee, H.W.H.; Fayer, M.D. Chem. Phys. Lett. 1984, 110, 7.
6. Molenkamp, L.W.; Wiersma, D.A. J. Chem. Phys. 1984, 80, 3054.
7. Hegarty, J.M.; Broer, M.M.; Golding, B.; Simpson, J.R.; MacChesney, J.B. Phys. Rev. Lett. 1983, 52, 2033.
8. Walsh, C.A.; Berg, M.; Narasimhan, L.R.; Fayer, M.D. J. Chem. Phys. 1987, 86, 77.
9. Thissen, H.P.H.; Dicker, A.I.M.; Völker, S. Chem. Phys. Lett. 1982, 92, 7.
10. Thissen, H.P.H.; van den Berg, R.E.; Völker, S.; Port, H. Chem. Phys. Lett. 1983, 97, 295.
11. Thissen, H.P.H.; van den Berg, R.E.; Völker, S. Chem. Phys. Lett. 1985, 120, 503.
12. Burkhalter, F.A.; Suter, G.W.; Wild, U.P.; Samoilenko, V.D.; Rasumova, N.V.; Personov, R.I. Chem. Phys. Lett. 1983, 94, 483.
13. Breinl, W.; Friedrich, J.; Haarer, D. Phys. Rev. B 1986, 34, 7271.
14. Lee, H.W.H.; Huston, A.L.; Gehrtz, M.; Moerner, W.E. Chem. Phys. Lett. 1985, 114, 491.

15. Carter, T.P.; Fearey, B.L.; Hayes, J.M.; Small, G.J. Chem. Phys. Lett. 1983, 102, 272.

16. van der Berg, R.; Völker, S. Chem. Phys. Lett. 1986, 127, 525.

17. Jankowiak, R.; Bässler, H. Chem. Phys. Lett. 1983, 95, 124.

18. Jankowiak, R.; Bässler, H., Silbey, R. Chem. Phys. Lett. 1986, 125, 139.

19. van der Berg, R.E.; Völker, S. J. Lumin. 1987, 38, 25.

20. Macfarlane, R.M.; Shelby, R.M. Opt. Commun. 1983, 45, 46.

21. Hayes, J.M.; Jankowiak, R.; Small, G.J. Persistent Spectral Hole-Burning: Science and Applications, Moerner, W.E., Ed., Springer-Verlag: Berlin, 1988.

22. Walsh, C.A.; Berg, M.; Narasimhan, L.R.; Fayer, M.D. Chem. Phys. Lett. 1986, 130, 6.

23. Walsh, C.A.; Berg, M.; Narasimhan, L.R.; Littau, K.A.; Fayer, M.D. Chem. Phys. Lett. 1987, 139, 66.

24. Narasimhan, L.R.; Pack, D.W.; Fayer, M.D. Chem. Phys. Lett. 1988, 152, 287.

25. Littau, K.A.; Bai, Y.S.; Fayer, M.D. Chem. Phys. Lett. 1989, 159, 1.

26. Littau, K.A.; Fayer, M.D. submitted to Chem. Phys. Lett.

27. van der Zaag, P.J.; Galaup, J.P.; Völker, S. Chem. Phys. Lett. 1990, 166, 263.

28. Breinl, W.; Friedrich, J.; Haarer, D. J. Chem. Phys. 1984, 81, 3915.

29. Meiler, J.; Friedrich, J. Chem. Phys. Lett. 1987, 134, 263.

30. Rebane, K.K. Cryst. Lett. Def. and Amorph. Mat. 1985, 12, 427.

31. Gorokhovskii, A.A.; Rebane, L.A. Izv. Akad. Nauk SSSR, Ser. Fiz. 1980, 44, 859.

32. Nakatsuka, H.; Inouye, K.; Uemura, S.; Yano, R. Chem. Phys. Lett. 1990, 171, 3.

33. Jankowiak, R.; Shu,L.; Kenney, M.J.; Small, G.J. J. Lumin. 1987, 36, 293.

34. Jankowiak, R.; Small, G.J. Science 1987, 237, 618.

35. Friedrich, J.; Haarer, D. In Optical Spectroscopy of Glasses Zschokke, I., Ed., D. Reidel Publishing Company: Dordrecht, 1986.

36. Knaak, W.; Meissner, M. In Phonon Scattering in Condensed Matter, Solid State Sciences, Eisenmenger, W., Lassman, K., Döttinger, S., Eds., Springer: Berlin, 1984, vol.51, p.416.

37. Loponen, M.T.; Dynes, R.C.; Narayanamurti, V.; Garno, J.P. Phys. Rev. B 1982, 25, 1161.

38. Jankowiak, R.; Hayes, J.M.; Small, G.J. Phys. Rev. B 1988, 38, 2084.

39. Fearey, B.L. Ph. D. Dissertation, Iowa State University, 1986.

40. Carter, T. P. Ph. D. Dissertation, Iowa State University, 1986.

41. Fearey, B. L.; Carter, T. P.; Small, G. J. J. Phys. Chem. 1983, 87, 3590.

42. Drell, P.; Chu, S. Optics. Commun., 1979, 28, 343.

43. Moerner, W.E. In Proceedings of Int. Conf.:Lasers'83, Society for Optical and Quantum Electronics, McLean, Va., 1984.

44. Romagnoli, M.; Moerner,W.E.; Schellenberg, F.M.; Levenson, M.D.; Bjorklund, G.C. J. Opt. Soc. Am. B 1984, 1, 341.

45. Walsh, C.A.; Fayer, M.D. J. Lumin. 1985, 34, 37.

46. Moerner, W.E.; Levenson, M.D. J. Opt. Soc. Am. B 1985, 2, 915.

47. Osad'ko, I.S.; Soldatov, S.L. Chem. Phys. 1988, 128, 125.

48. Kenney, M.J.; Jankowiak, R.; Small, G.J. Chem. Phys. in press.

49. Jankowiak, R.; Shu,L.; Kenney, M.J.; Small, G.J. J. Lumin. 1987, 36, 293.

50. Rebane, K.K., Rebane, L.A. In Persistent Spectral Hole-Burning: Science and Applications, Moerner, W.E., Ed., Springer-Verlag: Berlin, 1988.

51. de Vries, H.; Wiersma, D.A. J. Chem. Phys. 1980, 72, 1851.

52. Dehn, E. Algebraic Equations Columbia University Press: New York, 1930.

53. Julmukhambetov, A.U.; Osad'ko, I.S. Chem. Phys. 1983, 77, 247.

54. Gorokhovskii, A.A.; Kikas, Y.V. Zh. Prikl. Spektro. 1978, 28, 832.

55. Causgrove, T.P.; Struve, W.S. Iowa State University, 1986, unpublished results.

56. Lessing, H.E.; Richardt, D.; Von Jena, A. J. Mol. Struct. 1982, 84, 281.

57. Schellenberg F.M. IBM Research Report, San Jose, 1985.

SECTION III.

PHOTOCHEMICAL HOLE BURNING STUDY OF BACTERIORHODOPSIN

INTRODUCTION

Bacteriorhodopsin (BR) is the only protein of the purple membrane of the bacterium *Halobacterium Halobium* that grows in the natural brines where NaCl concentration is near saturation. This bacterium uses oxygen to synthesize ATP under aerobic conditions. When grown under anaerobic conditions, it develops a BR containing purple membrane that converts light energy to chemical potential associated with a gradient of hydrogen ions across the membrane. This chemical potential is used to synthesize ATP (1).

X-ray diffraction studies have shown that (2-4) BR in the membrane forms a rigid two-dimensional hexagonal lattice with a 63 A long unit cell. Electron diffraction studies have shown that (5,6) each protein molecule consists of seven α-helical rods which are about 40 A long, 10 A apart with three of them perpendicular to and four of them slightly tilted with respect to the membrane plane. Bacteriorhodopsin exists as a trimer around one of the three fold axes (2,3,6). Thus there is a strong protein-protein interaction due to the large contact area (7). Linear dichroism measurements (8) have shown that there is no mobility of BR in the membrane on a time scale of ~60 min while rhodopsin located in the viscous disk membrane has both rotational and translational mobility (9). The amino acid sequence of BR was determined by Khorana et al. (10) and established that BR consists of 248 amino acids with ~70% of the amino acid chain hydrophobic. Bacteriorhodopsin has molecular weight of 26,500 (10,11) and consists of a bacterioopsin (BO) and a retinal that is bound via a protonated Schiff base linkage to lysine-216 of BO (11,12). Retinal is tilted at an angle of about 20° to the plane of the membrane (13,14). Bacteriorhodopsin exists in two stable

forms, BR_{570} which contains all-*trans* retinal and BR^{C} which contains 13-*cis* retinal. Both forms are present in almost equal amounts in the dark adapted form while only BR_{570} is present in the light-adapted form (15,16).

Figure 1 shows the all-*trans* retinal chromophore in BR. Photoisomerization occurs about the C_{13}=C_{14} bond.

The most important features of the BR photocycle are summarized in Fig. 2. In Fig. 2, solid arrows indicate thermal reaction and dotted arrows photochemical reaction. The different states of the chromophore are represented by capital letters and by their absorption maxima in nm. A photocycle model of BR was originally proposed by Lozier et al. (17). In that model four observable ground states, K_{610}, L_{550}, M_{412} and O_{640}, were used. The intermediates of the BR photocycle were studied by low temperature spectrophotometry (18-21). The sequence of intermediates in the BR photocycle is very similar to that of rhodopsin although BR photochemistry is cyclic and does not include the detachment of retinal from the BO (22) while the rhodopsin photocycle does (15).

A batho-*trans*-BR (K_{610}) is formed below -120° C and even at liquid helium temperatures by irradiation of BR_{570} (18-21). Batho-*trans*-BR does not mean that it contains all-*trans* retinal but rather that it originates from all-*trans*-BR. It has been shown by low temperature spectrophotometry (18-21) and by pulsed laser photolysis at room temperature (23,24) that K_{610} and BR_{570} are interconvertible, depending on the wavelength of the irradiating light. Lumi-*trans*-BR (L_{550}) is produced by warming K_{610} above -120° C. Meta-*trans*-BR (M_{412}) can be observed by warming L_{550} above -90° C. But depending on the temperature ,e.g., <-90° C all of L_{550} can be directly converted to BR_{570}. In addition to the above

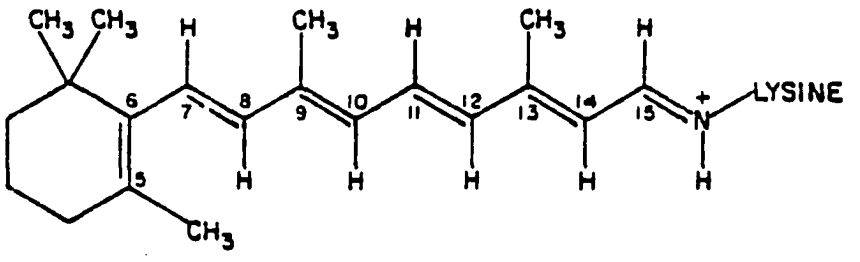

Figure 1. The all-*trans* retinal chromophore in bacteriorhodopsin is linked to a lysine residue of the protein by a protonated Schiff base linkage. Photoisomerization occurs about the C_{13}=C_{14} bond

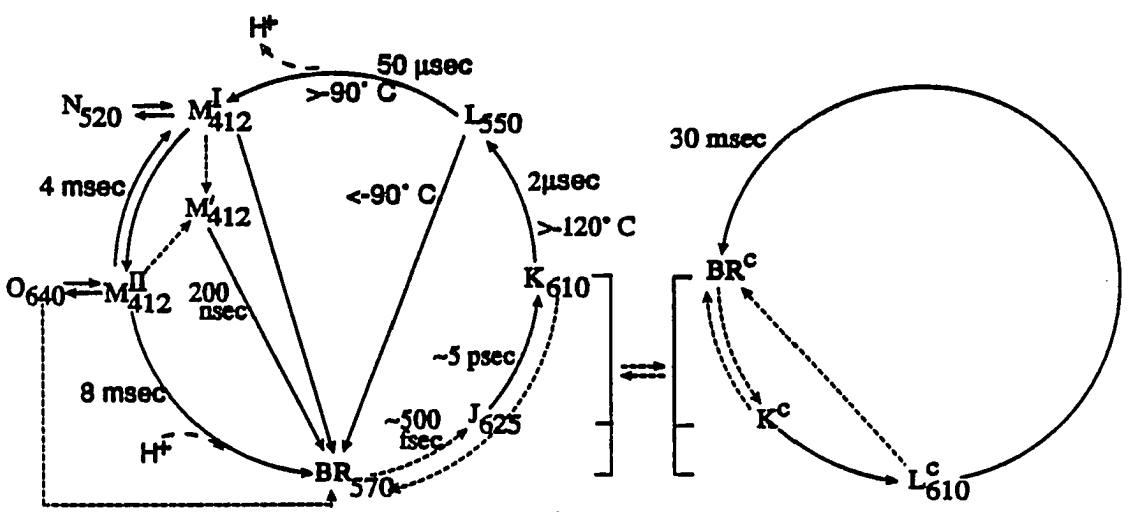

Figure 2 Two photocycle of BR. Left: BR_{570} (the light-adapted form), Right: BR^c (50% of dark-adapted form). Photochemical reactions are presented by dotted arrows and thermal reactions by solid arrows with transition temperatures of the intermediates

intermediates, N_{520} and O_{640} were also observed in photolysis experiments (1,17,25).

The photocycle of 13-*cis* BR of dark adapted BR is different from that of all-*trans* BR. Tokunaga et al. (26), by studies of a photostationary mixture at 77 K, showed that BR^c has a different primary bathoproduct K^c. Kalisky et al. (27) and Sperling et al. (16) observed a long-lived intermediate of BR^c (L^c) generated from K^c by laser photolysis at higher temperature.

Marcus et al. (28,29) and Campion et. al (30) observed that proton release from the shiff base linkage of retinal occurs during the transition between L_{550} and M_{412} by using the resonance Raman technique.

Kaufman et al. (31) observed an absorption increase at 635 nm with 6 psec rise time (laser limited) at room temperature and noted that its absorption spectrum was nearly same as that of K on a μsec time scale (17). In 1978, Ippen et al. (32) reported that a bathochromic intermediate occurs in 1.0±0.5 psec. This means that batho intermediate of BR appears rapidly after the excitation, like that of rhodopsin.

Later it was demonstrated that J_{625} (the precursor to K_{610}) forms in ~500 fsec and relaxes to K_{610} in 3~5 psec (33-36). Also Polland et al. (35) and Nuss et al. (33) observed that K_{610} decays to L_{550} in ~μsec time scale.

The detachment of the proton of the Schiff base linkage is observed during the transition of L_{550} to M_{412} (37) and causes a significant blue shift of the absorption spectrum of M_{412} (38,39).

Resonance Raman spectroscopy has played a very important role in identifying intermediates in the BR cycle. It is now believed that the primary photocycle event involves a trans to cis isomerization (1). It was Pettei et al. (40) who first postulated that the transient isomerization from all-*trans* to 13-*cis* retinal occurs during the BR_{570} photocycle by extracting the chromophore of M_{412}. The 13-*cis* retinal of M_{412} has been confirmed by resonance Raman spectroscopy (41). It was also observed that K_{610} contains 13-*cis* retinal protonated Schiff base linkage at room temperature (42) and 77 K (43,44). In 1988 Mathies et al. (45,46) and Dobler et al. (47) used femtosecond spectroscopy to directly determine that the 13-*trans* to 13-*cis* isomerization of retinal occurs in 100-200 fsec on the excited state potential surface.

Thus lifetime broadening (~50 cm^{-1}) cannot account for the large spectral width of BR_{570} (FWHM~2600 cm^{-1} at 1.6 K). The large absorption width could be inhomogeneously broadened. One way to determine the homogeneous and inhomogeneous contribution to the absorption band width is through spectral the hole burning studies. There was one unsuccessful spectral hole burning attempt of BR (48) in water/glycerol glasses at 1 K by Wolfrum and Haarer at IBM. The first report of low temperature optical hole burning of BR is presented in the paper I of this section of the dissertation. The results are discussed in terms of the degree of homogeneous broadening and broadening mechanisms.

EXPERIMENTAL APPARATUS

Figure 3 shows the burning laser system and double-beam spectrometer which is used in part of this experiment. No sharp hole was observed in preliminary experiment. Therefore, it is necessary to take a wide range scanning (~ tens of nm) to observe whether broad hole is present. Because the ring dye laser is tunable up to only 30 GHz, another light source having better tunability is required for reading holes. If in Fig. 1 of Section II, the probe beam is replaced by a spectrometer and leg 2 is ignored, it is identical to Fig. 3 in this section.

In order to provide a convenient and reproducible method of burning and probing holes in the exactly the same part of the sample by using two different beam paths, lens L_6 was mounted on a translational stage together with a 90° prism situated so that the stage could be reproducibly positioned to allow the laser beam to be sent through the sample in precisely the opposite direction of the probe beam. The prism is situated in the beam path for hole burning while L_6 was for hole reading. In this case, burn beam size was always maintained larger than probe beam size at the sample position because the burn beam is not focussed at the sample while probe beam was.

The light source used for probing the hole was a high pressure short-arc Xenon lamp (Canrad-Hanovia model 959C1980). The light from the Xenon lamp was dispersed by a 1.5 m monochrometer (Jobin-Yvon HR-1500). The grating of the monochromator has a linear dispersion of 0.19 nm / mm (2400 groves / mm grating) and is equipped with a stepping motor and controller. Microcomputer drives the scanning of the monochromator.

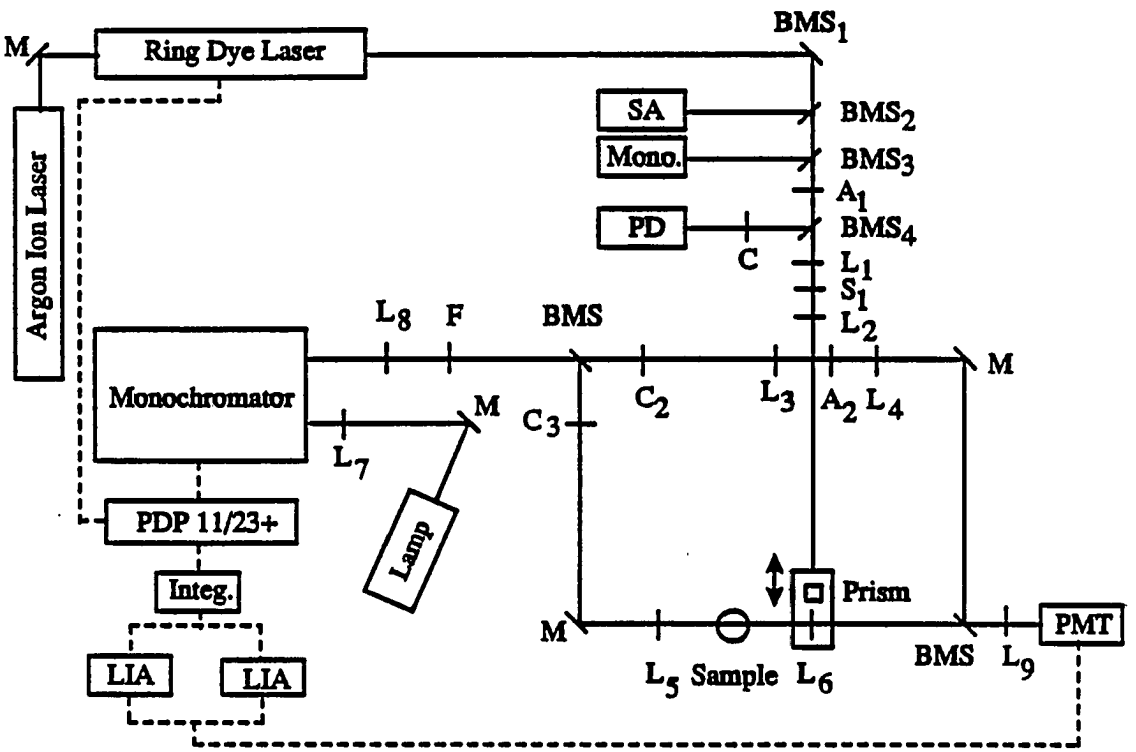

Figure 3. Hole burning experimental apparatus with double beam spectrophotometer. A: attenuator, BMS: beam splitter, C: chopper, F: optical filter, Integ.: integrator, L: lens, LIA: lock-in-amplifier, M: mirror, Mono: monochromator, S: shutter, PMT: photomultiplier tube

Details of the burn laser, the double beam absorption configuration and signal processing are described in experimental method of Section II of this dissertation.

PAPER I. PHOTOCHEMICAL HOLE BURNING IN BACTERIORHODOPSIN

153

Photochemical Hole Burning in Bacteriorhodopsin

In-Ja Lee, J.K. Gillie and Carey J. Johnson

Chemical Physics Letters 1989, 156, 227

ABSTRACT

Photochemical hole burning has been observed in the absorption spectrum of light-adapted bacteriorhodopsin and in its bathochromic intermediate K at 1.6 to 90 K. Hole widths (~800 cm^{-1}, hwhm) show evidence of large homogeneous linewidths, which are attributed to vibronic broadening. Holes were burned into the absorption spectrum of K with burn wavelengths from 514 to 650 nm. These results are discussed, and related to recent models of the excited-state dynamics in bacteriorhodopsin.

INTRODUCTION

Bacteriorhodopsin (BR) functions as a light-driven proton pump in which the primary photochemical event is isomerization of a retinal Schiff base from the all-trans to the 13-cis configuration (1-3). The photochemistry of BR has been the subject of extensive study, both at room temperature and at cryogenic temperatures (4,5). At room temperature the intermediate J is formed in 400-500 fsec (6,7) and decays in 2-3 psec (7-9) to the intermediate K, which has a lifetime of ~1 μsec (4,10). Several intermediates in the photocycle have been trapped at cryogenic temperatures and studied by low-temperature spectrophotometry. The intermediate K, for example, can be trapped at temperatures as high as 150 K (11). This intermediate is known to contain the protonated retinal Schiff base in a strained 13-cis conformation (12). In a low-temperature study, Iwasa et al. (13) found that irradiation of BR_{570} at 9 K with green light generates the red-shifted species identified as K. It was possible to reconvert K to BR_{570} by irradiation with deep red light (>660nm). A stable precursor to K has not beeen observed, even at temperatures of 6-9 K (11,13).

The absorption spectrum of bacteriorhodopsin is broad and unresolved at low temperature. Recent measurements of the excited-state dynamics in bacteriorhodopsin detected excited-state relaxation in 100-200 fs (14,15). Thus lifetime broadening can not account for the large spectral width of BR_{570} (FWHM ~ 2600 cm^{-1} at 1.6 K). The spectral profile of BR_{570} could be inhomogeneously broadened, for example by a shallow ground-state potential well susceptible to variations in the protein environment, and it could also be broadened by strong phonon or Franck-Condon coupling. To determine the homogeneous contribution

to the spectral width, we present in this letter the first low-temperature optical hole-burning study of BR_{570} and K. The results are discussed in terms of mechanism and degree of homogeneous broadening, and are related to the excited-state photochemistry of BR.

EXPERIMENTAL METHOD

Halobacterium halobium S9 (a gift from Professor W. Stoeckenius) was grown and its purple membrane isolated according to standard procedures (16). Samples were prepared in two forms: [1] purple membrane was suspended in 75% glycerol, 25% water, or [2] bacteriorhodopsin samples were solubilized with triton X. Samples were light adapted at 0° C by exposure for 10-20 min to white light from a tungsten lamp passed through and H_2O heat filter. Light adaptation was verified by a red shift in the spectrum. Optical densities were 0.7 in a 1 cm cell.

The samples were quickly cooled (<10 min) to 4.2 K in a Janis model 8-DT Super Vari-Temp liquid helium cryostat. Holes were burned with a Coherent 699-21 ring dye laser (linewidth ~ 0.07 cm^{-1}) operated with rhodamine 6G or DCM dye. Alternatively, a Coherent Innova 90-5 Ar ion laser was used for a 514 nm burn wavelength (resolution 0.2 cm^{-1}). The absorption and hole spectra were obtained either with a computer-controlled double-beam spectrometer, described elsewhere (resolution 0.2 cm^{-1}) (17), or with a Bruker model IFS-120 Fourier-transform spectrometer operating at a resolution of 4 cm^{-1}.

RESULTS

Figure 1a shows the absorption spectrum of solubilized light-adapted BR at 1.6 K recorded on the scanning double-beam spectrometer before and after irradiation at λ_B=566.1 nm with a burn intensity of 110 mW cm^{-2} for 5 min. The band width (FWHM, low energy side) is 940 cm^{-1}. The difference spectrum in fig.1b shows two broad holes, one at 550 nm (HWHM 800 cm^{-1} and other at 620 nm. No narrow hooes were found.

The absorption spectrum for BR in the form of membrane suspensions, taken with FT spectrophotometer, is shown in Fig. 2. To record these spectra, the sample was exposed to white light with a power density of ~ 1 mW cm^{-2} for 20 sec, sufficient to convert on the order of 10% of the sample to K. The spectrum in Fig. 2 shows increased tailing of the absorption band to the red compared to spectra recorded with a scanning monochromator (13) (dashed line in Fig. 2). Similar increased absorption in the red tail after exposure in the FT spectrophotometer (compared to Fig. 1a) was observed in solubilized BR. Repeated scanning of the FT spectrophotometer resulted in no further change in the spectral line shape. We interpret this result as the establishment of a photostationary distribution of BR and K. Since the spectral profile of the light source peaks in the red (>700 nm), the photostationary distribution is weighted in favor of BR and contains a relatively small amount of K.

Hole-burning studies were carried out on this photostationary distribution. Figure 3 shows the difference spectrum after laser excitation at λ_B = 577 nm (8 mW/cm^2, 10 min). A broad hole is centered at 630 nm and an antihole at 600 nm. The crosses show a Lorentzian fit to the low energy side of the hole with hwhm of

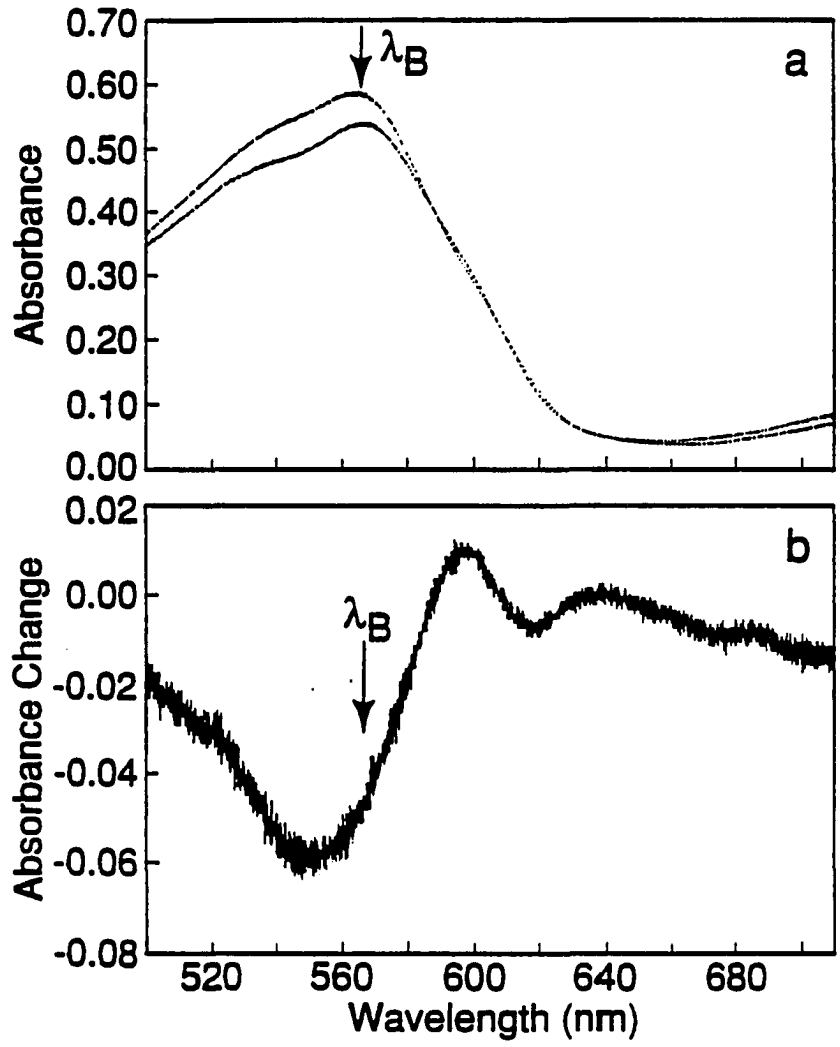

Figure 1. Absorption spectrum and difference spectrum of light-adapted solubilized bacteriorhodopsin. (a) Absorption spectrum before (top) and after (bottom) irradiation at 566.1nm for 5 min with 110 mW/cm^2 at 1.6 K. (b) Difference spectrum

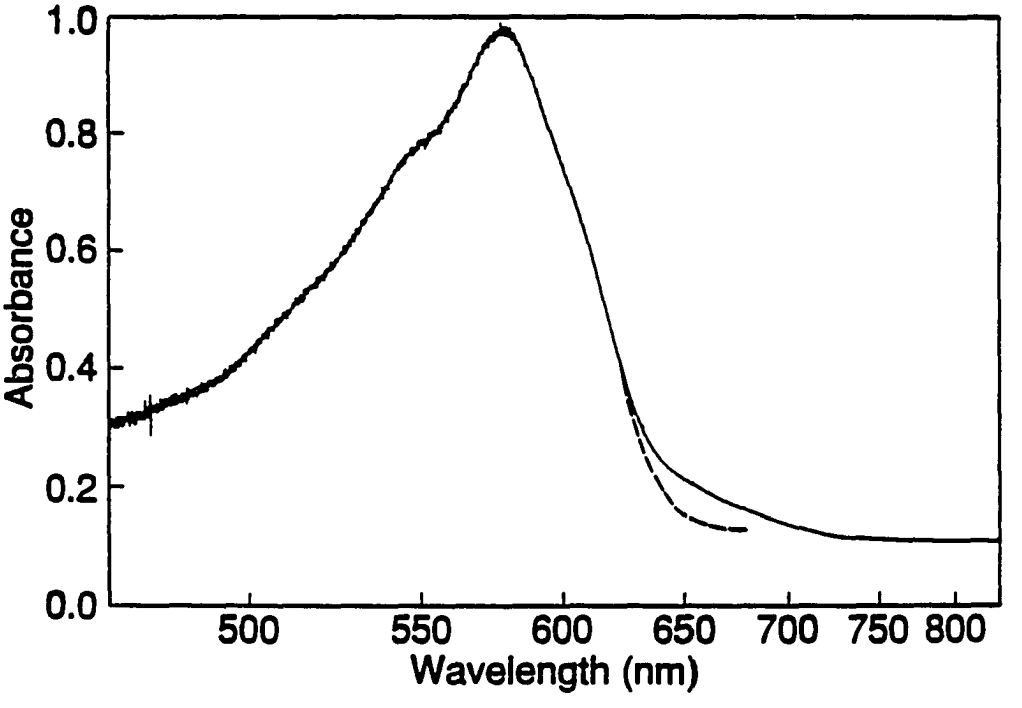

Figure 2. Absorption spectrum of light-adapted purple membrane suspension taken with FT spectrometer at 1.6 K. The dashed line shows the absorption profile expected for low exposure intensity (from ref. 14)

800 cm^{-1}. Similar holes were burned with irradiation wavelengths ranging from 514 to 650 nm at temperatures up to 90 K. A weaker antihole was observed in several difference spectra at 537 nm. No holes were observed near the BR peak absorption (575nm) when pre-burn and post-burn spectra were recorded on the FT spectrophotometer. Similar results were obtained with solubilized BR (absorption peak a 565 nm), where a broad hole was centered at 620 nm, but no hole was found near 565 nm. By comparison with Fig. 1, we conclude that the holes burned into the BR_{570} absorption band were subsequently erased by re-establishment of a photostationary distribution in recording the post-burn spectra. We cannot exclude the possibility that a sharp hole at the burn wavelength was not observed due to the 4 cm^{-1} resolution of the FT spectrometer.

Figure 4 shows the burn-wavelength dependence of the hole spectrum. The hole shifts by about 6 nm from blue to red as the burn wavelength λ_B is tuned from 514 nm to 650 nm (Table I.). Hole burning in K was also studied as a function of burn intensity and burn time. The hole width was independent of burn intensity and burn time over range from 10 to 250 mW cm^{-2}.

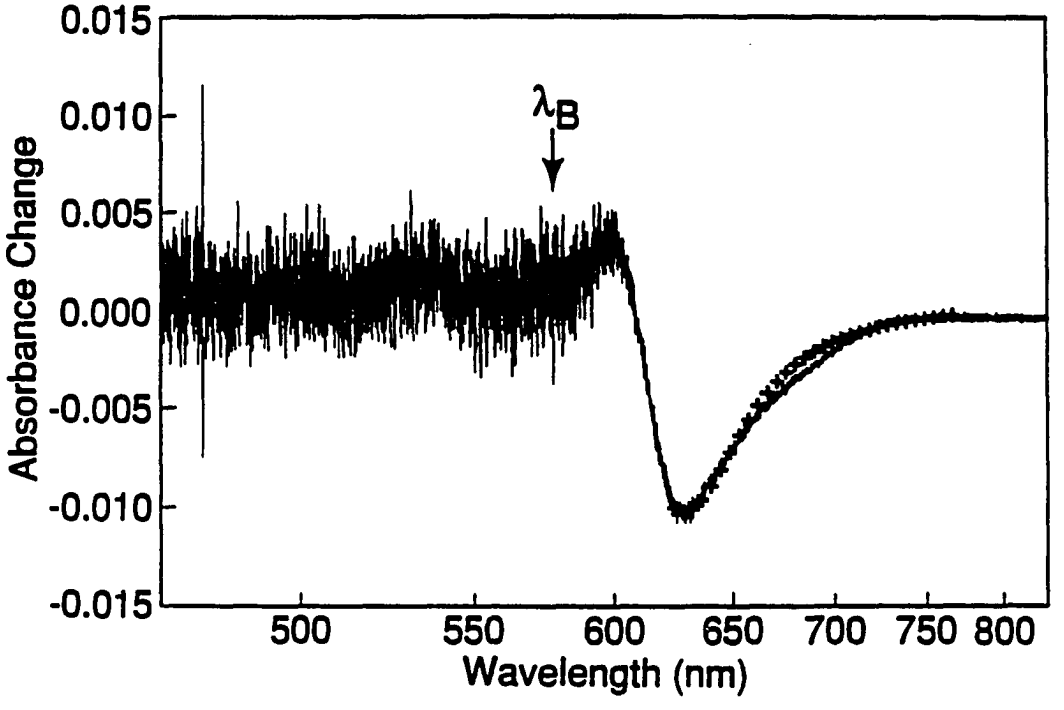

Figure 3. Difference absorption spectrum of purple membrane suspension at 1.6 K for laser excitation at 577.4 nm for 10 min at 8 mW/cm^2. The crosses show a Lorentzian fit to low energy side with hwhm 800 cm^{-1}

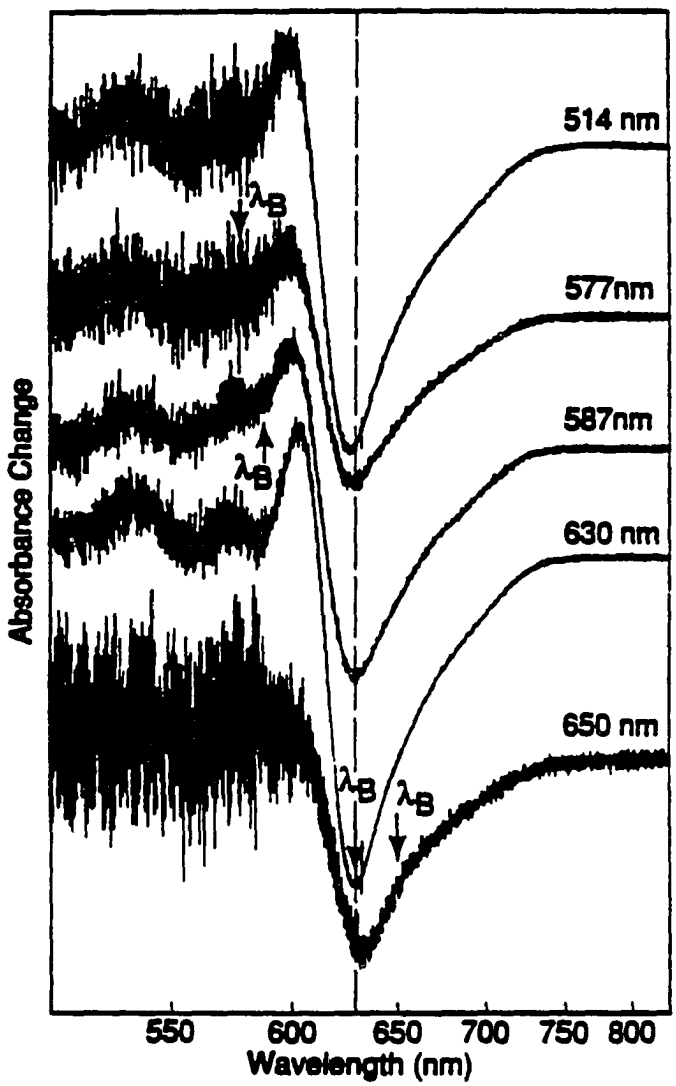

Figure 4. Excitation-wavelength dependence of difference spectrum (1.6 K). Burn wavelength were 514, 577, 587, 630 and 650 nm

DISCUSSION

Hole burning into the absorption band of BR_{570} is shown in Fig. 1 to result in a remarkably broad hole with hole maximum near the absorption maximum. The hole width (~800 cm^{-1} HWHM) is nearly as large as the BR_{570} absorption band width (~940 cm^{-1} HWHM). A rough estimate of the inhomogeneous contribution can be obtained as follows. If we take the hole width to be twice the homogeneous width, we have Γ_h~400 cm^{-1} (HWHM). (By homogeneous we mean mechanisms broadening the absorption width of single molecules.) The inhomogeneous contribution can be estimated by (18) $\Gamma_{inh} \approx \Gamma - \Gamma_h \approx 540$ cm^{-1}, consistent with an inhomogeneous width of ~500 cm^{-1} (HWHM) deduced by Myers et al. (19,20) from fits to resonance Raman cross sections and excitation profiles.

We consider here coupling of the elctronic transition to low-frequency torsional modes of the retinal Schiff base as a mechanism for the broad homogeneous width in BR_{570}. This mechanism has been suggested by a number of workers (14,15,19-22) as a model to explain spectroscopic properties of bacteriorhodopsin and rhodopsin. The torsional model is thus already based on a vast array of studies of these systems. Since torsional motion about the $C_{13}=C_{14}$ double bond double bond leading to its isomerization occurs in 100-200 fsec (14,15), strong Franck-Condon activity is likely in this mode. For the visual chromophore rhodopsin, Birge and co-workers have carried out semi-empirical calculations of the vibrational overlap integrals and have shown that the broad absorption band width can be explained by strong Franck-Condon activity associated with the

C_{11}=C_{12} torsional mode (21). In their simulation, an inhomogeneous contribution of 250 cm^{-1} (HWHM) combined with the calculated torsional vibronic activity is sufficient to generate a diffuse spectral contour at low temperatures. Similar arguments are expected to apply to the C_{13}=C_{14} torsional mode (isomerization coordinate) in bacteriorhodopsin. Myers et al. have also suggested that a torsional mode, modeled by a linear dissociative excited-state potential, could contribute significant width (500-600 cm^{-1} HWHM) to the absorption band (19,20). Vibronic activity associated with torsion about single bonds may also contribute to the observed line width, although the contribution from the C_6-C_7 single bond, which appears to broaden the spectral profile of all-trans retinal (22), seems not to play a major role in bacteriorhodopsin (19-21).

The vibronic mechanism of spectral broadening associated with torsional modes bears a strong resemblance to the theory of hole burning in systems characterized by strong electron-phonon coupling that has recently been developed by Small and co-workers and applied to primary donor state of photosynthetic reaction centers in Refs. 18, 23 and 24. In their theory, the strength of electron-phonon coupling is parametrised by the Huang-Rhys factor S. A rough estimate of $S\omega \approx 2000$ cm^{-1} (where ω is the tortional frequency) for BR can be made from the Stokes shift (~4000 cm^{-1} (14)), given approximately by $2S\omega$ (18). As a check, the approximate formula $\Gamma \sim \Gamma_{inh} + S\omega$ (18) gives $S\omega \sim 1500$ cm^{-1}. Assuming $\omega = 50$ cm^{-1}, we find S~40. (Since no strong low-frequency modes have been observed in the resonance Raman spectrum of bacteriorhodopsin, a frequency of 50 cm^{-1} is chosen

as an upper limit above which the torsional mode should have been observed directly or as a combination band (19).) Since the torsional frequency is not known, and the assumption of displaced harmonic potentials with no frequency change used to derive these formulas does not apply to the torsional mode, these numbers are merely intended to show that S is extremely large. We note that the excited-state displacement parameters determined from the Raman cross sections of observed Raman bands are all small ($\Delta_i<1$) (19). Thus the observed Raman bands cannot account for the large Huang-Rhys factor ($S=\Sigma\Delta_i^2/2$). Strong electron-phonon coupling characterized by $S\geq4$ in photosynthetic reaction centers finds precedent in charge-transfer states associated with aromatic donor aceptor complexes (25). There is no evidence for charge transfer of this degree upon excitation of the protonated retinal Schiff base, and a candidate for such a charge-transfer state has not been identified (26). Strong linear electron-phonon coupling has been observed in some systems without charge-transfer states (27). However, such cases appear to be the exception rather than the rule (28). We conclude that our observations are consistent with the torsional model. However, other possibilities, such as electron-phonon coupling, cannot be strictly ruled out.

The broad holes centered at 626-634 nm in Figs. 3 and 4 are burned into the absorption band of the intermediate K. Since no corresponding increase in optical density is observed at 575 nm, hole formation involves photochemical generation of a species distinct from BR_{570}. For example, a possible mechanism for hole burning in the K state is photochemical deprotonation of the retinal Schiff base

and, in fact, the blue-absorbing deprotonated intermediate M has been observed to form from a photostationary distribution of BR and K at room temperature upon radiation with intense laser pulses (29). The hole width (800 cm^{-1} HWHM) is evidence for strong Franck-Condon activity in the K absorption band as well. The excited-state potential surface for K, like BR, is known to lead readily to isomerization about the C_{13}=C_{14} double bond. Thus the hole width in K is also very likely associated with C_{13}=C_{14} vibronic activity. The hole width observed in BR and K are the same within the accuracy of the measurement (±50 cm^{-1}). We attribute this to the similarity in the protein environment and the torsional mechanism of homogeneous broadening in the two species.

The burn-wavelength dependence of the hole maximum (Table I) represents evidence of site inhomogeneous broadening of the K intermediate. Only when the burn wavelength is far removed from the hole center are shifts of more than 1 nm observed. Small shifts of the hole center from the absorption maximum toward the burn wavelength were also observed in photosynthetic reaction centers (30), and are consistent with a large homogeneous absorption width on the order of the site inhomogeneous broadening (23). Experiments are planned to study the burn-wavelength dependence of hole burning in the BR_{570} absorption band.

We turn finally to a brief discussion of the 600 nm antihole. The increased optical density at 600 nm is 1/2 to 1/3 as large as the decrease at 630 nm in all difference spectra with burn wavelengths 514 to 630 nm. At this point we can only speculate about the origin of the antohole. Possible explanations are: [1] an

intermediate formed by photo-excitation of K and trapped at temperatures up to ~60 K; [2] a species formed thermally from K, such as the intermediate KL absorbing at 600 nm (31), due to local heating in the sample. Further experiments are planned regarding the 600 nm feature.

Table I. Burn wavelength dependence of hole and antihole maximum at 1.6 K

Burn wavelength (nm)	Hole maximum (nm)	Antihole maximum (nm)
514	627.2	598.0
567	628.6	600.3
577	629.2	600.3
587	629.7	600.1
597	629.8	601.0
622	630.5	600.9
630	629.8	603.5
650	633.5	600.3

ACKNOWLEDGMENT

Illuminating discussions with Professor G. J. Small are gratefully acknowledged. IJL and JKG ackowledge support from the Division of Material Research of NSF through grant DMR-8612270. CKJ acknowledges partial support for this research from Research Corporation.

REFERENCES

1. Oesterhelt, D.; Stoeckenius, W. Nature New Biol. 1971, 233, 149.
2. Stoeckenius, W.; Bogomolni, R.A. Ann. Rev. Biochem. 1982, 51, 587.
3. Braiman, M.; Mathies, R. Biochemistry 1980, 19, 5421.
4. Ottolenghi, M. Advan. Photochem. 1980, 12, 97.
5. Hochstrasser, R.M.; Johnson, C.K. In Ultrashort Laser Pulses, Kaiser, W. Ed.; Springer: Berlin, 1988.
6. Nuss, M.C.; Zinth, W.; Kaiser, W.; Kolling, E.; Oesterhelt, D. Chem. Phys. Lett. 1985, 117, 1.
7. Petrich, J.W.; Breton, J.; Martin, J.L.; Antonetti, A. Chem. Phys. Lett. 1987, 137, 369.
8. Polland, H.-J.; Franz, M.A.; Zinth, W.; Kaiser, W.; Kolling, E.; Oesterhelt, D. Biophys. J. 1986, 49, 651.
9. Sharkov. A.V.; Pakulev, A.Y.; Chekalin, S.V.; Matveetz, Y.A. Biochim. Biophys. Acta 1985, 808, 94.
10. Milder, S.J.; Kliger, D.S. Biophys. J. 1988, 53, 465.
11. Iwasa, T.; Tokunaga, T.; Yoshizawa Biophys. Struct. Mech. 1980, 6, 253.
12. Braiman, M.; Mathies, R. Proc. Natl. Acad. Sci. USA 1982, 79, 403.
13. Iwasa, T.; Tokunaga, F.; Yoshizawa, T. FEBS Lett. 1979, 101, 121.
14. Dobler, J.; Zinth, W.; Kaiser, W.; Oesterhelt, D. Chem. Phys. Lett. 1988, 144, 215.

15. Mathies, R.A.; Brito Cruz, C.H.; Polland, W.T.; Shank, C.V. Science, 1988, 240, 777.

16. Oesterhelt, D.; Stoeckenius, W. Methods Enzymol. 1974, 31, 667.

17. Fearey, B.L.; Carter, T.P.; Small, G.J. J. Phys. Chem. 1983, 87, 3590.

18. Hayes, J.M.; Gillie, J.K.; Tang, D.; Small, G.J. Biochim. Biophys. Acta 1988, 932, 287.

19. Myers, A.B.; Harris, R.A.; Mathies, R.A. J. Chem. Phys. 1983, 79, 603.

20. Myers, A.B.; Trulson, M.O.; Pardoen, J.A.; Heeremans, C.; Lugtenburg, J.; Mathies, R.A. J. Chem. Phys. 1986, 84, 633.

21. Birge, R.R.; Bocian, D.F.; Hubbard, L.M. J. Am. Chem. Soc. 1982, 104, 1196.

22. Warshel, A.; Karplus, M. J. Am. Chem. Soc. 1974, 96, 5677.

23. Hayes, J.M.; Small, G.J. J. Phys. Chem. 1986, 90, 4928.

24. Gillie, J.K.; Fearey, B.L.; Hayes, J.M.; Small, G.J.; Golbeck, J.H. Chem. Phys. Lett. 1987, 134, 316.

25. Haarer, D.; Philpott, M.R. In Spectroscopy and Excitation Dynamics of Condensed Molecular Systems, Agranovich, V.M., Hochstrasser, R.M., Eds.; North-Holland: Amsterdam, 1983, p 27.

26. Grossjean, M.F.; Tavan P. J. Chem. Phys. 1988, 88, 4884.

27. Small, G.J. J. Chem. Phys. 1970, 52, 656;
Chereson, P.H.; Friedman, P.S.; Kopelman, R. J. Chem. Phys. 1972, 3716.

28. Macfarlane, R.M.; Shelby, R.M. J. Lumin. 1987, 36, 179;

Rebane, K.K.; Gorokhovskii, A.A. J. Lumin. 1987, 36, 273;

Fearey, B.L.; Carter, T.P.; Small, G.J. J. Phys. Chem. 1983, 87, 3590.

29. Grieger, I.; Atkinson, G.H. Biochemistry 1984, 24, 5660.

30. Boxer, S.G.; Lockhart, D.J.; Middendorf, T.R. Chem. Phys. Lett. 1986, 123, 477.

31. Shichida, Y.; Mutuoka, S.; Hidaka, Y.; Yoshizawa, T. Biochim. Biophys. Acta 1983, 723, 240.

CONCLUSIONS

Photochemical hole burning has been observed in the absorption spectrum of light-adapted BR (BR_{570}) and its bathochromic intermediate K_{610} at the temperatures ranging from 1.6 K to 90 K. Both BR_{570} and K_{610} show same hole width of ~800 cm^{-1} (hwhm) which is evidence for large homogeneous broadening. Strong electron-phonon coupling and coupling to a torsional mode mechanism were considered as mechanisms for the large homogeneous broadening of BR_{570}. The first mechanism, which requires a large S value (~40), inconsistent with the S value obtained from resonance Raman data. Since the torsional motion about the C_{13}=C_{14} double bond occurs in 100-200 fsec, strong Franck-Condon activity seems likely for in this mode. It is concluded that the large homogeneous broadening comes from the coupling of electronic transition to the torsional mode about the C_{13}=C_{14} double bond of retinal although there is also probably a small contribution by the torsional mode about C_6-C_7 single bond.

The hole width of ~800 cm^{-1} burned in K_{610} is also likely related to the torsional mode of C_{13}=C_{14} double bond. The burn wavelength dependent hole spectra of K_{610} show a small shift of hole position which indicates a large homogeneous width on the order of site inhomogeneous broadening.

REFERENCES

1. Stoeckenius, W.; Bogomolini, R.A. Ann. Rev. Biochem. 1982, 52, 587.
2. Balurock, A.; Stoeckenius, W. Nature (London) New Biol. 1971, 233, 152.
3. Herderson, R. J. Mol. Biol. 1975, 93, 123.
4. Blaurock, A. J. Mol. Biol. 1975, 93, 139.
5. Ebrey, T.G.; Becher, B.; Meo, B.; Kilbride, P.; Honig, B. J. Mol. Biol. 1977,112, 377.
6. Uwin, P.N.T.; Henderson, R. J. Mol. Biol. 1975, 94, 425.
7. Korenstein, R.; Hess, B. Methods. Enzymol. 1982, 88, 193.
8. Korenstein, R.; Hess, B. FEBS Lett. 1978, 89, 15.
9. Liebman, P.A.; Eutine Science 1974, 185, 457.
10. Khorana, H.G.; Gerber, G.E.; Herlihy, W.C.; Gray, C.P.; Anderegg, R.J.; Nihei, K.; Biemann, K. Proc. Natl. Acad. Sci. USA 1979, 76, 5046.
11. Ovchinnikow, A. Yu.; Abdulaev, N.G.; Feigina, M.Yu.; Kiselev, A.V.; Lobanov, N.A. FEBS Lett. 1979, 100, 219.
12. Oesterhelt, D.; Stoeckenius, W. Proc. Natl. Acad. Sci. USA 1973, 70, 289.
13. Heyn, M.P.; Cherry, B.J.; Muller, U. J. Mol. Biol. 1977, 117, 607.
14. Bamberg, E.; Apell, H.-J.; Dencher, N.A.; Sperling, H.; Laüger, P. Biophys. Struct. Mech. 1979, 5, 277.
15. Ottolenghi, M., Adv. Photochem., 1980, 12, 97.
16. Sperling, W.; Karl, P.; Raffety, Ch. N.; Dencher, N.A. Biophys. Struct. Mech. 1977, 3, 79.

17. Lozier, R.H.; Bogomolni, R.A.; Stoeckenius, W. Biophys. J. 1975, 45, 955.

18. Tokunaga, F.; Iwasa, T. Methods. Enzymol. 1982, 38, 163.

19. Iwasa, T.; Tokunaga, F.; Yoshizawa, T. Photochem. Photobiol. 1981, 33, 539.

20. Iwasa, T.; Tokunaga, F.; Yoshizawa, T. FEBS Lett. 1979, 101, 121.

21. Iwasa, T. Tokunaga, F.; Yoshizawa, T. Biophys. Struct. Mech. 1980, 6, 253.

22. Stoeckenius, W.; Lozier, R.J. J. Supramol. Struct. 1974, 2, 769.

23. Goldschmidt, C.R.; Ottolenghi, M.; Korenstein, R. Biophys. J. 1976, 16, 839.

24. Goldschmidt, C.R.; Kalisky, O.; Rosenfeld, T.; Ottolenghi, M. Biophys. J. 1977, 17, 179.

25. Dencher, N.; Willms, M. Biophys. Struct. Mech. 1975, 1, 259.

26. Tokunaga, F.; Iwasa, T.; Yoshizawa, T. FEBS Lett. 1976, 72, 33.

27. Kalisky, O.; Goldschmidt, C.R.; Ottolenghi, M. Biophys. J. 1977, 19, 185.

28. Marcus, M.A.; Lewis, A. Science 1977, 195, 1382.

29. Marcus, M.A.; Lewis, A. Biochemistry 1978, 17, 4722.

30. Campion, A.; Terner, J.; El-Sayed, M.A. Nature, 1977, 65, 659.

31. Kaufman, K.J.; Rentzepis, P.M.; Stoeckenius, W.; Lewis, A. Biochem. Biophys. Res. Commun. 1976, 68, 1109.

32. Ippen, E.P.; Shank, C.V.; Lewis, A.; Marcus, M.A. Science 1978, 200, 1279.

33 Nuss, M.C.; Zinth, W.; Kaiser, W.; Kölling, E.; Oesterhelt, D. Chem. Phys. Lett. 1985, 117, 1.

34. Sharkov, A.V.; Pakulev, A.V.; Chekalin, S.V.; Matveetz Biochim. Biophys. Acta 1985, 808, 94.

35. Polland, H.-J.; Franz, M.A.; Zinth, W.; Kaisser, W.; Kölling, E,; Oesterhelt, D. Biophys. J. 1986, 49, 651.

36. Petrich, J.W.;; Breton, J.; Martin, J.L.; Antonetti, A. Chem. Phys. Lett. 1987, 137, 4.

37. Stockburger, M.; Alshuth, T.; Oesterhelt, D.; Gärtner, W. In Spectroscopy of Biological Systems, Clark, R.J.H., Hesler, R.E., Eds.; Wiley: New York, 1986.

38. Schulten, K.; Dinur, U.; Honig, B. J. Chem. Phys. 1980, 73, 3927.

39. Tavan, P.; Schulten, K.; Oesterhelt, D. Biophys. J. 1985, 47, 415.

40. Pettei, M.J.; Yudd, A.P.; Nakanishi, K., Henselman, R.; Stoeckenius, W. Biochemistry 1977, 16, 1955.

41. Braiman, M.; Mathies, R. Biochemistry 1980, 19, 5421.

42. Terner, J.; Hsieh, C.-L.; Burns, A.R.; El-Sayed, M.A. Proc. Natl. Acad. Sci. USA 1979, 76, 3046.

43. Braiman, M.; Mathies, R. Proc. Natl. Acad. Sci. USA 1982, 79, 403.

44. Pande, J.; Callender, R.H.; Ebrey, T.G. Proc. Natl. Acad. Sci. USA 1981, 78, 7379.

45. Mathies, R.A.; Brito Cruz, C.H.; Pollard, W.T.; Shank, C.V. Science 1988, 240, 777.

46. Pollard, W.T.; Brito Cruz, C.H.; Shanck, C.V.; Mathies, R.A. J. Chem. Phys. 1989, 90, 199.

47. Dobler,J.; Zinth, W.; Kaiser, W.; Oesterhelt, D., Chem. Phys. Lett. 1988, 144, 215.

48. El-Sayed, M.A.; Karvaly, B.; Fukumoto, J.M. Proc. Natl. Acad. Sci. USA 1981, 78, 7512.

GENERAL CONCLUSIONS

The theory proposed to simulate hole profiles for arbitrarily strong electron-phonon coupling in short burn time limit was extended to examine the hole profiles at arbitrary burn time. The shapes of real- and pseudo-PSBH in the hole burned spectra in amorphous solids strongly depend on burn time and burn wavelength. As burn time increase, hole burning through PSB becomes more important. At shorter wavelengths, the pseudo-PSBH is getting larger compared to the real-PSBH.

The antihole spectrum was deconvolved from the hole spectrum using the simulated hole spectrnm. From the deconvolved antihole profile, it is concluded that NPHB of antenna complex of PSI-200 predominantly creates sites whose zero-phonon transitions are shifted to higher energy relative to preburn sites.

The first observation of the antihole of a porphyrin in an amorphous solid is presented. The antihole was polarized oppositely to the hole and distributed throughout the inhomogeneous absorption band. Vibronic frequencies and Franck-Condon factors of some vivrations were measured. A positive correlation between the site distributions for Q_x and Q_y is observed.

The extent of hole burning of Ox720 in PVOH has been studied as a function of burn intensity for fixed burn fluences. It was shown that the hole depth increased logarithmically with burn time over several decades. Although the triplet quantum yield of Ox720 is as low as 0.04, it is observed that the triplet bottleneck effect plays an important role on hole burning (both on hole broadening and hole growth) when burn intensities become large. By comparing calculated

and measured constant fluence curves, the longest lifetime of the spin sublevels in the triplet state was obtained.

The large differences in the magnitude of the slopes between the measured and calculated curves may be explained mostly by the effect of dispersive kinetics and partly by hole saturation broadening.

Spectral difussion in ~μsec range using the persistent hole burning was not observed in the Ox720 in PVOH. However, it might be possible to be observed when transient hole burning is used.

Photochemical hole burning has been observed in the absorption spectrum of light-adapted BR (BR_{570}) and its bathochromic intermediate K_{610} at 1.6 K to 90 K. Both of BR_{570} and K_{610} show a hole width of ~800 cm^{-1} (hwhm) which is evidence for large homogeneous broadening. Since torsional motion about C_{13}=C_{14} double bond occurs in 100-200 fsec, strong Franck-Condon activity seems be in this mode. It is concluded that large homogeneous broadening comes from the coupling of the electronic transition to the torsional mode about the C_{13}=C_{14} double bond of retinal although there is also a small contribution by the torsional mode about the C_6-C_7 single bond.

The hole width of ~800 cm^{-1} burned in K_{610} is also likely related to the torsional mode of the C_{13}=C_{14} double bond. The burn wavelength dependent hole burning of K_{610} shows a small shift of hole position which indicates a large homogeneous width on the order of site inhomogeneous broadening.

ACKNOWLEDGMENTS

I would like to express my sincere thanks to Prof. Gerald J. Small, my research advisor, for his advice, guidance and patience throughout the course of this study. The work described in this dissertation could not have been completed without his helpful advice, valuable insight and patient discussions.

I am greatly indebted to Dr. John M. Hayes for his valuable advice and guidance on experimental and theoretical aspect of my research as well as proofreading of this dissertation. I always learned something from our discussion.

I would like to thank Dr. R. Jankowiak and Dr. N. R. S. Reddy for their advice on theoretical and experimental aspects of my research as well as proofreading of this dissertation. I wish to thank to Prof. C. K. Johnson of Univ. Kansas for his many discussions of the bacteriorhodopsin project.

I also owe thanks to other members of the group, particularly Dr. M. J. Kenney and Dr. J. K. Gillie who helped me get started and showed me how to perform the experiments. I would also like to express my thanks to Dr. K. S. Song and Mrs. S. Song for their friendship during my graduate study.

I would like to express my sincere gratitude to Prof. Keon Kim of Korea University for his encouragement and advice.

Most importantly I would like to sincerely thank to my parents, grand mother and parents-in-law who have always supported me and encouraged me in everything I have done.

Finally my sincere thanks to my husband, Tae-kyun, for his encouragement, support, patience and love.